UNIVERSITY OF CAPE TOWN
IYUNIVESITHI YASEKAPA • UNIVERSITEIT VAN KAAPSTAD

FACULTY OF ENGINEERING AND BUILT ENVIRONMENT

DEPARTMENT OF CIVIL ENGINEERING

THE BEHAVIOUR OF PATCH REPAIRED AND FRP STRENGTHENED REINFORCED CONCRETE BEAMS: AN EXPERIMENTAL INVESTIGATION

Prepared by: **ThabisoDladla**

Supervisor: **Prof. P. Moyo**

Co-supervisor:**Prof. H. Beushausen**

THIS THESIS HAS BEEN SUBMITTED TO THE DEPARTMENT OF CIVIL ENGINEERING, FACULTY OF ENGINEERING AND BUILT ENVIRONMENT, UNIVERSITY OF CAPE TOWN, IN PARTIAL FULLFILLMENT OF THE REQUIREMENTS FOR AN MSc DEGREE IN CIVIL ENGINEERING

PLAGIARISM DECLARATION

THESIS SUPERVISOR: PROF P. MOYO

1. I know the meaning of plagiarism and declare that all the work in the document, save for that which properly acknowledged, is my own.
2. I have used the Harvard Convention for citation and referencing. Each significant contribution to and quotation in this research forms the work or works of other people that has been attributed and has been cited and referenced.
3. I have not allowed and will not allow anyone to copy my work with the intension of passing it as his or her own work.

Name: Thabiso Dladla Student No: DLDTHA001

Date: AUGUST, 2014 Signature: .

Abstract

The aim of this study was to investigate the effect of extent of simulated uniform corrosion on reinforced concrete beams that have been patch repaired and strengthened in flexure. The most widespread cause of deterioration of reinforced concrete structures is due to corrosion of reinforcement (Bentur et al., 1997). According to Taljsten (2006) some reasons for the corrosion of structures can be attributed to incorrect design and poor construction methods, just to mention a few. Hollaway (2006) suggests that corrosion reduces the area of steel at the corrosion sites therefore decreasing load carrying capacity. The reduced steel area due to corrosion of steel in reinforced concrete beams is considered critical when it can lead to premature failure of a structure. Elgarf (1999) argues that large reductions in flexural capacity, strength and rigidity, which render a beam inadequate for serviceability loads are most likely to occur when localized pitting has extended to many sites resulting in extensive and relatively uniform levels of corrosion.

Upgrading of structures is not only required for deteriorating structures but could be due to errors in design or construction and increased demand of traffic (Taljsten, 2006). Where possible rehabilitation and retrofitting of reinforced concrete members has become favourable compared to demolishing and reconstruction.

Numerous studies have been devoted to the method of retrofit of non-corroded studies some of which were conducted by; Hollaway and Leeming (1999), Bonacci et al. (2001), Khalifa and Nanni (2002), Bren et al. (2004). However less research is available on corroded beams which have been patch repaired and strengthened with Carbon Fibre Reinforced Polymer (CFRP). The purpose of this dissertation was to add information on the behaviour of patch repaired and strengthened (RS) beams.

This experimental study was conducted under four point loading and included a total of 15 beams; of which 3 were control beams and the remaining 12 beams were RS beams. The beams had dimensions of 155mm x 254mm x 2000mm. The RS beams were subjected to simulated corrosion process instead of accelerated corrosion. Simulated corrosion was done by reducing the steel area, as corrosion does, by means of milling the steel. The degree of corrosion that was being simulated was that of 5% area loss over the damage lengths of 450mm, 800mm,

1300mm and 1800mm. The term damage extent is used to describe the different lengths of damage which were investigated for the same steel area loss. The damage imposed on the tensile reinforcement was a simulation of uniform corrosion which reinforced structures have been known to experience mostly in coastal environments. The 12 RS beams were subdivided into 4 of 3 beams each; where each set was related to the damage extent of 450mm, 800mm, 1300mm and 1800mm.The patch repair lengths were of a similar length to the damage length. CFRP plate was bonded to the centre of the beam's soffit and all CFRP plates had a length of 1700mm. The cracking behaviour of the beams was monitored by marking the crack patterns at every 10kN load interval. The crack width for each beam was measured with a crack width gauge ruler. The mid-span load-deflection behaviour was analysed from the results that were collected electronically with linear variable differential transducers (LVDTs) and load cell equipment. The concrete compression strain was measured at mid-span using demec targets and used to develop neutral axis results.

The damage progression for all the beams was monitored for all beams by means of crack mapping. It was observed that flexural cracks would develop in the maximum moment region at low loads. As the loads increased flexural shear cracks developed in the direction of the applied loads. The control beam had a higher cracking load than the RS beams. From crack mapping it was observed that for increasing damage extent of 450mm, 1300mm and 1800mm there was a decrease in cracking loads; the results were compared to the finite element models (FEM) prepared in a different parallel study conducted at the University of Cape Town. It was also observed that for the average crack spacing of RS beams was lower than the control beams; furthermore for increasing damage extent there was a decrease in average crack spacing. The RS beams failed by debonding of the CFRP plate, by means of epoxy splitting, and subsequently concrete crushing in the extreme compression zone near one of the load application zones.

From the load deflection behaviour it was observed that the yield loads and peak loads of the RS beams were found to be mostly greater than the control beam results. The higher loads of the RS beams were achieved at the expense of ductility. The RS beams were less ductile than the control beams. There was an increase in the yield loads and peak loads, from the experimental results, for increasing damage extent of 450mm, 800mm and 1800mm. The FEM yield

and peak loads also increased for the RS beams with increasing damage extent of 450mm, 800mm and 1300mm.

The experimental results indicated a decreasing ductility for increasing damage extent of 450mm, 800mm and 1300mm. The FEM results similarly displayed a decrease in ductility for increasing damage extent. The FEM e rigidity results of the RS beams were lower than the control beams whereas the average experimental results indicated the control beam as more rigid than the RS beams.

The neutral axis of the control beam was lower than that of the RS beams. It was observed that the neutral axis would decrease with increasing loads until failure for all the beams. Furthermore a pattern was established for the neutral axis and damage extent where the neutral axis would decrease with increasing damage extent.

Acknowledgements

The author would like to thank the following people for their support and assistance during the dissertation period:

- My parents for all the encouragement and support throughout the dissertation period, and to my friends for their continued support.
- My supervisor, Professor Pilate Moyo, for all the time he dedicated towards my study and the manner in which he always challenged me to test the boundaries of my post graduate dissertation.
- A personal thank you must go to the Concrete Structures Materials Integrity Research Unit (CoMSIRU) for workshops and motivation of continued growth as an individual.
- Special thanks to SANRAL for providing the financial assistance needed in order undertake a dissertation of this nature
- Appreciation must also be given to the University of Cape Town laboratory and workshop staff. Mr Noor Hassen and his staff for all their assistance when needed to help out.
- PhD student K. Matongo with the connection and calibration of the testing equipment in the laboratory.
- Kevin Kimbrey for the donations of all the CFRP, bonding agents and patch repair mortar needed throughout the experimental program.

TABLE OF CONTENTS

List of figures

List of tables

Glossary of terms

Accelerated steel corrosion – Steel corrosion at a faster-than-normal rate by subjecting steel to anodic current.

Anode - The electrode in electrolysis where steel corrosion occurs.

Bar spacing - The distance between parallel reinforcing bars, measured centre- to- centre of the bars perpendicular to their longitudinal axes.

Bond strength - Resistance to separation of a repair or CFRP from substrate concrete.

Bonding agent - A material applied to a suitable substrate to enhance bond between it and a new repair layer or CFRP laminate.

CFRP – Carbon Fibre Reinforced Polymer

Cathode - The electrode at which chemical reduction occurs.

Composite - A combination of two or more constituent materials such as a substrate concrete and a repair.

Concrete substrate – The original concrete. However, when FRP repair follows patch repair then it is a combination of existing concrete and patch repair.

Concrete Cracking – When the structure has visible cracking on the surface, dismemberment of the concrete as a whole.

Corrosion - Destruction of metal by a chemical, electrochemical, or electrolytic reaction with-in its environment.

Corrosion agents – Compounds such as water and oxygen that promote corrosion.

Corrosion cracks – Cracks on concrete due to steel corrosion.

Corrosion rate – The rate of loss of steel.

Cracked section - A section with a crack.

Debonding– A separation at the interface between the substrate and adherent material.

Deformation – A change in shape or size.

Debonding– When the CFRP laminate detaches from the original substrate or patch repair material, caused by excessive loading

Depth of the neutral axis – A distance from the outer surface of concrete to the neutral axis (in this thesis it is often measured from the compression face).

Deterioration - Physical manifestation of failure of a material (e.g., cracking, delamination, flaking, pitting, scaling, spalling, staining) caused by service conditions or internal autogenous influences.

Durability - The ability of a structure or its components to maintain serviceability in a given environment over a specified time.

Fibre reinforced polymer (FRP) – A general term for a composite material that consists of a polymer matrix reinforced with cloth, strands, or any other fibre form.

Interface – The interfacial boundary between two materials, e.g., an existing concrete substrate and a bonded patch repair material or CFRP laminate.

Interfacial bond – The bond between two different substances e.g. patch repair and CFRP

Laminate – One or more layers of fibre bound together in a cured resin matrix.

Degree/Level of steel corrosion – Degree of steel lost due to corrosion measured here as percentage mass loss of steel or as percentage loss in the area of steel.

Load-bearing capacity - The maximum load that a structure or structural element can withstand before it ultimately fails.

Neutral axis - A line in the plane of a structural member subject to bending where the longitudinal stress is zero.

Simulated corrosion – Steel was ground to emulate the accelerated corrosion process.

Patch Repair – A material used to substitute a portion of removed damaged concrete

Pitting - Development of relatively small surface cavities in corrosion of steel.

Propagate – When a crack increases in length and size over time whilst under loading

Repair - To replace or correct deteriorated, damaged, or faulty materials, components, or elements of a structure.

Spall – A fragment of the cover concrete that is detached from the parent concrete.

Static load – A single applied load at a constant rate or time

Stiffness - Resistance to deformation.

Stirrup - Reinforcement used to resist shear and torsion stresses in a structural member.

Strain - The change in length, per unit of length, in a linear dimension of a body; measured here in micro strains.

Stress - Intensity of force per unit area.

List of symbols

δ = predicted deflection
A_q= area of mass of steel consumed/lost
A_s' = Area of compression reinforcing steel
A_s = Residual area of tensile reinforcement after corrosion
b = Width of concrete section
c = Concrete cover depth
d = Bar diameter
d' = Distance from the extreme compression fibre to the centroid of compression reinforcing steel
E_c = concrete elastic modulus
E_f = concrete elastic modulus
f_{ct} = Tensile strength of concrete
F_s = Internal tensile force carried by the tensile steel reinforcement
F_{uls} = Ultimate tensile strength of tensile steel reinforcement
fy = Yield stress of tensile steel reinforcement
h = Height of the beam
Ig = Gross second moment of area of a beam
l = beam span
M = External applied moment
M_{cr} = Cracking moment of a beam
M_{uls} = Ultimate capacity of the beam
r = Radius of uncorroded steel bars
ε_{su} = Ultimate strain of tensile steel reinforcement
ε_u = Ultimate strain of concrete in compression
ε_y = Yield strain of tensile steel reinforcement

Chapter 1

1. Introduction

1.1 Background

The deterioration of reinforced concrete structures, particularly bridges near the coast, is a worldwide problem and has motivated the development of various retrofit methods.

Literature (Bentur et al., 1997; Hollaway and Leeming, 1999; Balaguru et al., 2009) suggests that the most widespread cause of deterioration of reinforced concrete structures is pitting corrosion of reinforcement. Corrosion of steel in concrete beams is considered critical when leads to premature collapse or when it results in compromised fitness of purpose of a structure. The premature failure affects both the serviceability limit state (SLS) and the ultimate limit state (ULS), of which the latter is the main subject of this study. Corrosion reduces the area of steel at the corrosion sites therefore decreasing its load carrying capacity (Bentur et al., 1997; Hollaway, 2006).The premature failure affects both the serviceability limit state (SLS) and the ultimate limit state (ULS), of which the latter was focused on in this study.

One of the common approaches of rehabilitating corroded members has been through the use of patch repairs. Patch repairs using cementitious mortars are the most popular due to their re-passivation ability (Bentur et al., 1997). In addition, they also allow the damaged regions to be cleaned and protected from further corrosion through the use of protective coatings. The selection of patch repair materials depends largely on its compatibility with the concrete substrate.

In certain cases of extreme deterioration there may be a need for upgrading structural members. Upgrading of structures is not only required for deteriorating structures but could be due to errors in design or construction. Where it is necessary to restore the load carrying capacity of RC structures, strengthening techniques are used. Increased demand of traffic in case of bridges can also be a reason for an upgrade of a structure (Taljsten, 2006). For this reason rehabilitation and retrofitting of structures has become increasingly important. The idea of replacement of an entire structure is at times inconceivable for the client due to the cost of demolition and reconstruction. Besides replacement being costly, it would also cause traffic problems (with regard to bridges applications) which would have economic consequences. The time for

replacing an entire structure would far exceed that of rehabilitation, should rehabilitation be possible. Where rehabilitation is possible it is often the optimal solution in terms of cost versus the life span of the structure.

Steel plates were used as the first form of strengthening but were rather complicated to install and proved challenging in the long term especially in regards to durability (Taljsten, 2006). According to Taljsten durability challenge of the steel plates was mainly brought about by the corrosive nature of steel. As a result, alternative materials such as Fibre Reinforced Polymers (FRPs) were discovered. From these FRPs a number of strengthening systems were developed some of which are: near surface mounted systems (NSM), laminate systems, plate systems, sheet systems and pre-stressed systems.

The combination of patch repair and flexural strengthening has been seen as the most effective retrofit method (Malumbela et al., 2011; Ray et al., 2011). Unfortunately there aren't many studies that have been conducted on the behaviour of patch repaired and strengthened beams. This gap in literature motivated the experimental investigation that was conducted in this thesis.

1.2 Statement of the problem

The rehabilitation and retrofitting of reinforced concrete structures has become a major priority in many countries and as such has spurred much research.

Limited work on the behaviour of patch repaired and strengthened beams in flexure have been reported in literature. Past literature has focused on cracked RC beam members which have corroded and subsequently strengthened in flexure without patch repair (Hollaway, 1999; Hollaway and Leeming, 1999; Bonacci et al., 2001; Khalifa and Nanni 2002; Ashour et al., 2002; Bren et al., 2004). There is however a paucity in research of corroded beams that have been patch repaired and strengthened; as commonly done in the field. This study seeks to investigate the behaviour beams that have been subjected to extensive uniform corrosion which have been patch repaired and strengthened in flexure. To that end the aim of the study is to provide information that could help improve CFRP strengthening design. There have been no

studies conducted on the effect of varying damage extent on patch repaired beams and strengthened beams.

1.3 Research objectives

The following objectives have been set for the study:

- Investigate how the presence of voids, in the epoxy bond between the CFRP plate and concrete substrate, affects the debonding failure mode of the patch repaired and strengthened beams
- Investigate the cracking behaviour (crack width and crack spacing) of patch repaired and strengthened beams compared to control beam behaviour
- Evaluate the effect of the damage extent on the cracking behaviour (crack width and crack spacing) of patch repaired and strengthened beams.
- Investigate the mode of failure of the patch repaired and strengthened beams
- Investigate the yield load, peak load, rigidity behaviour of patch repaired and strengthened beam compared to the control beams
- Evaluate the effect of the damage extent on yield load, peak load, rigidity and ductility of the patch repaired and strengthened beams

1.4 Structure and content of thesis

The breakdown of chapters of this research is outlined as follows:

Chapter 1 – Introduction

This chapter provides the background to the study of patch repaired and strengthened beams. It also provides the objectives of the investigation and the layout of the entire dissertation.

Chapter 2 – Literature review

The literature review begins with a *Corrosion background* which has been identified as the main cause of deteriorated structures. It is the reason why the research topic was chosen and is

provided to give insight to the problems caused by corrosion and why it has captivated the interest of many researchers.

The *Patch repair* section deals with the process involved in the patch repair procedure. It also covers the patch repair mortars that have been used and explains how repair mortar is selected in contemporary engineering for retrofitting reasons.

A background to *FRP materials* is presented as it is one of the rehabilitation techniques used in the experimental study. A *review of FRP strengthened beams* highlights the present knowledge of strengthened beams in flexure only. A discussion is made on beam retrofitted with externally bonded CFRP (EB-CFRP). The failure modes of strengthened beams are presented of which *debonding failure* is mentioned as the most common failure mode in the past experiments.

Covered next is the behaviour of *non-corroded strengthened beams* followed by the behaviour of *corroded beams* and *corroded retrofitted beams*.

In the end a brief background is provided on *Thermography* and subsequently a brief discussion on thermography applications.

Chapter 3 – Methodology

This chapter provides an outline of the procedures followed in the experimental investigation. The design procedure is covered, laboratory preparations and testing procedure.

Chapter 4 – Results and discussion

This chapter contains the damage progression, load – deflection and neutral axis results obtained from the experimental tests

Chapter 5 – Conclusion and recommendations

Concluding remarks and recommendations for improvement of future studies related to this work are discussed.

Chapter 2

2. Literature review

2.1 Introduction

Reinforced concrete structures have been found to have a finite life. The structures with significant problems are those that are exposed to marine environments, de-icing salts on highways, aggressive industrial environments and to a lesser extent those which have exposed to the natural weather conditions (Hollaway and Leeming, 1999). From an economic perspective it is often more beneficial to repair wherever possible instead of demolishing and rebuilding structures.

The use of externally bonded steel/FRP has been proven to an effective retrofitting method, which economic and convenient to the users (Hollaway and Leeming 1999; Bank 2006; Taljsten 2006). Initially externally bonded steel plates were used but the disadvantages inherent in steel stimulated the search into other possible materials which lead to the use of fibre reinforced polymers (FRP). FRP material became popular as it was more versatile strengthening than the material than steel, which is covered later in the chapter.

The construction industry has been known to favour the patch repair of structures as a maintenance strategy but there is a growing interest in FRP materials as a method of upgrading structural systems. The literature review presents some insight into the process of patch repair and how it affects beam behaviour. It further provides a minor history of FRP strengthening in flexure where it goes on to describe how strengthening has altered beam behaviour. It was also observed that there is a paucity of literature of the combined use of patch repair and FRP strengthening in flexure,which is provided where possible. A study conducted by Bonnacci et al. (2001) shows that many studies involving FRP strengthening undergo brittle failure by debonding of FRP; this result inspired this study to investigate possible methods that could identify the cause of debonding which came in form of thermographic imaging and whether the prescence of voids may have an influence with that.

2.2 General aspects of corrosion

Reinforced concrete is a relatively new construction material, applied extensively in the 20th century, which was developed due to the improved performance of the combined materials (Bentur et al., 1997). Nounu and Chaudhary (1999) claimed that the dynamic growth of concrete usage came during the 1960s. The popularity of reinforced concrete comes from the complimetary action of concrete and reinforcement steel. The cementitious material of concrete provides a protective coating over the steel thus making the composite quite durable if designed appropriately. Although the concrete provides some cathodic protection over the steel, corrosion of steel cannot be avoided in severe environmental conditions.

There are two types of corrosion that have been found in bridge structures namely: pitting corrosion (Figure 2.1) and general corrosion. Pitting corrosion is described as a localized form of corrosion of a metal surface which takes the form of cavities. In beams pitting corrosion normally exists due to the presence of cracks caused by over loading of the structure. Although pitting corrosion is localized it can be found at various points along the length of the beams due to cracks or inadequate cover (which relates to durability). General corrosion is described as corrosion that proceeds at a constant rate for the entire length for which the metal surface is exposed to the environment. General corrosion has been found in various bridge members one of which are beam members that have been damaged by impact loads or spalled due to corrosion and other forms of chemical attack. Since corrosion is such a big player in the deterioration of bridge elements a brief technical background was provided as it relates to this study.

2.2.1 Mechanisms of steel corrosion

Corrosion of steel involves an electrochemical reaction whereby iron atoms (Fe) are removed from the steel and dissolved into the surrounding solution. In concrete there exist pores which act as the medium through which the electrochemical reaction can be carried through. The removal of iron from the steel, also known as oxidation, leads to the reduction of the cross section of the steel which consequently translates to higher stresses. Stress is defined as a ratio of force over area in structures hence the increase in stress with the reduction in area of steel. The increase in stresses in the diminished steel can result in a safety risk or even lead to failure.

The dissolved iron (ferrous Fe^{2+}) into the aqueous solution can react with hydroxide (OH^-) ions and dissolved oxygen molecules within the concrete pore solution to form corrosion products

also known as rust. The rust induces expansive forces (due to the limited space) within the concrete which could lead to the spalling of concrete.

The corrosion process involves two separate but coupled reactions on different steel sites one being the anode and the other the cathode. The anode involves oxidation where the onset of electron flow starts also known as electrical current, (Equation 2.1). The anode is where the loss of iron occurs, (Figure 2.1).

$$2Fe - 4 \text{ electrons} = 2Fe^{2+} \quad (2.1)$$

The cathode is the term given to the position where reduction of the ferrous ions occurs, which also involves ionic flow, (Equation 2.2). The ferrous ions are reduced near this region to form the corrosion products noted before as rust, Figure 2.2.

$$O^{2-} + 4 \text{ electrons} = 4(OH^{-}) \quad (2.2)$$

The presence of the pore solution is a critical component of the reaction without which the corrosion process would cease to exist. The presence of oxygen is also important for the reaction to occur as for every oxygen molecule 2 ferrous atoms are required. Thus it can be noted that for corrosion to occur there are some prerequisite situations that are required.

2.2.2 Likelihood of corrosion occurring

In order for corrosion to occur there are certain compositional variations that must exist within the pore solution medium (Fulton, 2008):

- local differences in applied stresses

- Variations in local environmental conditions e.g. different oxygen levels at steel level

- Variations in chemical activity (electro-potential differences) e.g. different metals in contact, steel made up of different crystals thereby making it heterogeneous etc.

Bentur et al. (1997) mentions that even with the presence of the prerequisite corrosion conditions it may not necessarily imply that the corrosion process will be of significance. The corrosion rate is affected by parameters such as: the presence of oxygen around the steel, the cover thickness, the presence of the passivation layer (protective film of gamma ferric oxide), high concrete electrical resistance etc.

Figure 2.1: Pitting corrosion of reinforced concrete

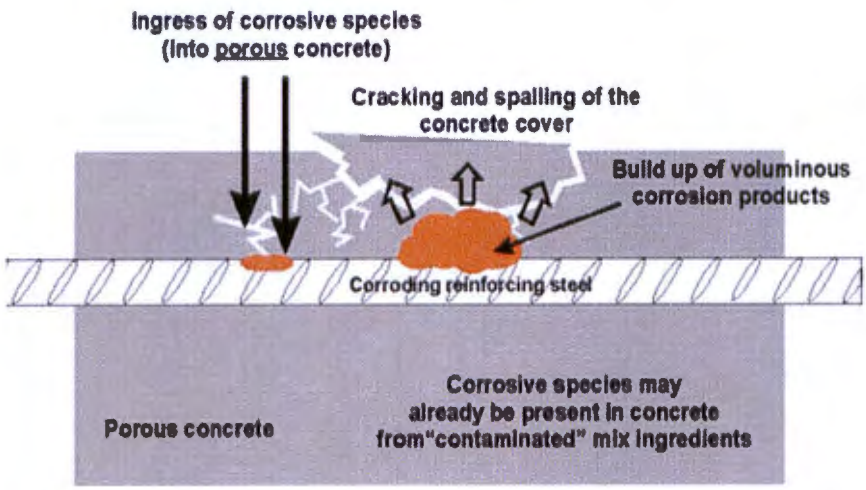

Figure 2.2: Spalling of reinforced concrete

Other than compositional variations, the presence of cracks in concrete has been found to exacerbate corrosion damage and reduce the service life of concrete due to the rapid initiation of steel corrosion. Where cracks are present there is easy access to the steel reinforcement. Furthermore there is a correlation that has been found with increasing crack width and increased corrosion rates for concrete exposed to chloride-induced corrosion (Fulton, 2008). It is evident that corrosion requires a unique set of conditions for initiation to occur not forgetting that there are other elements that exacerbate corrosion initiation such as Carbon dioxide (CO_2) and Sulphates (SO_4^{2-}) by reducing the pH of the concrete and nullifying the passivation layer.

2.2.3 Bond between corroding reinforcement and concrete

Besides the reduction in area of reinforcement corrosion affects the bond strength between concrete and steel. Before the 1990s there were conflicting results on the relationship between bond strength and degree of corrosion. The conflicting results were ascribed to the test that was being used (Almusallam and Al-gahtani, 1996). Almusallam and Al-gahtani (1996) mention some existing bond strength tests which are:

- Concentric pull-out test is used to compare the bond strength of different concretes. The concrete surrounding the rebar is in compression which eliminates the presence of tension cracks and also improves the bond strength of the specimens.

- Tension pull-out test is an improved form of the concentric test but eliminates the compression on the reinforcement.

- Bond beam test has larger specimens than the other tests. It is more representative of the bond stress conditions in flexure, therefore considered more reliable

- There are other modified beam tests such as: the Bureau of standards beam test, the University of West Virginia test, RILEM/CEB/FIP beam test and the Cantilever bond test.

Due to its simplicity the concentric pull-out test is the most widely used by researchers (Almusallam and Al-gahtani, 1996). Although different bond strength tests exist it has become well known that bond strength tends to increase initially up to a certain point of degree of corrosion, after which the bond strength decreases (Almusallam and Al-gahtani 1996; Cabrera 1996; Mangat and Elgarf 1999; Lee et al. 2002; Almusallam 2001). Work by Almusallam and Al-gahtani (1996) was based on the cantilever bond test. The study focused on the effect of corrosion on bond strength between concrete and steel. The bond behaviour investigation consisted of parameters such as: ultimate bond strength, free-end slip and the modes of failure in pre-cracking, cracking and post-cracking stages. The results obtained from the investigation indicated that for the pre-cracked stage the ultimate bond strength increased by 13% leading up to 4% degree of corrosion, (Figure 2.3a), after which the ultimate bond strength decreased. The slip at ultimate load decreased in the pre-cracking stage, this decrease was attributed to the reactionary confinement caused by the increase in corrosion products. This reduction in slip is the cause for the increase in ultimate bond strength in the initial stages of corrosion. In Figure 2.3b

the uncorroded beams (0%) displays a linear relationship leading to 40kN. Thereafter there is an increase in slip for small gains in bond resistance (Almusallam and Al-gahtani, 1996). For the corroded beams the linear relationship is higher than the uncorroded beams up to 4% degree corrosion (Almusallam and Al-gahtani 1996). In the cracking stage the linear relationship of load and slip is similar to un-corroded beams. The linear relationship between load and slip of the post cracking stage exhibited a sudden drop. The sudden drop of the load slip curve at ultimate load was attributed to sudden splitting of concrete cover over the bar due to corrosion cracks.

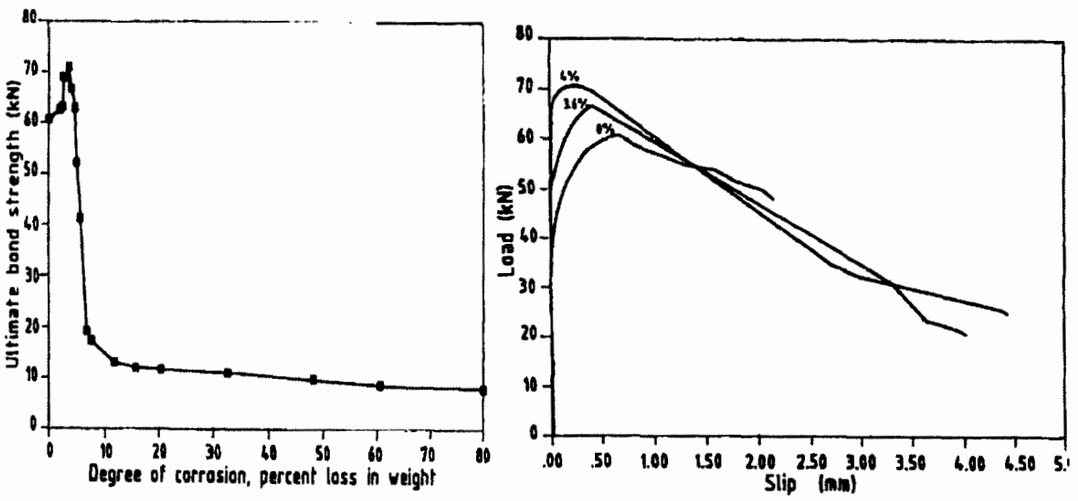

Figure 2.3: a) Ultimate bond strength vs degree of corrosion, b) Relationship between load and slip pre-cracking stage (Almusallam and Al-gahtani 1996)

From the bond strength-corrosion degree curve, (Figure 2.3a), it was noted that the bond strength remains relatively unchanged for corrosion ranging between 7.8%-80% (Almusallam and Al-gahtani, 1996). The bond strength at high levels of corrosion is highly diminished; this is due to the degradation of the lugs of reinforcement thus acting like a plain bar. The other reason for the low bond strength at high corrosion degrees was attributed to the crack width.

Another study by Mangat and Elgarf (1999) realizing the shortcomings of the other bond strength test methods adopted the RILEM/CEB/FIP beam specimen for testing with some modifications The study investigated low levels of corrosion degree in the range of 0-5%. The investigation revealed bond strength increased leading up to 0.4% degree of corrosion. The bond strength increased to as much as 25% at the corrosion degree of 0.4%.

The difference in bond strength increase at low levels of corrosion has been said to be dependent on corrosion rate. Mangat and Elgarf (1999) mention that at corrosion rates greater than $0.25mA/cm^2$ there is no increase in bond strength which contradicts the behaviour observed in both studies by Almusallam and Al-gahtani (1996), (Figure 2.3a), and Mangat and Elgarf (1999). Although the results varied for the different experiments, the bond strength behaviour however was found to be the same, showing that bond strength increases up to a certain level thereafter it decreases for corrosion rates less than $0.25mA/cm^2$.

2.3 Patch repair rehabilitation scheme

The effect of corrosion as the main deterioration mechanism of structures necessitated the development of durability repair. Ballim et al. (2009) efine durability of concrete structures as thethe ability of concrete to resist the design environment over the design life, without loss of serviceability and any need for rehabilition. Patch repair system were necessitated by the premature deterioration of reinforced concrete members. The patch repair system gained popularity due to the re-passivation effect it provided. It also allows for the corroded reinforcement to be cleaned and coated so that the corrosion reaction can no longer continue.

2.3.1 Patch repair process

Before the implementation of the patch repair process an initial assessment on the amount of damage on the deteriorated structure is required. The assessment includes the following (Bentur et al., 1997):

i. Causes of corrosion on steel, whether it is carbonation induced corrosion or chloride induced corrosion the latter being more critical

ii. The extent of the damage and influence on the serviceability of the structure

iii. The projected progress of damage

The initial assessment assists in the determination of the strategy that should be adopted in order to provide the optimal repair solution. Patch repair is a commonly favoured repair method as it restores the alkalinity of concrete (re- passivation) which was disturbed by carbonation or chlorides to an approximate pH of 12.5 – 13.5. The patch repair method for corrosion damaged concrete consists of several steps (Bentur et al., 1997):

i. Removal of damaged concrete (At least 20mm beyond the steel) and exposure of the exposed steel.

ii. Treatment of steel by removing the corrosion products on the steel and adding steel or fibre rods if the cross section loss is extreme. A protective coating can also be applied if chosen.

iii. Treatment of the surface concrete is also required before any patching can be done.

iv. Application of the repair mortar. External membranes can be applied over the patch repair or all of the concrete to enhance protection.

2.3.2 Types of repair mortars

In the past simple repair materials were used to replace damaged concrete such as: Portland cement based concrete, mortars, grouts or gunites(Morgan et al., 1996). Since the 1960s new enhanced concrete repair materials have been introduced and used in the civil engineering industry. Morgan et al. (1996) states that the repair mortars that have been used post the 1960s era have ranged from polymer modifiers for Portland cement to pure polymers (epoxy), polyesters and polyurethane systems. The repair mortars that exist can be classified into 3 categories namely: resin mortars, polymer modified cementitous materials and plain cementitous materials (Morgan et al. 1996; Bentur et al. 1997; Río et al. 2005).

Table 1: Typical mechanical properties of repair materials (Morgan et al., 1996)

Property	Resin mortar	Polymer modified cementitious mortar	Plain cementitious mortar
Compressive strength (MPa)	50 -100	30 - 60	20 - 50
Tensile strength (MPa)	10 -15	5 - 10	2 - 5
Modulus of elasticity in compression (GPa)	10 - 20	15 - 25	20 - 30
Coefficient of thermal expansion (per °C)	25-30 x^{-6}	10 - 20 x 10^{-6}	10 x 10^{-6}
Water absorption (% by mass)	1 - 2	0,1 - 0,5	5 - 15
Maximum service temperature (°C)	40 - 80	100 - 300	300

Portland cement based repair materials fared well for a period of time but became challenged by aggressive environments. Initially engineers believed that the solution was to provide repair

materials that were compatible with the concrete substrate but this could not hold for all cases for example concrete with bad durability conditions could not be replaced with an equivalent bad repair material which is porous and would not prevent further deterioration. This led to engineers seeking solutions for better repair materials. In this contemporary age, engineers are faced with the issues of durable repair where consideration of environment for which the repair is to be applied is considered important.

The properties of the polymer modified cementitious materials can be explained as being between the resin mortar and the plain cementitious mortar. Polymer modifiers are blended with cementitious materials to provide an efficient bond with the concrete substrate. The polymer mortars have their advantages and disadvantages. The advantages of such a mortar are as follows: it can provide an impermeable protective cover for the reinforcement; it can also provide a strong bond with the concrete substrate thus eliminating the need for a primer (Bentur et al., 1997). On the contrary performance problems have been experienced with polymer mortars due to the inhomogeneity with the concrete substrate properties e.g. the thermal coefficient of expansion of the polymer mortar is more than 5 times larger whereas the modulus of elasticity is much lower (Bentur et al., 1997). The polymer binders normally used are epoxy or polyester polymers which have different properties thereby influencing the mortar properties differently. Although polymeric mortar can provide physical protection to the steel it cannot provide chemical re-passivation as the cementitious mortar does (Bentur et al., 1997).

Cementitious mortar traditionally was found to be inadequate on its own therefore have generally been combined with polymeric additives to improve ductility, flexural strength, bonding and workability of the mortar. It is evident that different mortars affect the behaviour of the repaired beams differently when related to compatibility of: Young's modulus, compressive strength, tensile strength and shear properties of the bonding agent at the concrete-mortar interface, dimensional stability, chemical stability and transport properties of the repair material just to list a few.

2.4 Structural performance indicators for corrosion damaged structures

Corrosion damage of reinforced concrete beams requires performance indicators to quantify damage. Structural performance assessment involves defining appropriate performance indicators and comparing the current state of a structure or structural component with these

indicators. Examples of performance indicators include ultimate load capacity, deflections, stiffness and ductility which can be inferred from load-deflection measurements and strain measurements.

2.4.1 Stiffness

El Maaddawy et al. (2005) defined deflection capacity as the deflection of a member at failure.Loss of cross-sectional area of steel affects the stiffness of RC members. To determine the effect of the loss in area due to corrosion on stiffness, load-deflection relationships of tested RC members can be used (Nounu and Chaudhary, 1999; Rio et al., 2005; Sahamitmongkol et al., 2008).

2.4.2 Ultimate capacity and Ductility

Although ultimate capacity cannot be used as a performance indicator in practice, it is a good measure of performance in research work. Corrosion damage reduces the area of reinforcing steel and reduces the ultimate capacity of the structure. Malumbela et al. (2011) found that a 1% mass loss of steel reduced the flexural load capacity by 0.8%. Malumbela reviewed past literature and cites the work by Mangat and Elgarf (1999b) where the average mass loss of steel was used and it was found that 1% loss in average mass of steel was related to 1.4% loss in load bearing capacity. It was shown later that the maximum mass loss is more critical than the average mass loss.

Ductility is defined as the non-linear behaviour of the beams. Ductility is important as a design parameter as it allows members to provide enough warning signs before failure. Ductility description of load-deflection curves is normally presented as: displacement ductility, curvature ductility and energy ductility.

It is clear that corrosion compromises the performance of the affected RC structures; therefore, there is a growing need for repairing and restoration of the service life of old and new structures before reaching the ultimate limit state. But, before any repair or strengthening activity can take place, it is good practice to establish the level of deterioration by using appropriate measures of redeeming the structure.

This research will adopt all the performance indicators mentioned above to investigate the changes that are brought about by the application of patch repair alone and both patch repair and FRP strengthening on damaged beams.

2.5 General aspects of FRP strengthening of beams

2.5.1 Introduction

The deterioration of existing structures has aroused the interest of many engineers to find alternative techniques of rehabilitation. In this context the studies regarding the use of fibre reinforced polymer (FRP) have appeared. In the past 20, years the use of fibre composites in construction have been the fastest growing new areas in the field of civil engineering (Taljsten, 2006).

Taljsten (2006) also mentions that the use of fibre composites in the field of civil engineering is relatively new but they have long been used in other fields i.e. aviation and space, automobile, and boat industries. The science of the composites has been well established from the aerospace industry during the 1950's. Although the science of the composites is well established it cannot be automatically transferred to the civil engineering field. The civil engineering field has different demands in terms of: life - span, durability and higher static long term loads. This is in contrast to the aviation and space industry which are subjected to dynamic loading over a short term period. For the reasons mentioned previously it is apparent that the design methods used in the space industry cannot be directly transferred to the civil engineering industry.

Structures tend to lose their structural integrity before serving their expected life (Neagoe, 2011). Retrofitting of concrete structures is essential to restore or strengthen the structures integrity where it has been compromised due to various factors. Some of which are: the deterioration of structures which alters their properties, increased demand on structures thereby exceeding the designed loads, mistakes in design or in construction and exposure to unpredicted loads e.g. truck collision or seismic activity.

The remedy of the lost structural integrity has been achieved through retrofitting methods of repair or strengthening or both methods together. Many innovative strengthening techniques and materials have been developed and used over the years. Steel was the first strengthening material that gained popularity due to its high tensile strength and ductile properties. The chal-

lenges that came with the use of steel, i.e. corrosive nature, complication of application etc., were frustrating and this led to the search of alternative materials which is where fibre reinforced polymers (FRP) came into play. In the last 20 years several techniques have been developed for flexural strengthening, using fibre composites on existing structures, with the aim of improving their ultimate failure and serviceability.

2.5.2 Concepts and historical background

2.5.2.1 Concepts

In terms of structural strengthening there have been recent developments related to the materials, methods and techniques used. The state of the art material that is used in contemporary civil engineering strengthening is that of fibre reinforced polymer (FRP) composites.

FRP materials used to strengthen and repair load bearing members form part of a collective of *retrofitting techniques*. Retrofitting applications can be classified broadly into two types. The first being *strengthening*, where the original structure's strength is increased when compared to the original un-strengthened beam. The increase in strength capacity is necessitated by increased demands, deteriorated structures or seismic activities. The other type of FRP retrofitting can be classified as *repair*. In this case the beams are repaired to restore the characteristic properties (load-carrying capacity and ductility) of beam back to what is was before deterioration occurred. The use of the repair technique, as mentioned in the earlier section, also allows for cleaning of corrosion products and the re-passivation of reinforcement steel.

Two primary methods are used to attach FRP composites to already cast concrete structures for retrofitting purposes: adhesively bonding FRP or hand layup. There exists a new method known as *near surface mounting* which is also used for strengthening.

2.5.2.2 Historical background of fibre composites

The idea of FRP application grew out of the experience gained from retrofitting of reinforced concrete structures using steel plates. Due to the vast problems with steel material researchers found an alternative material to use; that material being FRP.

The use of FRP composites for retrofitting concrete structures is presumed to have initiated in the 1980s in Switzerland and in Japan. Taljsten (2006) states that the initial development of the

FRP strengthening technique with prefabricated laminates took place in Switzerland by Meier (1987), in the late 1980s, at the Swiss Federal Laboratories for Material Testing and Research (EMPA). The first to study the use of thin CFRP laminate used for flexural strengthening of reinforced concrete beams was Meier, in 1987. Much research has been done since then, with researchers such as Triantafillou and Plevris (1992) who completed comprehensive analytical and experimental studies of the short term flexural behaviour of the FRP strengthened reinforced concrete. Other researchers the likes of Saadatmanesh and Ehsani (1991) have also provided important information which improved the field of study. Other researchers such as Of and Bonacci (2001) and Ceci et al. (2011) completed review studies on the former studied the trends of non-corroded strengthened beams while the latter performed a statistical analyses of existing literature.

Since the late 1980s the body of literature has grown drastically covering many different aspects (fatigue, preloaded structures, deteriorated structures etc.) for different applications such as shear strengthening, torsional strengthening etc. Certain professional organisations have developed general purpose design guides for the use of externally bonded FRP strengthening products of concrete structures. Some design codes that have emerged include TR 55; 2004, FIB, 2001; ACI, 2002 and CSA; 2002 just to mention a few. Although the design codes have been proposed their acceptance by practicing engineers has not taken off due to certain limitations such as debonding failure and cost of material.

An FRP strengthening strip known as Carbodur was developed at EMPA and commercialized by Sika (Neagoe, 2011). The Carbodur strips have been used in numerous applications in buildings and bridge structures. The Carbodur material is the same FRP material which was used for the purpose of this experiment.

2.5.3 Material properties of FRP

2.5.3.1 Description of composite material

FRP composites are comprised of fibres and a matrix. Fibre composites can either consist of glass fibres, boron fibres, aramid fibres or carbon fibres in a polymeric matrix. The fibres and matrix material are preformed to form plates under factory conditions normally by the pultrusion process (Neagoe, 2011).

The adhesive substance used to bond the laminate to the concrete surface is normally a hardy two-component epoxy adhesive, when combined with the fibre becomes a fibre composite on the surface of the structure.

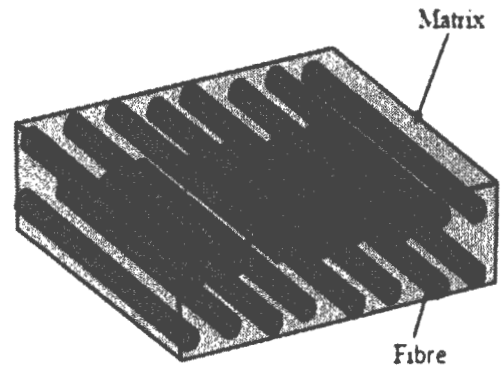

Figure 2.4: Schematic representation of a unidirectional FRP plate (Obaidat et al., 2011)

The composites can be manufactured as unidirectional, (Figure 2.4), and bi- or multidirectional. The unidirectional composites have all their fibres facing one direction whereas the latter terms refer to composites with fibres in more than one direction. Typical values for properties of the fibres are given in Table 2. The fibres are all liner elastic up to failure. The main purpose for the matrix in the composite is to act as a medium for stress transfer between the fibres and to provide environmental protection.

Table 2: Typical properties of fibres (Neagoe, 2011)

Material	Elastic modulus (GPa)	Tensile strength (MPa)	Ultimate tensile strain (%)
Carbon			
High strength	215 - 235	3500 - 4800	1.4 - 2.0
Ultra-high strength	215 - 235	3500 - 6000	1.5 - 2.3
High modulus	350 - 700	2100 - 2400	0.5 - 0.9
Ultra-high modulus	500 - 700	2100 - 2400	0.2 - 0.4
Glass			
E	70	1900 - 3000	3.0 - 4.5
S	85 - 90	3500 - 4800	4.5 - 5.5
Aramid			
Low modulus	70 - 80	3500 - 4100	4.3 - 5.0
High modulus	115 - 130	3500 - 4000	2.5 - 5.0

The mechanical properties of composites depend largely on the volume of fibres used, the type of fibres used, fibre orientation and the matrix bond properties. The fibres provide the strength and stiffness of the composite hence the anisotropic properties found in composites. Fibres act as the load carrying constituents of composites and occupy the largest volume in a composite laminate. For the purposes of strengthening unidirectional composites are normally used. FRP materials have high tensile strength normally higher than that of steel. When FRP are externally bonded to beams it acts as additional reinforcement, when using section analysis.

In the case of EB CFRP beams the concrete structure and the bonded fibre composite form a relationship that has a greater strength than the original structure. Besides strengthening for bending FRP's can also be used to strengthen structures in shear, torsion and axial loads (Taljsten, 2006).

2.5.3.2 Carbon fibres and polymeradhesives

As mentioned earlier there are three types of fibres which are carbon, glass and aramid. Carbon fibres offer the highest modulus of all reinforcing fibres, (Table 2). Carbon fibres also offer the highest tensile strength compared to the either fibres and a higher modulus. In addition, carbon fibres have high fatigue strength, low coefficient of linear thermal expansion. Although carbon

fibres have superior properties than those of its counterparts the cost of the fibres is higher than the aramid and glass fibres

Polymeric materials often referred to as matrices after cure, can be classified into two categories based on their reaction to heating and cooling: thermosets and thermoplastics (Hota et al., 2006). Thermoplastics are said to be available as a solid in granular form, whereas thermosets are found in liquid form. Choosing the type of polymer to form a matrix is important because of its role on the in-plane shear properties and interlaminar shear properties.

Adhesives are used to attach the composites to the concrete substrates. The most common types of adhesives are acrylics, epoxies and urethanes. Epoxies provide high bond strength with high temperature resistance (Neagoe, 2011). Epoxy materials have better performance, in terms of mechanical properties, as compared to other organic resins.

2.5.3.3 Advantages and disadvantages

The body of literature dictates that unique properties of FRPs, over its counterparts steel and aluminium alloys, have made it the extreme favourite. Some of the advantages that rendered FRPs the dominant strengthening material are: high corrosion resistance, low strength to weight ratio, improved fire resistance, reduced freeze/thaw damage, less mechanical fixing, high tensile strength, short time of construction, easy handling and transportation and possibly less costly in the long term. Although the cost of FRP material is initially higher than that of steel the FRP properties make the life cycle costs lower than that of steel due to the high resistance to corrosion which would require less maintenance should the need arise. Other properties include lower transportation costs, lower cost of workmanship, construction period and ease of application.

The potential disadvantages of FRP composites are: cost of acquisition and mechanical damage Considering the pros and cons of FRPs over metals, it is evident that FRPs are a more superior strengthening material, which is why many engineers have chosen to use it for retrofitting.

2.6 General background on FRP strengthened beams

The investigation of the behaviour of retrofitted reinforced concrete has become an important research field. There have been numerous experimental investigations which have been conducted but before that are discussed; a preliminary theoretical background is required.

The load deflection graphs of an un-strengthened (Unplated) reinforced concrete beam and a strengthened (plated) beam are shown in Figure 2.5 (Hollaway et al., 1999). The beams were tested under four point loading. The load-deflection curves of the beams exhibit 3 regions of behaviour where the stiffness changes as shown below in Figure 2.5 (Hollaway et al., 1999)

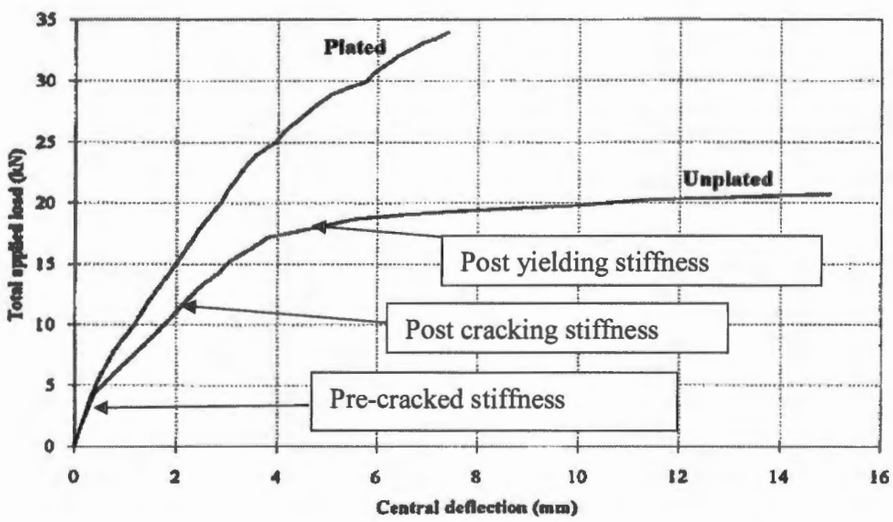

Figure 2.5: Comparison of typical load/deflection response of control beam and a strengthened beam (Hollaway, 1999)

The different stages of stiffness are described as a function of un-cracked section, cracked and yielding of the longitudinal reinforcement. The first stage the unplated beam exhibits the region of highest stiffness at low loads. This first stage represents the beam before cracking occurs,referred to as the pre-cracked stiffness region on Figure 2.5. As the load increases on the beam the stresses at the extreme top and bottom of the beam increase until the tensile strength of the beam is reached, which is when cracks start appearing and the second stage begins. The presence of cracks reduces the stiffness of the beam which is indicated by the change in the gradient, this region is termed the post cracking stiffness. The post cracking stiffness is assumed to be approximately linear. In the third stage the tensile concrete is assumed to have a

negligible effect, the tensile reinforcement also yields at this stage. When tensile reinforcement yields it is referred to as the post yielding stiffness. It is important to note that the un-plated behaviour described here is that assuming the member is designed to be under reinforced. The yielding of the tensile reinforcement leads to a further reduction of the composite material stiffness. When the steel yields the beams undergo large deflections due to the ductility of the member until failure of the compression face occurs. Before compression failure of concrete occurs it will be preceded by numerous flexural cracks near the region of highest moments and shear cracks near the supports of the beams.

The behaviour of strengthened beams is also represented in Figure 2.5, with the condition that the composite plate nearly covers or completely covers the full width of the soffit of the beam (Hollaway, 1999). The plated/strengthened beams load versus deflection response was described as being similar to the un-plated beam when the loads are low. This was explained by the absence of cracks in the early stages, which meant that the FRP has little or no effect on the second moment of area hence flexural rigidity at this stage (Hollaway, 1999).

Hollaway (1999) further mentions that the post cracking stiffness of the strengthened beam becomes significantly higher than the un-strengthened beams. The higher stiffness is explained by the addition of stiffness due to the composite plate coming into play when the concrete section below the neutral axis (tensile concrete) has become ineffective. The cracked tensile concrete releases tensile stresses which are then transferred to the composite plate and the steel reinforcement bars (rebar's). The increase in stiffness is subject to the composite plate properties and dimensions. The addition of the composite plate to the soffit of the beam also restricts the widening of cracks (also referred to as tension stiffening) which results in improved performance of the concrete in the tensile zone. It is important to note that tensile stresses that are transferred to the FRP induce interfacial stresses between the FRP and concrete which can lead to debonding near the cracks if high enough, this will be covered in the next topic of failure modes. Going back to the post cracked stage of the strengthened beam where tensile stresses are shared between the tensile reinforcement and the FRP it is important to note that the yield stress increases. A study conducted by Maadaway and Soudki (2005) increases in yield load of 31% and 32% for two CFRP strengthening schemes. The increase in yield stress due to the fact that for a given applied load the yield stress is higher for the strengthened beam as the FRP takes some of the tensile stress therefore prolonging the yielding of the steel reinforcement.

Once yielding initiates the post yielding stiffness decreases, like the un-plated beam behaviour, but remains higher due to the continued support of tension component by the FRP. The ultimate load of the strengthened beam is generally higher than that of the control beam. The higher ultimate load of the strengthened beams was evident in a study by Maadaway and Soudki (2005), with increases of up to 52% and 58% for two CFRP strengthening schemes. The behaviour of strengthened beam after yielding is controlled by the linear elastic properties of the FRP. The linear elastic properties of the strengthened beam the affects the properties of beam i.e. stiffness, yield stress and failure load which increase the stiffness and load carrying capacity but decreases the ductility.

Hollaway et al. (1999) mentions that for a strengthened beam with a shear span to beam depth ratio of 3, the crack propagation would normally be found in the constant moment region which are referred to as flexural cracks. The crack path develops in an upwards direction with the crack width remaining narrow due to the tension stiffening effect. Flexural shear cracks start developing later near the support with further increases in load. The flexural shear cracks follow the direction towards the point loads. The progression of the flexural shear cracks with increased loads would tend to shift closer to the plate ends until debonding failure occurred by means of cover separation. This failure mechanism of cover separation was that found occurring in the experimental study by Hollaway et al. (1999). The cover separation was described as extending to the length of the shear span and occasionally past the mid-span of the beam. The cracking contrast of the strengthened beams and un-plated beams are therefore quite different. This was evident in the strengthened beams which had a lower mean crack height due to the increased neutral axis depth.

2.7 Failure modes of flexurally strengthened beams

Beams that have been strengthened flexurally with FRP can fail in different modes. When beams are strengthened the preferred mode of failure is that which is ductile and will utilize the properties of the FRP fully. There are a number of failure modes that have been identified in literature. Different books call the failure modes by slightly different names but they are in essence the same failure modes. Esfahani et al. (2007) proposed that different failure modes can be divided into 5 categories namely, (Figure 2.6):

i. Flexural failure by crushing of compressive concrete before or after yielding of tensile steel

ii. Rupture of FRP laminate after yielding of tensile steel.

iii. Cover delamination at the end of FRP

iv. Debonding of FRP from substrate:

a) Plate end interfacial debonding

b) Interfacial debonding induced by flexural cracks

c) Interfacial debonding induced by flexural shear cracks

v. Shear Failure

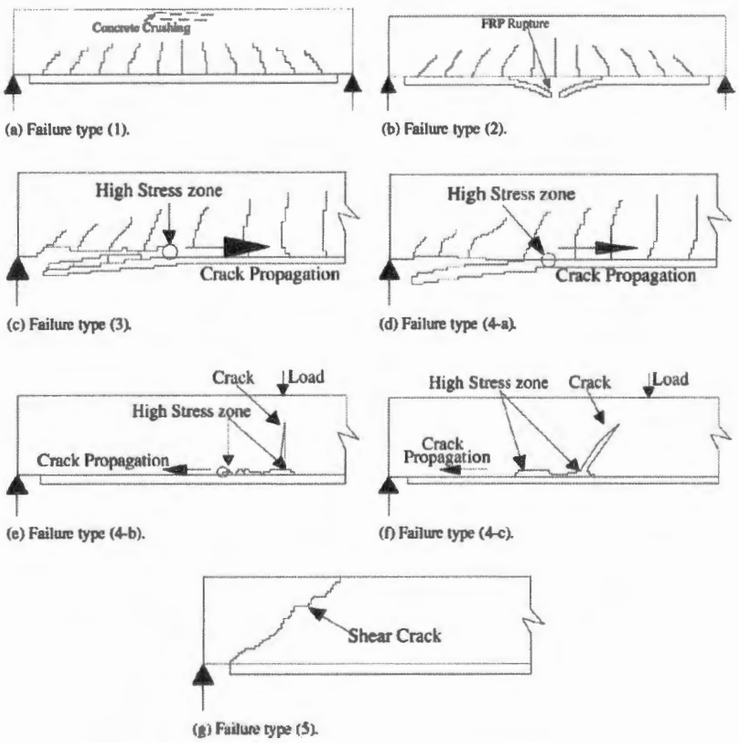

Figure 2.6: Common types of failure modes observed from literature (Esfahani et al., 2007)

Hollaway and Teng (2008) provide good description of how the failure modes can be differentiated into two main categories that is: flexural failure of the critical section, which is by concrete crushing or FRP rupture after steel yielding. The failure mode of concrete crushing occurs when the composite action (bond) of the FRP and the concrete is maintained up to

failure of the beam (Hollaway and Teng, 2008). While FRP rupture (debonding) involves loss of bonding between FRP and concrete. Debonding failure has been found to be the most common failure mode in past experiments. An investigation conducted by Bonacci et al.(2001) found that in 23 different studies debonding was prevalent in a database compiled of literature up to 1999. This database included 127 beam specimens that were strengthened without any prior damage.

"Reported failure modes for the specimens included in the database were 63% by debonding of FRP, 16% by tensile rupture of FRP, 12% by concrete flexural compression, and 9% by beam shear" (Bonacci et al., 2001).

It is evident that debonding failure is problematic and that it underutilizes the FRP material due to its unpredictable occurrence. In the database from Bonacci et al. (2001) the average debonding strain was found to occur at 49% of rupture strain. The flexural FRP design process by Taljsten (2006) also emphasizes that debonding occurs at strains below 60% of the rupture strain. Bonacci and Maalej (2006) also point out that debonding is a function of the relative stiffness of tensile reinforcement and FRP stiffness as both control the cracking patterns of beams and thus the failure mode of flexurally strengthened beams.

The description provided by Oehlers and Seracino (2004), Hollaway and Teng (2008) differentiates debonding failure under into 3categories namely: intermediate crack (IC) debonding, critical diagonal crack (CDC) debonding and plate end debonding. Plate end debonding, relates to failure mode 4-a, initiates from the plate end and propagates towards the beams mid-span. IC debonding was described as that failure mode (debonding) which relates to flexural cracks (4-b) or flexural shear cracks (4-c) in high moment regions. IC debonding tends to propagate at the concrete-adhesive interface towards the end of the plate. CDC debonding occurs near the region of high shear capacity region and is related to a single inclined crack across which rigid body shear displacement occurs. CDC debonding is commonly associated with shear failure, it can be subdivided into 4 categories (linked to failure modes 3 and 5):

i. critical diagonal crack (CDC) debonding

ii. CDC debonding with concrete cover separation

iii. Concrete cover separation

iv. Plate end interfacial debonding

It is important to note that CDC debonding failure can only occur if the bonded FRP plate length extends in to the region where the CDC forms, which is near the support as the shear force is high in this region and the bending moment non existent.

2.7.1 Debonding failure

Numerous experimental studies that have been done on strengthened beams with EB-FRP indicate debonding failure as the most common failure mode. As mentioned in the previous section, debonding failure is an important issue as it prevents the full ultimate capacity of the retrofitted beam from being achieved it is extremely hard to predict.

The unpredictability of debonding has led researchers such as Buyukozturk et al. (2004); Smith and Teng (2002); Camata et al. (2007); Pešić and Pilakoutas (2003), just to mention a few, to analytical investigations for explanations of various failure mechanisms. The aforementioned researchers identified interfacial stresses as the cause of debonding, which is why in the past 2 decades there has been much research on interfacial stresses. Buyukozturk et al. 2004 described the possible types debonding failures of reinforced concrete (RC) beams strengthened by EB-FRP as the separation of the following: concrete-rebar interface, cover separation, concrete-adhesive interface, adhesive delamination and adhesive-FRP interface.

Interfacial failure described by Buyukozturk et al. 2004 and Smith and Teng 2002 attributed debonding failure to the high interfacial stresses which have been found at material discontinuities (i.e. plate end, Figure 2.7) and near crack formations, which is in line with the descriptions provided by Hollaway and Teng (2008). Interfacial stresses are composed of two main components which are interfacial shear stress (τ) and interfacial normal stress (σ_y), as shown in Figure 2.7. These high interfacial stresses play and important role in some of the debonding modes. Smith and Teng (2001) describe the difficulty faced by many researchers at establishing clear solutions towards the characterisation of debonding failure.

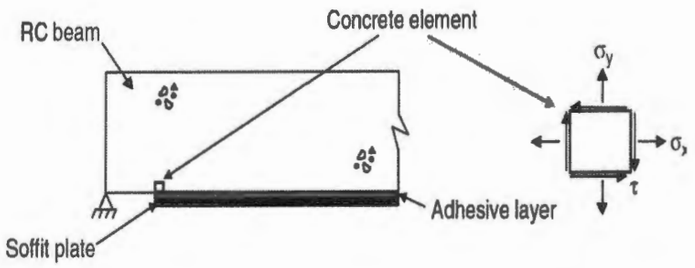

Figure 2.7: Stresses acting on a concrete element at plate end (Hollaway and Teng, 2008)

From the covered literature two approaches have been mentioned: the strength approach and the fracture mechanics approach. Smith and Teng (2001) describes the strength models as solutions that are defined by linear elastic materials only and are based on the assumption that shear and normal stresses remain constant across the thickness of the adhesive layer. The aforementioned assumption enables for simple closed form solutions to be developed. Several methods have been developed using the strength approach with the majority providing simple and accurate results whereas others involve higher-order analysis, the latter providing more accurate and more involved solutions. The difference between the approximate and the higher-order analysis based on the assumption of the adhesive layer, the former assumes constant interfacial stresses and the latter considers stress variations of stresses in the adhesive layer. Smith and Teng (2001) mention that the approximate solutions which assume linear elastic materials can be divided into two groups based on the different assumptions which are: the staged analysis approach and the deformation compatibility approach. Figure 2.8 shows the interfacial stresses behaviour of the different models. The diagram indicates that shear stresses decreases in a gentle parabolic manner from the FRP plate end, likewise with the normal stress behaviour but the decrease is drastic initially from the FRP plate end but tends to zero towards the FRP plate centre.

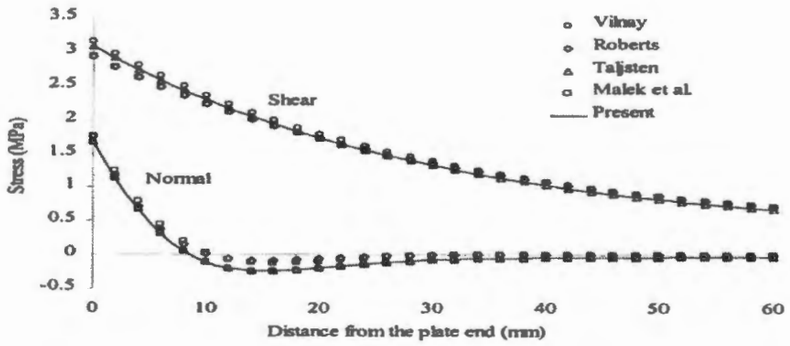

Figure 2.8: Comparison of some of the interfacial stress model that have been developed (Smith and Teng, 2001)

Hollaway and Teng (2008) mentions that for a simply supported beam the magnitude of inter-facial stresses, in the region between the support and plate end, greatly depends on the elastic modulus and thickness of FRP and adhesive layer. In order to understand debonding behaviour Hollaway and Teng (2008) mention that knowledge on bond behaviour is required between the FRP plate and the concrete substrate. Simple pull-off tests and finite element modelling (FEM) have been used by various researchers in the attempt of understanding bond behaviour. Good bond slip models (Figure 2.9) have been proposed by Lu et al. (2005) for modelling purposes in search of bond strength cognizance.

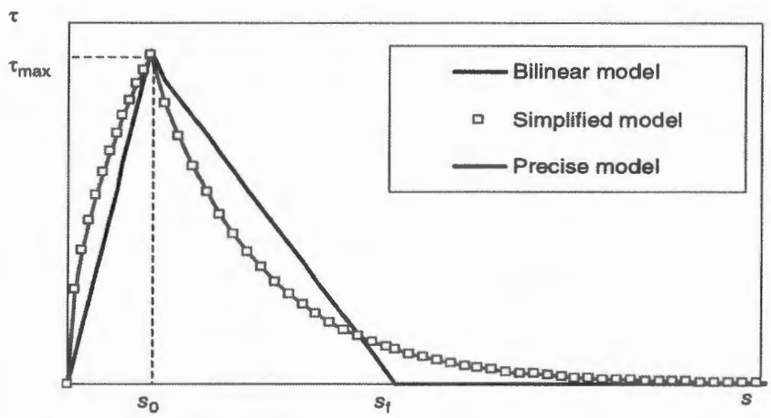

Figure 2.9: Bond slip model by Lu et al. (2005) as described by Hollaway and Teng (2008)

The bond strength, of FRP-concrete interface, is described as the ultimate tensile force that can be resisted by the FRP plate in a simple pull-off test before debonding. Hollaway and Teng (2008) reviewing works of various researchers claim that the bond strength increases as the bond length increases but when a threshold length is reached no further increase in the ultimate load exists. The threshold length is referred to as the effective bond length. Although a long FRP bond will not increase the ultimate tensile strength it improves the ductility of the beam (Hollaway and Teng, 2008). There exist a number of theoretical bond strength models that have been developed to predict bond strength of adhesive-concrete interface. Hollaway and Teng (2008) citing works by Lu et al. (2005) states that the bond strength model developed by Chen and Teng (2001) have been found to provide the most accurate predictions of test results.

The second approach is that of fracture mechanics. This method uses the elastic and fracture material properties for the prediction of debonding mechanism.

The brief analytical solutions that have been covered in this literature are not the focus of the current investigation but were mentioned to show the direction of the field of strengthened beams with EB-FRP and to provide a process of thinking concerning debonding failure. The hope by many researchers is that understanding debonding behaviour will lead to the development of design practice of strengthened members.

Plate end debonding is complicated because it is affected by many parameters such as percentage of reinforcement present (tension and shear reinforcement), FRP plate dimension in relation to the concrete substrate and the region in which the bonded FRP is placed i.e. the entire FRP length could be in the pure bending region or the FRP length could extend all the way to the support where the bending moment is zero, for simply supported beams, and the shear maximum. It is therefore apparent that many factors control the type of failure mechanism that occurs and consequently the behaviour (e.g. load carrying capacity, ductility etc.) of the beams.

2.8 Existing literature on the behaviour of strengthened beams

2.8.1 Introduction

Various literatures pertaining to CFRP strengthened beams were covered to give a big picture of research in the field. In the literature covered a progression of the field of flexural strengthening of beams in bending was observed. In this section a compendium is provided on CFRP flexural strengthening of rectangular beams for four point bending under static loading.

It is now generally recognized that the use of externally bonded CFRP on flexural members is a practical efficient and sound method of strengthening and upgrading the inadequate structures (Spadea et al., 1998). Taljsten (2006) mentions that the first studies of FRP strengthening were recorded in EMPA by Meier in 1989. Taljsten further goes on to describe many other related investigations, by other researchers such as Saadatmanesh and Eshani (1991), Meier and Kaiser (1991), Triantafillou and Plevriset al. (1992) etc., all focusing on FRP strengthening of virgin beams. Although the field of strengthening was not new, steel strengthening was in existence before, it was new in the sense of the material that was being used. Many of the earlier studies in the field of flexurally strengthened members for bending focused on the effect of: orientation of fibres in FRP, FRP thickness, FRP width, the effect of reinforcement ratio, anchorage, predamaged (by pre-cracking beams before strengthening) and sustained loads on the load carrying capacity, stiffness and ductility of the retrofitted beams. Soon the benefits of external strengthening were realized and the direction of research steered towards retrofitting of beams as found in the field, particular corroded beams. Various retrofit methods were tested; patch repair only (by cutting out the old concrete substrate and replacing it or filling the cracked regions with epoxy etc.), FRP strengthening only and a combination of patch repair and FRP

strengthening. Recently over the last decade, the latter retrofit method has gained traction and has been noted as the most effective retrofit method. The combined retrofit method is favoured because patch repair provides re-passivation capability, bond restoration between steel and concrete, it also allows for mitigation measures taken in form of cathodic protection. Meanwhile strengthening has been shown to have the ability to reduce mass loss due to corrosion.

2.8.2 The behaviour of non-corroded reinforced concrete beams retrofitted with CFRP

Research has demonstrated that the addition of CFRP to reinforced concrete beams can increase the load carrying capacity and the stiffness of beams. A study conducted by Toutanji et al. (2006) on a strengthened beam with CFRP laminates which displayed a maximum load increase of 170.2%. Other studies have also been executed by the likes of David and Djelal (1998), Hollaway (1999), Hollaway and Leeming (1999), Bonacci et al. (2001), Khalifa and Nanni (2002), Ashour et al. (2004), Bren et al. (2004), Benjeddou et al. (2007), Fayyadh and Abdul Razak (2012).

The effect of the thickness and width of CFRP on the behaviour of strengthened beams was investigated by Brena et al. (2004), Benjeddou et al. (2007) and Esfahani et al. (2007). The investigation of the effect of reinforcement ratio on the behaviour of strengthened beams was also performed by Esfahani et al. (2007).

2.8.2.1 The effect of reinforcement ratio, CFRP width and thickness on strengthened beams in flexure

In the past there are many parameters which were investigated e.g. tensile reinforcement ratio, CFRP: width, thickness, anchorage, cracking etc. on the behaviour of strengthened beams only. There are many studies which covered similar topics but only a few are mentioned in this literature due to the fact that the other results were confirmatory.

Esfahani et al. (2007) performed an experiment that covered most of the aforementioned parameters but mostly focused on the effects of tensile reinforcement ratio on the strengthened beams. The experiment consisted of 12 beams of which three beams served as the control beams for the different tensile reinforcement of diameters 12mm ($0.3\rho_{bal}$), 16mm ($0.6\rho_{bal}$) and 20mm ($0.8\rho_{bal}$), also given as a ratio of the balanced reinforcement ratio. The beams were

designed to be under reinforced to attain a ductile behaviour of steel i.e. yielding of reinforcement and crushing of compressive concrete.

2.8.2.2 Reinforcement ratio

Increasing the tensile reinforcement ratio was found to have a major influence on the the behaviour of the strengthened beams, there was a change in the cracking patterns of the beams. The control beams exhibited large spaced cracks whereas the strengthened beams showed more cracks at smaller intervals. The change in cracking patterns have been observed in much of the literature but due to the addition of CFRP laminates to the soffit of beams by the likes of Shahawy et al. (1996) and Kachlev et al. (2000). According to Esfahani the reduced cracks are a result of increased tensile force (T_s) due to the increased reinforcement cross sectional area which provides an additional tension stiffening effect. Esfahani further mentions that higher yield strength and ultimate strength of the steel could also lead to reduced cracks due to the increase in tensile force. Increasing the tensile reinforcement changed the failure mode of some of the beams from tensile rupture of the CFRP laminate to cover splitting and debonding of CFRP at the plate ends.

The study conducted by Ross et al. (1999) also investigated the effect of reinforcement ratio on strengthened beams. In order to evaluate the results an enhancement ratio was developed (R_E). The enhancement ratio was defined as the ratio of the peak load of the strengthened beams to the peak load of the control beam. The R_E ratio was plotted as a function of reinforcement a ratio, and as a function of composite area to steel area . The notable conclusion drawn from the study was that lightly reinforced concrete beams ($\rho \leq 0.01$) had significant flexural strength enhancement for thin FRP plates (Ross et al., 1999). Heavily reinforced beams required comparable strength enhancement by increasing FRP area or using a similar composite ratio.

2.8.2.3 CFRP width and thickness

The body of literature has continously shown that flexural strengthening of beams with CFRP improves the performance of beams considerably if designed correctly. The addition of CFRP externally increases the carrying capacity and stiffness of beams as mentioned in the theoretical background and has been proven experimentally by numerous experiments.

Esfahani et al. (2007) found that increasing the width and/or thickness of CFRP did in fact increase the load carrying capacity and the stiffness of the strengthened beams when compared to the control beams. Furthermore increasing the width only or the thickness only of CFRP changed the failure modes of the beams with $0.6\rho_{bal}$ and$0.8\rho_{bal}$ tensile reinforcement.

Brena et al. (2004) confirmed the results of increasing load carrying capacity and stiffness as a result of increasing width or thickness in their own experiment. Although this study was slightly different; where the width and thickness was done for constant area. The effect of varying thickness was also investigated for varying area with constant width. The specimens of constant CFRP area with decreased thickness and wider were found to have increased load carrying capacity but lower FRP stiffness than beams with increased thickness and decreased width of the same area. This decrease in FRP stiffness was attributed to the decrease in second moment of area. The beams with wider CFRP and same area were also found to have larger deformations, which were explained by lower interface shear stresses associated with contact the larger area. The increase in post yield stiffness and yielded stiffness was found to be negligible. Strengthened beams with varying areas were found to have significant increases in post yield stiffness and yielded stiffness. The Yield load and ultimate load of the varying area of composites also increased with resultant decrease of ultimate load deflection.

Another study done by Benjeddou et al. (2007) showed that increasing the CFRP plate width affected the failure mode of the repaired beams. The failure mode changed from plate end debonding to cover separation with an increase (double) in CFRP width. The change in failure mode was attributed to increased bonding which resulted in cover separation. Although the failure modes changed both beams had higher load carrying capacities than the control beam. Doubling the CFRP width resulted in a 10% load capacity increase.

2.8.2.4 CFRP length

An investigation was performed by Obaidat et al. (2011) on the effect of CFRP length on pre-damaged beams. A total of six beams were strengthened in flexure and two control beams cast. The beams had the same dimensions, 150mm x 300mm x 1960mm, and were strengthened in flexure with 50mm wide CFRP laminates of three different lengths, length one was 1560mm which was the equivalent of the beams span (beam RF1), the second length was 1040mm (RF2) and the last length was 520mm (RF3) which is also equal to the distance between the ap-

plied loads, as shown in Figure 2.10. For each strengthening length there were two beams. The beams were preloaded until cracks appeared, at the load of 95kN, and unloaded before they were strengthened.

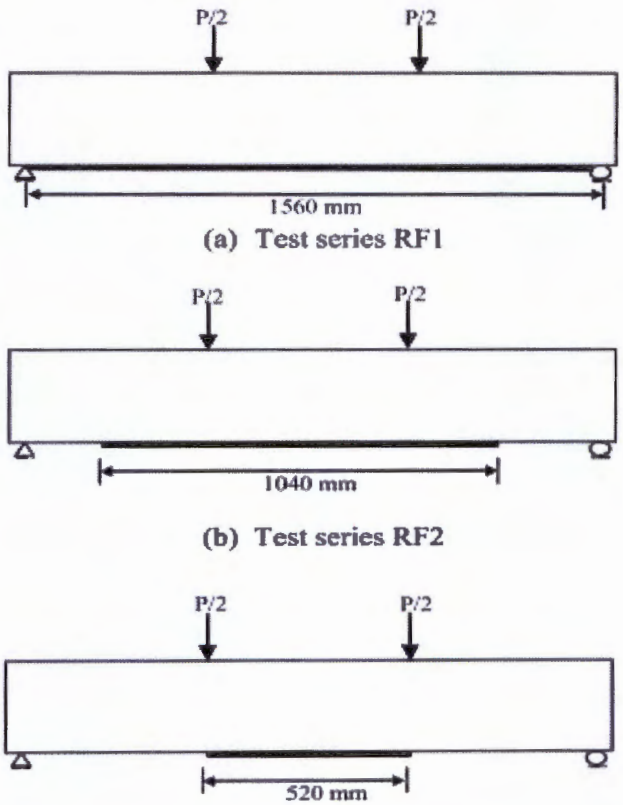

Figure 2.10: Lengths of CFRP laminates beam RF1, RF2 and RF3 (Obaidat et al., 2011)

The control beams failed in a typical ductile manner from under-reinforcement of reinforced concrete member. The maximum load of 118kN was obtained for the mean control beam behaviour which was less than all the strengthened beams.

The crack patterns of the retrofitted beams were significantly different to that of the control beams. The retrofitted beams had many flexural cracks with smaller width, which was indicative of the confinement imposed by the CFRP laminates. Obaidat mentioned that the decrease in stiffness, after cracking, for the retrofitted beams was smaller than the control beams, as shown in Figure 2.11. The smaller decrease in stiffness was attributed to the CFRP which prevents crack widening. The study also revealed that the longer the CFRP was the stiffer the

beam became. The longer CFRP strips provided more anchorage outside the maximum moment region.

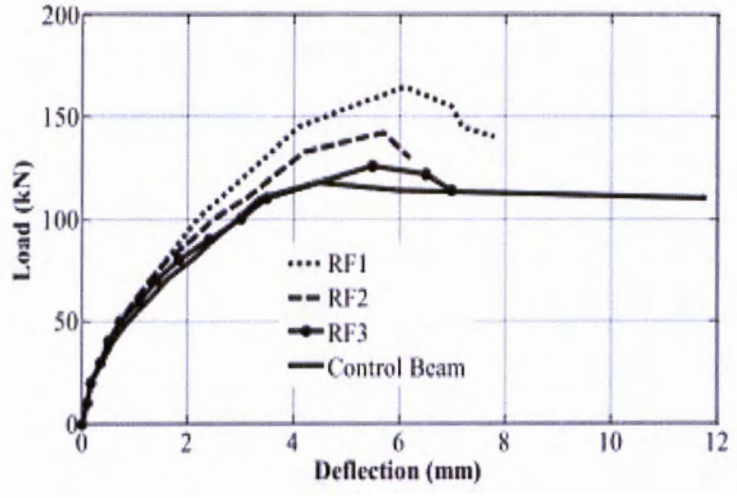

Figure 2.11: Comparison between the mean load-deflection curves for the retrofitted beams and the control beam (Obaidat et al., 2011)

The mean load-deflection curve revealed the increase in maximum load for beams RF1, RF2 and RF3 as 33%, 20% and 7% respectively. All the beams failed in a brittle manner of plate end debonding of the CFRP plate from the concrete. The shorter CFRP strengthened beams debonded earlier due to the high plate end stresses that formed. This study showed the importance of anchorage in improving the strengthened beams ultimate capacity, stiffness and ductility.

2.8.2.5 Anchorage

Although an investigation of the effect of anchorage was done by Esfahani et al. (2007) it was not as comprehensive as the other parameters. The beams 'without anchorage' failed by cover splitting for increased thickness and increased width of the CFRP, which is premature failure and under utilizes the CFRP.

An extensive study on the effect of anchorage was carried out by Spadea et al. (1998). The study involved 4 beams, 3were externally bonded CFRP plates on the beams soffit . 2 beams of the 3 strengthened beams, were rife with anchorage support from the plate ends to between the plate ends in a intermittent manner. For the purpose of structural load response data of the: load

at first cracking, load at yielding of steel and the percentage of ultimate loads up to the no slip composite action was collected. The load at first cracking although not precise was enhanced marginally, compared to the control beam, for the strengthened beams by 13% -20% of the ultimate loads. The loads at yielding for the strengthened beams were also higher than that of the control beam. The load of the composite action for the strengthened beams were as follows: 85% of the ultimate load for the unanchored strengthened beam (A3.1), 87% of the ultimate load for the anchored strengthened beam (A3.2) and 98.7% of the ultimate load for the anchored, but different scheme to the previous beam, and strengthened beam (A3.3).

The control beam failed at the ultimate load of 57.2kN in the conventional ductile manner of yielding of steel followed by crushing of the concrete compressive zone. Beam A3.1 carried an additional 17.6kN load prior to failure whereas beams A3.2 and A3.3 exhibited much more ductile behaviour than beam A3.1 and both carried an additional load of approximately 24kN higher than beam A3.

The study revealed that bonding CFRP externally without anchorage resulted in severe deficiency in the deflection and rotational capacity (Spadea et al., 1998). Beam A3.1, did not have anchorage, underwent brittle debonding failure and had low ductility of approximately 20-30% less that of the control beam. From the study conducted by Spadea et al. (1998) it was shown that CFRP efficiency could be improved by up to 85% of the ultimate capacity.

Hollaway et al. (1999) also endeavoured to investigate the effects of anchorage at the plate ends. In his investigation he found that anchorage had the greatest benefit when the ratio of maximum shear force to bending moment is high, in which case the anchorage resists the peeling stresses at the ends of the external plate.

2.8.2.6 Cracking and strains

The experiment conducted by Brena et al. (2004) measured four strain points along the FRP from one of the points of load application towards the support but 228mm from the support. The strain results indicated that at low loads the highest strains occurred in the region of maximum moments directly below one of the load points, near the mid-span of the beam subjected to four point bending. The strains at the two points which were in between the strain gauges near the support and directly below the load point were the lowest. The highest strains

occurred at points near the supports and point load application. The high strains were attributed to preformed cracks that had been intentionally placed, by means of inserting a steel plate in concrete of dimensions 0.2mm thick and 6mm high.

2.8.2.7 Concrete strength

The study by Benjeddou et al. (2007) also revealed that increasing the concrete strength could improve the load carrying capacity of the control beams and the damaged beams which had been strengthened. The comparison of load carrying capacity having different strengths 21 Mpa and 38 MPa was made. Both beams had control beams and strengthened damaged beams (90%). The strengthened beams with the strength of 21MPa displayed 50% increase in load carrying capacity whereas the beams with 38MPa strength had 56% strength increase when compared to the control beam.

2.8.2.8 Pre-damaged beams

It is also established that pre-damaged beams by pre-cracking before CFRP strengthening had an equivalent or better performance compared to the control beam, some studies that have covered this topic are Arduini and Nanni (1997), Benjeddou et al. (2007), Obaidat et al. (2011) just to mention a few. The investigation implemented by Benjeddou et al. (2007) focused on the effect of damage degree, by means of loading until cracks form prior to strengthening. The investigation looked at damage levels 0%, 80%, 90% and 100%. The CFRP strengthened beams after they had been damaged and loaded to failure had higher load capacities and were more stiff than the control beam but less ductile than the control beams (Benjeddou et al., 2007). As a result the conclusion was that strengthening for any damage levels is still effective tool for the rehabilitation of damaged beams.

Another similar result was obtained by Fayyadh and Abdul Razak (2012). In this study the results were ascertained by monitoring the flexural stiffness recovery, crack patterns, load capacity and failure modes of the retrofitted beams. The flexural stiffness change was calculated based on the secant modulus of the load against deflection curves. The experiment consisted of 4 beams, the first being the control beam (DB), the second was a repaired beam after predamaged under the design load limit (RBD), whilst the third was predamaged to the steel yield limit (RBY) and the fourth was predamaged to the ultimate load limit (RBU). The

results obtained confirmed the effectiveness of CFRP strengthening as a repair technique with increased stiffness of 17%, 10% and 4.6% for RBD, RBY and RBU respectively. The load capacity increased by 83%, 56% and 48% for the pre- repair damage levels 35% (RBD), 66% (RBY) and 100% (RBU) respectively (Fayyadh and Abdul Razak, 2012).

2.8.3 The behaviour of corroded beams and retrofitted corrosion damaged beams

There are numerous studies that have been devoted to the method of corroded reinforced concrete beams retrofitted with CFRP. However there is a paucity of research on corroded beams that are patch repaired and strengthened in flexure with CFRP.

Corrosion of structures has been noted as the most common environmental chemical attack found on many structures. Corroded beams have been found to behave much like the control beams (non - corroded beams). Corrosion becomes detrimental to beam members when there is loss of the cross sectional area of tensile reinforcement. The reduced tensile reinforcement cross sectional area has an effect on the moment capacity of the beam and can be shown through moment capacity equations from internal (sectional) forces, refer to methodology section.

2.8.3.1 Corroded beam behaviour

Maaddawy and Soudki (2005) conducted a study on CFRP repair to extend service life of corroded reinforced concrete beams using the accelerated corrosion process. Various degrees of corrosion were used up to 31%. The study involved a total of 14 beams. Three beams were not corroded, six of the corroded beams were strengthened with CFRP and the remaining five corroded beams were not strengthened or repaired. Some of the corroded beams were subjected to sustained loads and two different CFRP strengthening schemes were used. The corroded beams were labelled in two groups A and B. The Group A beams consisted of the beams that were not subjected to sustained loading. Group A consisted of 6 beams; there was the control beam (UU), two un-corroded repaired (UR) with CFRP strengthening schemes I and II, one corroded unrepaired with no sustained load (CUN) and two corroded repaired with no sustained load (CRN) with two CFRP schemes I and II. Group B consisted of 8 beams that were all corroded. Goup B was divided in two: the corroded unrepaired under sustained loading (CUS) with vary-

ing degrees of corrosion and the corroded r epaired (scheme I) under sustained loading (CRS) with varying degrees of corrosion.

Corrosion of steel significantly reduced the yield loads and ultimate loads of the corroded and unrepaired (CU) reinforced concrete beams. The corroded beam CUN had a significant reduction in yield load and ultimate load compared to the control beams. The yield load of the corroded (8.9% steel mass loss) beam decreased by 8% relative to the virgin beam (Maaddawy and Soudki, 2005). The ultimate strength of the corroded (8.9% steel mass loss) and unrepaired beams were about 6% lower than that of the virgin beams (Maaddawy and Soudki, 2005). The CUS beams all had a reduction in yield load and ultimate load which was found to be proportional to the degree of corrosion (9.7, 15.4, 22.8 and 30%), where a higher corrosion degree resulted in the reduction of the yield load by 11, 18, 25 and 31%, respectively (Maaddawy and Soudki, 2005). The ultimate loads were reduced by 12, 14, 14.5 and 24% respectively (Maaddawy and Soudki, 2005). It was observed that most of the corroded beams, except the beam with 30% degree of corrosion, had higher ductility than the control beam.

In a study conducted by Sahamitmongkol et al. (2008) a total of 11 beams were tested, two control beams, three corroded beams and 6 patch repaired corroded beams. Accelerated corrosion degree of 2.5% was used for three corrosion lengths: short, medium and full length. The effect of increasing corroded lengths was observed by absent shear cracks thought to be inhibited by the formation of longitudinal cracks as a result of corrosion expansive product (rust). In the investigation it was found that for increasing accelerated corroded lengths, of the corroded beams, there was decrease in the ultimate load carrying capacity by 4.5% to 6% when compared to the control beams, as shown figure 2.12 below:

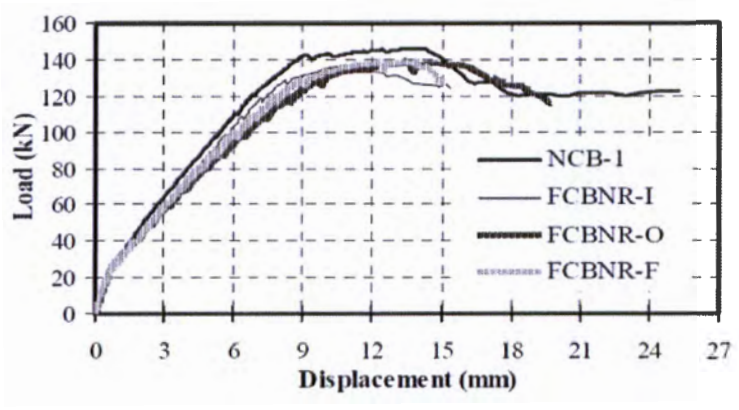

Figure 2.12: Load - deflection relationship of corroded specimens with control specimens (Sahamitmongkol et al.,2008)

The stiffness of all corroded beams was significantly less than that of the control beam; the decrease in stiffness was explained by the bond degradation between the tensile reinforcement and concrete and the formation of longitudinal corrosion cracks. The ductility of the corroded beams was also found to be less than the control beam. The load deflection curve of a corroded beam compared to the control beam.

A similar result for corroded beams was observed in another study by Al-Saidy et al. (2010). The experimental program consisted of 10 reinforced concrete beams. 1 control beam (C_0), three corroded beams (C_5, C_{10} and C_{15}) and 6 corroded beams (M5S1, M5S2, M10S2, M15S2, M15S2-2L and M15S3) were strengthened with three different CFRP schemes 1, scheme 2 and scheme 3. The beams strengthened and corroded were subjected to accelerated corrosion, three degrees of corrosion were investigated 5%, 10% and 15%.

The difference between the corroded beams was the extent of corrosion to which the beam had been subjected to. The general trend of the corroded beams was lower yield load and ultimate load compared to the control beam (Al-Saidy et al., 2010). Al-Saidy et al. (2010) also observed that the corroded beams with 5% and 10% corrosion had similar yield and ultimate load, as shown in Figure 2.13 below.

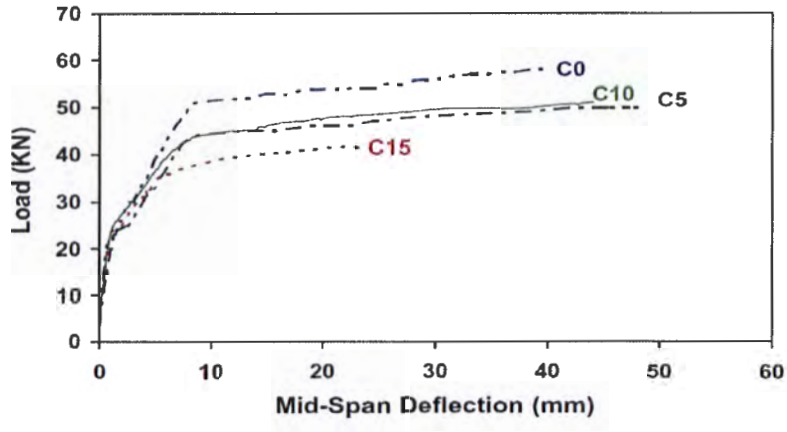

Figure 2.13: Load deflection behaviour of the control beam and corroded beams (Al-Saidy et al., 2010)

The behaviour of beam C_{10} was against the expected lower ultimate load than that of beam C_5, due to the loss of cross sectional area. The corroded beams C_5 and C_{10} appeared to be more ductile than the control beam whereas beam C_{15} was clearly less ductile than the control beam.

The reduced serviceability and ultimate capacity of beams due to corrosion spurred on the various retrofitting methods. The retrofit methods covered in the following section include that of patch repair, CFRP flexural strengthening and the combination of patch repair and CFRP strengthening.

2.8.3.2 The behaviour of patch repaired corroded beams

Patch repair rehabilitation method was developed to enable cleaning (removal of rust and epoxy painting) of the rusty bars and re-passivation. Different repair materials were developed in search of a durable patch repair material but it was established that durability is a function of environment in which the structure is located.

Nounu and Chaudhary (1999) and Rio et al. (2005) supported the claim that the durability of repair materials depends on the compatibility to concrete substrate with regards to good physical and chemical properties which resemble the concrete structure being repaired. Although compatibility of the repair material to the concrete substrate is important the adaptability of the repair material to the environment is equally important. The literature in this section pertains to the influences of patch repair material on the structural performance of the repaired corroded

beams. Structural performance of the patch repaired corroded beams was evaluated compared to control beam and corroded unrepaired beams.

2.8.3.2.1 Load carrying capacity

Various results were found in literature regarding the effect of repair material and its ability to restore the load carrying capacity of the deteriorated (corroded) structures. It is important to note that all experiments mentioned implemented accelerated corrosion to deteriorate the beams so as to replicate the corrosion problems experienced in the field.

Nounu and Chaudhary (1999) conducted test on beams before (short term) and after (long term) extreme weathering (drying and wetting periods as well as 1hour spraying sessions 3 times a day). The tests conducted on the non-weathered repaired beams indicated that there was no difference between the two repair materials (OPC and micro flowing concrete) in the short term as both restored 70% of the load carrying capacity of the control beams. Unfortunately the properties of the two repair materials were not indicated due to commercial reasons. The reasoning for the similar restoring effect, in the short term, of the two repair materials was not given and without the data it is hard to make any assumptions although the most plausible assumption would be due to the similarity of the properties of the two repair materials but this is disproved by the long term results.

In the long term (the weathered beams) the micro-concrete repaired beam restored 90% of the control beams load carrying capacity whereas the OPC repaired beam was only able to restore 50% of the load carrying capacity of the control beam. The 90% restoration of the micro-concrete was attributed to the higher resistance to weathering than the OPC repair material, which means the micro concrete is more durable.

In another study done by Sahamitmongkol et al. (2008), the researchers supported further the idea that different repair materials affect the behaviour of beams differently. Two repair materials were chosen that of polymer modified material (PM) and epoxy based repair material (EB).

This study also went on to look another parameter of the effect of patching area. 3 patching lengths were of interest 300mm, 1000mm and 1700mm (being the entire length of the beam).

The results found for the PM repaired beams for the varying patching lengths suggested that for increasing patching length there was a decrease in the ultimate load in the range of 4.5%-6%.

In contrast the epoxy repaired beams had increased ultimate loads, for increasing repair lengths, which can be considered as strengthening rather than restoring as found in the other previously mentioned repair materials. This was due to the high tensile strength of the repair material, which is further explained in the cracking behaviour. The increase in the ultimate load of the beam that was fully repaired (1700mm) suggest that the repair material could be modelled as an increased tensile force when considering the internal force equilibrium, whereas if concrete was there instead the tensile force contribution could be ignored in analysis.

Another study by Malumbela et al. (2011) revealed that patch repairs slightly increased the load bearing capacity, by approximately 2.5%, of the corroded beams and significantly increased the stiffness of the repaired beam. This was explained as patch repairs adding additional tensile force towards the internal force structure of the corroded beam.

Contradictory information has been found on the effect repair materials on the ultimate capacity, on the one side they have restoring capabilities and on the other they have a strengthening capacity. Nounu and Chaudhary (1999) showed that patch repair was unable to restore the capacity of corroded beams. Another study by Rio et al. (2005) showed that the patch repaired beams (polymer cementitious mortar, epoxy mortar and PCC) all had lower ultimate load capacity than the control beam. On the contrary studies conducted by Sahamitmongkol et al. (2008) and Malumbela et al. (2011) found that patch repairs could have a strengthening effect due to better mechanical properties than that of the substrate concrete. It was observed that the epoxy based material improved the ultimate capacity more than the cementitious repair materials. The epoxy material has high tensile strength but is not as rigid as the other repair materials. In practice the cementitious materials are the preferred patch repair material used, for its repassivation capabilities and restorative nature.

2.8.3.2.2 Durability of repair materials

Nounu and Chaudhary (1999)conducted electrochemical tests on two repair materials OPC and micro flowing concrete. The micro-concrete had higher resistance to chloride ingress as lower corrosion rates were observed from the electrochemical interactions. The higher resistance to chloride ingress of the micro concrete supports the results found from the restoring effect of the

original load carrying capacity for the two repair materials. The higher corrosion resistance of the micro-concrete suggests that its micro-structure is less porous than that of the OPC material. The lower pores in the micro concrete may have circumvented the electrochemical reaction thereby lowering the corrosion rate.

The micro concrete overall proved to be the more durable and had a better restoring capacity than the OPC repair material in the long term. It is important to note that repair materials can be designed for durability by improving the micro structure of the material such that it is not easily permeable. Reduced permeability is important to reduce chloride ingress and the formation of corrosion cracks.

The durability results found from the various literatures once again shows how durability of the different repair mortars differs. This is due to the different microstructures within the repair materials, for instance micro concrete materials with lots of fines will be less porous than material with less fines. The amount of cement used in the concrete is also important as it affects the interfacial transition zone which found around aggregates and forms the weakest part of concrete due to its porosity (Fulton, 2008). The micro structure of resin materials is not well known as it is normally used as an adhesive in structural applications. Another important factor that affects durability is the formation of cracks in concrete structures which allow for the corrosion initiation to occur provided the conditions allow for it.

2.8.3.2.3 Cracking patterns of repaired beams

Nounu and Chaudhary (1999) investigated cracking behaviour of the repaired beams for unweathered (short term) and weathered (long term) repaired beams. In the short term the OPC repaired beams were found to crack mainly in the concrete substrate with nominal cracks in the repair zone in the region of high bending moments. The main cracks were observed on the edges of the repair material. On the other hand the micro concrete cracks were found to be similar to the control beams with cracks present in the repair material and concrete substrate; this could suggest that the micro concrete was compatible with the concrete substrate.

Prior to structural testing of the weathered (long term) beams the crack patterns were observed once again. The OPC repaired beams were cracked within the repair zone. From the OPC repaired beams longitudinal cracks were observed which were explained by corrosion effect and the loss of bonding between the steel and concrete. On the other hand the failure of the weath-

ered (long term) free flowing micro-concrete was through sudden collapse of the compression zone of the beam. In the long term the results indicated that the increased impermeability of the micro concrete may have reduced crack propagation therefore allowing the bond (between the repair material and concrete) and stiffness of the structure to remain intact thereby improving the restoring capability of the micro concrete.

In the study conducted by Sahamitmongkol et al. (2008) the cracking behaviour was found to be different for the different repair materials. The PM repaired beams all exhibited cracks at the vertical concrete-repair material interface. There were flexural cracks in the in the repair material followed by the development of shear cracks at the shear span. The EB repaired beams for the repair lengths 1000mm and 1700mm had no flexural cracks in the repair area due to the high tensile strength of the epoxy material. Instead cracks developed on the concrete substrate from the horizontal concrete-repair material interface. For the full length repair of 1700mm the EB repaired beam had smaller shear cracks instead of 1 large crack also due to the tensile strength of the epoxy repair material, the beam failed by tensile rupture unlike all the other beams which had failed by flexural compression crushing like the control beam.

2.8.3.2.4 Deformation behaviour of the patch repaired beams

Nounu and Chaudhary (1999) also investigated the deflections of the short term repaired beams, for both OPC and micro concrete, were slightly higher than the deflections of the control beams. The absence of the repair material properties made it hard to develop any reasons for the different deformation behaviour of the repaired beams to the control beams. In the long term the load-deflection graph of the OPC repaired beams exhibited approximately linear load-deflection plots which were steep thus translating to high stiffness. The total deflection of the micro concrete repaired beams in the long term was found to be double that of the OPC repaired beams. The difference in the load-deflection behaviour of the two repair materials was attributed to the stiffness of the OPC repaired beam being higher than the micro concrete repaired beam therefore resulting lower deformation.

In another investigation conducted by Río et al. (2005) the deformations of the repaired beams (cement and glass fibre mortar) were found to be equal or lower than those observed in the control beam, up to the observed moment of 23kNm. The changes in the deformations were a result of the different properties of the repair material to the original concrete. The cement and

glass fibre mortar had a higher compressive strength than the concrete substrate, the former with 70 MPa and the latter with 24 MPa. The lower deformations could have been due to the Young's modulus of the repair material being higher than that of the original concrete, the modulus of the repair mortar given as 30 GPa and an assumed 26 GPa for concrete (SANS10100-1).

The study by Sahamitmongkol et al. (2008) found that the deflections of the epoxy based repaired beams were different before and after first crack. Before first cracking, the deflections for the longer repair lengths were higher than that of the short repair length (300mm). This was explained by the smaller repair area of lower stiffness as opposed to the larger areas with lower stiffness which decreased the overall stiffness of the beams. After first cracking the deflections of the epoxy based repair beams with longer repair lengths were found to be lower than the smaller repair length mainly due to the development of flexural and shear cracks that could not form properly in the fully repaired beams.

2.8.3.3 CFRP strengthened corroded beams

In the study by Maaddawy and Soudki (2005) the ultimate load of the corroded and strengthened (CRN-50-I and CRN-50-II) beams, not subjected to sustained load, had an increase of 41% over the control beam. The yield load of the CRN was on average 11% higher than the control beams. The stiffness of the repaired beams CRN was on average 16% higher than that of the control beam. The CFRP strengthened corroded (CRS) beams had mixed yield load results compared to the control beam results. For instance the CRS beam with steel mass losses of 9.5% displayed an increase in yield load of 9.6%. The CRS beam with 15.7% steel mass loss had the same yield whereas the remaining CRS with steel mass losses 23.7 and 31% had reduction in yield load of 11.9% and 17.8% respectively. However the CRS beams all had higher ultimate loads of 32, 32.4, 26.2 and 23.6% than the control beams. The CRS beams had significantly reduced ductility averaging 46% less than the corroded un-strengthened beams.

In another study by Al-Saidy et al. (2010) it was shown that strengthened beams M5S2, M10S2 and M15S2, with different corrosion levels but the same strengthening scheme, were able to recover the original strength of the control beams with the exception of M15S2, refer to Figure 2.14 below.

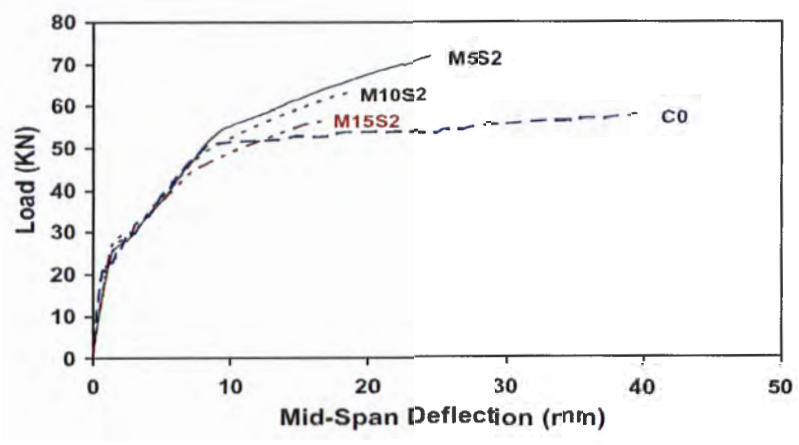

Figure 2.14: Load-deflection curve of the strengthened corroded beams and a control beam (Al-Saidy et al., 2010)

The ultimate strength of M5S2 and M10S2 were 23.9% and 9.3%, respectively, greater than the control beam C0 (Al-Saidy et al., 2010). The ultimate capacity of M15S2 was 2% less than that of the control beam C0. In addition, the ductility of all the strengthened corroded beams was less than the control beam, with M5S2 having the highest ultimate deflection and M15S2 the lowest ultimate deflection (Al-Saidy et al., 2010).

From the aforementioned investigations it can be asserted that strengthening of corroded beams can increase the yield load and ultimate load carrying capacity. The extent of strengthening depends heavily on the degree of corrosion and strengthening scheme, which could be a variation of anchorage scheme, CFRP layers/thickness etc. A higher degree of corrosion would result in lower yield load and lower ultimate load carrying capacity, ceteris paribus. The stiffness of the strengthened damaged beams also would depend on the CFRP material used and the anchoring system used.

2.8.3.4 Patch repaired and strengthened corroded beams

Malumbela et al. (2011) conducted a study at the University of Cape Town, as part of an extensive experiment on the behaviour of corroded, patched and FRP repaired beams under sustained loads. The corroded beams developed longitudinal cracks on the sides of the beams and on the tensile faces of the beams. The cover concrete within the corroded region started separating from the rest of the beam at loads between 60% and 70% of the failure load.

Part of the investigation focused on the behaviour of CFRP flexurally strengthened corroded beams that had been patch repaired. Although the investigation focused on differently repaired beams the conclusion that was drawn was that the combined use of patch repair and CFRP strengthening for retrofitting corroded beams would provide the best performance. The load capacity of the FRP-repaired beams was found to be approximately 50% larger than the capacity of the control beam.

Xie and Hu (2012) conducted studies at the Guangdong University of Technology which observed the behaviour of corroded beams that had been retrofitted by three different methods: direct CFRP strengthening, CFRP strengthening after the conventional patch repair method and lastly was a retrofit method designed by the authors which was a combination of CFRP strengthening after V-notch repairs. The retrofitting schemes yielded increases of the ultimate load carrying capacity of 57.1%, 16.3% and 93.8%, for corrosion levels between 15% and 50%, compared to the control. Beams that were strengthened with all the different retrofit methods displayed decreases in the ultimate load capacities of strengthened beams with damage levels greater than 50%. The effect of increasing CFRP stiffness was also investigated for the different retrofit methods, increasing stiffness results were obtained for increasing CFRP thickness. The ultimate load was also found to increase with increasing CFRP thickness. The relationship between CFRP thickness and load capacity was a non- linear relation, with a decrease of the increase rate of the load capacity with increasing CFRP thickness. The decrease of the increase rate was linked to the debonding failure modes that were obtained from the beams strengthened with more CFRP layers.

2.9 Infrared thermography

2.9.1 Background

Infrared rays were first discovered by Sir William Herschel in 1800 (Maldague, 1993). The discovery of the infrared rays was part of an experiment conducted by Herschel investigating the amount of heat produced by the different colours of light. Herschel used a prism to separate the different colours of light and measured the temperature of each colour using a mercury thermometer (Maldague, 1993). The experiment revealed that the temperature increased from violet, at one end of the spectrum, to red at the other end of the spectrum. The highest tempera-

ture was recorded beyond the red end of the spectrum where there was not any visible light, now known as infrared radiation.

2.9.2 Basic theory

Currently there exists many instruments which are being used for temperature measurement i.e. glass thermometer, thermocouple, thermal resistance, liquid crystals and radiation measurements. Radiation instruments have gained popularity over the decades which have led to Non-destructive evaluation of materials using thermography (TNDE). TNDE can be divided into passive approach and active approach (Maldague, 1993). The former method tests materials which are of a different temperature to ambient. Passive approach is more suited for industrial applications as it has been used in the production of materials, in the medical industry for visuals within the human body, in the military for night vision, for forest fire detection, astronomy etc. On the contrary the active approach requires an external heat stimulus to enable inspection, and is used for Non-destructive testing (NDT). The active approach can be further subdivided according to the external stimulus used to: pulse thermography, step heating, locking thermography and vibro-thermography (Maldague et al., 2002). In the case where the stimulus is done by introducing a heat source, the external heat source introduces a thermal front which propagates through the material by means of diffusion (Maldague, 1993). When using pulse thermography the presence of defects reduces the diffusion rate thus presenting different temperatures. The temperature evolution curve can be plotted by using the equation 3.1 below:

$$\Delta T = \frac{Q}{e\sqrt{\prod \times t}} \tag{2.1}$$

Where ΔT represents the temperature increase of the surface, Q is the quantity of energy absorbed, t referring to the time and $e = \sqrt{K\rho C}$ is the thermal effusivity of the material where K the thermal conductivity, ρ the mass density, C the specific heat. There are various stimulation techniques available for the detection of defects such as; thermal pulse, periodic thermal cycling which has been identified as time consuming therefore not practical and thermal mass.

Maldague (1993) mentioned that there exist different configurations when using the thermal pulse heating method a) point heating: uniform heating can be obtained from point to point but it is a rather slow process b) line heating where good uniformity can be obtained and c) surface heating for which uniform heating is hard to obtain, the method can be applied through static means or mobile. Point heating and line heating are normally used when the defect depth is known and constant.

Two methods of observation are possible: that of reflection, where both the thermal source and detector unit are located on the same side and the second method is that of transmission, which applies to conditions where the thermal source and detector unit are on opposite sides. The latter allows for detection of defects close to the heated surface whereas the former allows for detection of defects at the rear end (Maldague, 1993).

Maldague (1993) further described how detectors can be divided into two categories: thermal and photonic detectors. The thermal detectors use infrared radiation which is absorbed and produces temperature differentials in the detector. There are many thermal detectors which can be used i.e. the glass thermometer, thermal resistances, thermocouples etc. but the most widely uses thermal detector is the pyroelectricvidicon tube. Photonic detectors absorb energy and affects atomic states and free electrons within a semiconductor.

Maldague (2002) provides basic theory which is useful for understanding thermography; radiometry, emissivity and temperature measurement. Radiometry is described as the measurement of radiated electromagnetic energy which can be translated back to temperature values in the camera if calibrated properly. The thermal emissions (temperature) are described by the radiation emitted by the black body. The black body is described as capable of absorbing all radiation, whatever the wavelength. The blackbody refers to the thermal emission of solids where it is defined by Plank's law of thermal equilibrium, as shown by the equation 3.2 below:

$$N_{\lambda,b} = \frac{2hc^2}{\lambda^5\left(1 - e^{\frac{hc}{\lambda KT}}\right)} \tag{2.2}$$

Where h is Plank's constant, c the velocity of light, λ the wavelength of emitted radiation (μm), K is Boltzmann's constant $(1.381 \times 10^{-23} JK^{-1})$ and T is the temperature (K) of the black body, the subscript b denotes the black body.

In the case of real objects complete radiation is not possible due to energy loss that occurs. The fraction of the blackbody spectral radiance that is given is termed emissivity (ε). Where emissivity is low the material will tend to behave like a mirror which makes it hard to measure it temperature by radiative method (Maldague, 2002). Emissivity of objects is divided into two parts namely grey bodies and coloured bodies. The former referring to objects where the emissivity is independent of the wavelength and the latter describes objects with an emissivity dependent on the wavelength

Maldague (2002) suggests that the IR cameras available currently use the focal plane arrays (FPA). They are based on two types of detector arrays: Photonic cooled detectors (PCD) and uncooled micro-bolometers. PCD FPA's work on the principle of measuring excitation generated by incipient photons. The photonic excitation is measured by the change in electrical conductivity or generated voltage (Maldague, 2002). On the other hand the uncooled microbolometers FPA's are low cost and produce IR measurement from IR radiation of the FPA surface which is grooved to make mosaic of thermal masses.

2.9.3 Heat transfer modelling

Heat transfer modelling for thermography can be done using the analytical approach or the finite difference method. The analytical approach becomes complex when considering materials that are not isotropic and have complex shapes. The governing equation used is the Fourier diffusion equation with boundary conditions relevant to the situation being modelled. The finite difference method is used for complex shapes.

2.9.4 Experimental studies on Non-destructive testing of concrete structures with infrared thermography

Galietti et al. (2006) conducted a study where infrared was used to detect defects of well-known dimensions in the bond between concrete and FRP. 16 voids were investigated which were made inserting foils of Teflon in-between the FRP and concrete. The surface of the samples were analysed with a thermographic camera after impulsive heating. A Flirthermocam-

erawas adopted with a 320 x 257 Focal Plane Array. The neural networks (NN) were used for detection of defects. The results obtained from the thermographic analysis were processed in form of matrices of temperature values, and analysed as small region of thermograms concurrently 63x67 pixels (Galietti et al., 2006). The samples were also analysed by means of ultrasonic system in the C-scan and D-scan. The thermographic analysis was found to be the cheapest and quickest technique to be used.

Another study by Maierhofer et al. (2006) used impulse-thermography for the detection of voids. It was mentioned in literature that there are various types of active thermal excitation that can be used i.e. ultrasound exciter, halogen lamps, eddy current transducers etc. This was evident in a study by Lai et al. (2012) who used pulsed thermography to investigated the debond behaviour of CFRP-concrete beams.

There exists a large gap in literature into the use of active thermography for NDT. Researchers are mainly looking at active methods due to ease of application and good results.

2.10 Chapter summary

Corrosion of concrete has been identified as possibly detrimental to the safety of its users. Corrosion leads to reduced capacity which could lead to failure. Corrosion requires moisture and oxygen for the reaction to occur. Corrosion of reinforcement also leads to reduced bond between concrete and steel.

Almusallam and Al-gahtani (1996) illustrated that bond strength increases with the increase in corrosion prior to crack initiation, but a continuous loss of bond strength is observed after 4% degree of corrosion. After 8% degree of corrosion the bond strength remained steady around 13% even for 80% degree of corrosion.

Based on the experimental results of past studies covered in this literature review the following was observed:

i. The use of FRP laminates in strengthening concrete beams increases the load carrying capacity and reduces the ductility of the strengthened beams. Crack formation for the strengthened beams is smaller and more evenly distributed. The use of additional FRP layers can increase the ultimate load capacity and further reduce the ductility of the strengthened beams. Additional FRP layers decrease the chances of rupture failure of

CFRP. The use of anchorages improves the response of strengthened beams as debonding failure can be averted. The brittle nature of the strengthened beams may incite the use of higher factors of safety in design. The bond strength between the CFRP plate and concrete is a very critical factor of the strengthened beam behaviour.

ii. Corrosion of the tensile reinforcement of rectangular concrete beams leads to reduced beam performance with regard to load carrying capacity, yield load and stiffness.

iii. Strengthening corroded beams in flexure is an effective retrofit method as the ultimate capacity of strengthened beams can be increased beyond that of the control beams.

iv. Patch repaired and strengthened corroded beams can increase the ultimate capacity and stiffness of the damaged beams

v. Thermography is capable of detection of defects between CFRP and concrete

Chapter 3

3. Experimental Methodology

3.1 Experimental work

The experimental work was aimed at providing information with regard to the effect of the extent of damage on the structural behaviour of reinforced concrete beams strengthened in flexure. Damage was simulated as a reduction in the area of reinforcing steel, typically caused by uniform corrosion. The reinforcement was not corroded using the conventional accelerated corrosion technique; instead a simulated corrosion method was used by means of grinding the tensile reinforcement to simulate 5% corrosion level, which is explained later.

The experimental work consisted of testing a total of 15 simply supported beams, each tested under four point loading, as shown in Figure 3.1. Three beams were used as the control beams while the other 12 beams were retrofitted by patch repair and strengthening in flexure using FRP. The purpose of the control beam was to determine the un-strengthened beam original behaviour i.e. ductility and load carrying capacity for comparative reasons. All beams had the same cross sectional dimensions, reinforcement layout and CFRP strengthening scheme.

3.2 Design and details of the reinforced concrete beams

The designed failure mechanism of the control beam was by compressive concrete crushing in the critical moment region and yielding of longitudinal reinforcement. The design was based on SANS 10100-1 to achieve under reinforced behaviour so as to attain good ductility of the beams before failure. The beam was simply supported with a span of 1800mm as shown in Figure 3.1. The bending moment diagram as a result of the four point loading is shown in Figure 3.4. In between the loads exists the region of maximum moment and zero shear whereas at the beam ends is the region of zero moment and maximum shear. The shear span to effective depth of 3.2 was the result of the design, which according to SANS 10100-1 is the region of shear- flexural crack formation. The design calculations of the beam can be found in Appendix A.

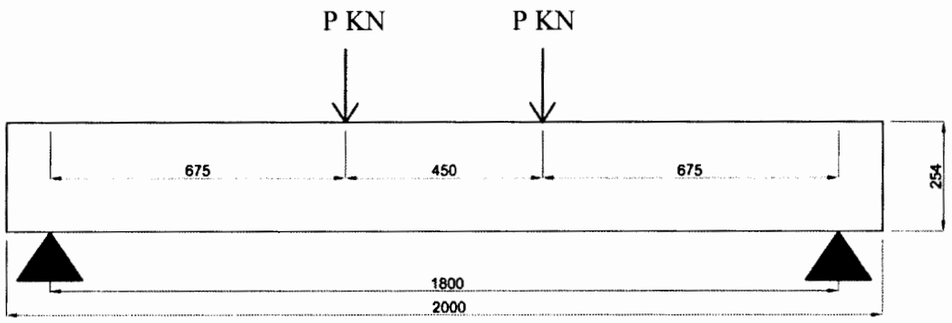

Figure 3.1: Beam under four point loading including cross sectional dimensions

The beams had a rectangular cross section with the dimensions 155mm width, 254mm depth and 2000mm length, as shown in figure 3.2. Two 20mm diameter bars were provided as tensile reinforcement with the area of 628mm^2 and two 8mm diameter bars, with an area of 101mm^2, were provided for the longitudinal compression reinforcement (Figure 3.2). Shear strength of the beams was provided by 8mm stirrups at the minimum spacing of 80mm, this was done to ensure that the beams fail in flexure as opposed to shear failure.

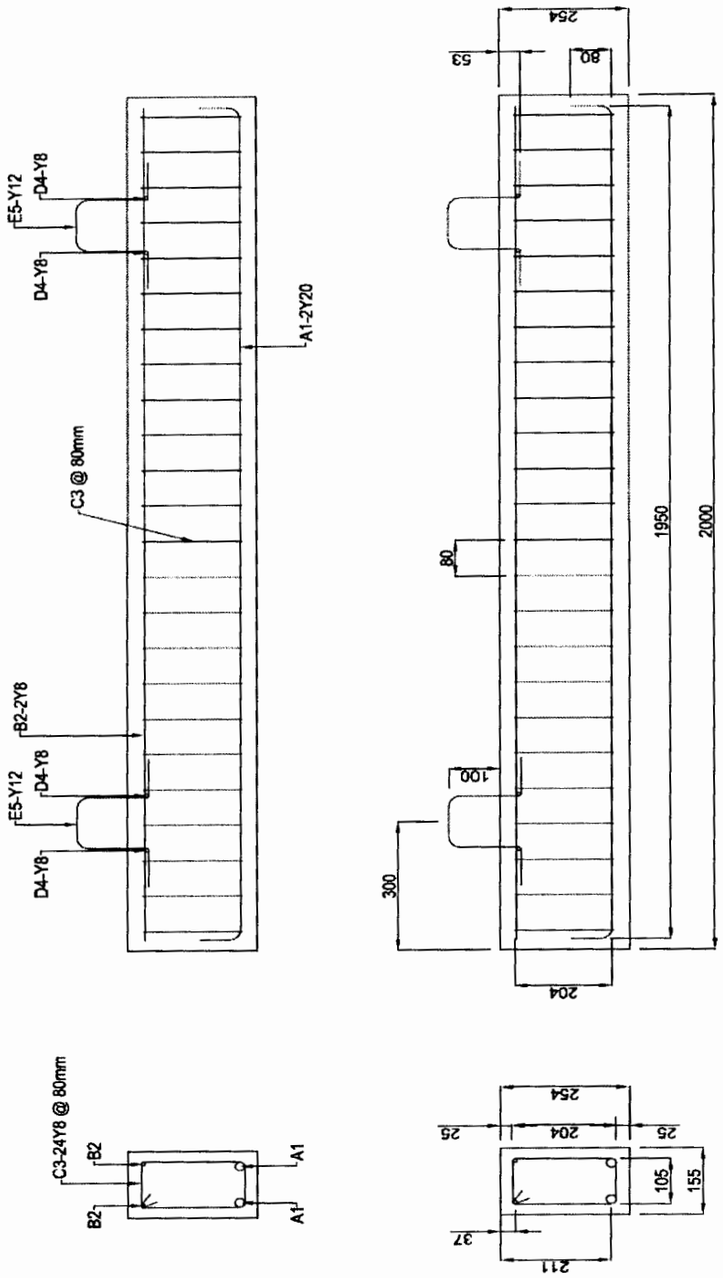

Figure 3.2: Reinforcement layout of all the beams

Lifting hooks were provided so that cranes could be used to hoist the beams to any destination. The effective depth (d) of the beam was 211mm (Figure 3.2).

3.3 Design for CFRP strengthening in flexure

The detailed design of CFRP strengthening is given in Appendix C. The design of CFRP strengthening was done in accordance with recommendations in Taljsten (2006). The design for flexural strengthening with CFRP was done in two stages. The first stage determined the internal moment capacity of the control beam. The second stage involved the calculation of the internal moment capacity when the beam was damaged with the cross section of the tensile reinforcement was reduced by 5%. The difference of the moment capacities was then used to determine the CFRP required for restoring and surpassing the original moment capacity of the section. The CFRP product that was used was a Carbodur plate S512 with an area of 60mm^2. Once the CFRP area had been determined the failure mode of the strengthened beam was determined by a due process of strain checks. The neutral axis of the strengthened beams was determined by force equilibrium using the ultimate limit state (ULS), in accordance with SANS10100-1.

The stress strain behaviour of FRP, concrete and steel that was used in the design process is provided in the Figure 3.3 below:

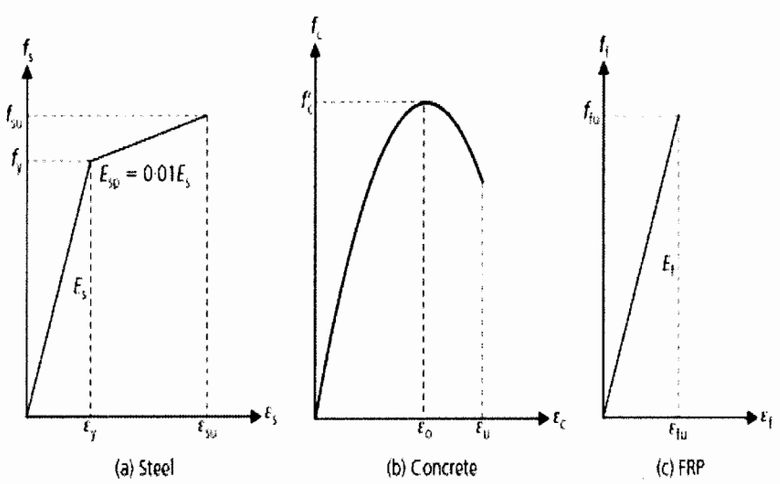

Figure 3.3: Stress strain relations of steel, concrete and FRP materials (Taljsten., 2006)

Taljsten (2006) states that when the beam's actual strain is known design for strengthening can initiate. An assumption is made at this stage of strengthening design where the beam either reaches crushing in the compression zone or the laminate reaches its ultimate limit strain. There

are 4 modes of failure associated with a double-reinforced cross-section, concrete crushing and laminate failure namely:

i. Failure in laminate with yielding in the compression steel reinforcement
ii. Failure in laminate without yielding in the compression steel reinforcement
iii. Crushing of concrete as well as yielding in the compression steel reinforcement
iv. Crushing of concrete without yielding in the compression steel reinforcement

The design process by Taljsten (2006) was developed by using strain compatibility conditions for the different failure modes in the force equilibrium equation to formulate comparative parameter where the longitudinal reinforcement yields (ρ_{f1}) and where the compression reinforcement doesn't yield (ρ_{f2}), refer to Equation C3 and C4 in Appendix C. The aforementioned comparative equations were compared to the equations for a normally-reinforced strengthened cross-section (ρ_{fu}), balanced strengthened cross-section (ρ_{fn}) and an over-reinforced strengthened cross-section (ρ_{fo}), provided in Appendix C as Equation C5, C6 and C7 respectively. Normally-reinforced strengthened ρ_{fu} is the case of the laminate fails first, ρ_{fn} is the balanced failure where concrete crushes simultaneously as the laminate failure and ρ_{fo} is the over reinforced failure where concrete crushing occurs prior to laminate failure. The comparative parameters were then used to describe the 4 modes of failure described earlier:

i. $\rho_{fu} \leq \rho_{f1} \leq \rho_{fo}$

ii. $\rho_{f2} > \rho_{fu}, \rho_{fn}$

iii. $\rho_{f1} > \rho_{fn}, \rho_{fo}$

iv. $\rho_{fn} \leq \rho_{f2} \leq \rho_{fo}$

After the mode of failure was determined the neutral axis, as determined for ULS (Figure 3.4), was used to check the strains of the CFRP and longitudinal reinforcement. The strains were checked for a presumed failure of concrete crushing and yielding of tensile reinforcement, as would be done for un-strengthened beams. This mode of failure dictates that the concrete strain capacity (ε_{cu}) is reached. The strains of longitudinal steel reinforcement were above the yield strain of steel which implied that both the compressive reinforcement and tensile reinforcement

yield at failure. The CFRP debonding strain was used to ensure failure didn't occur prematurely before the yielding of tensile reinforcement. The assumed ductile failure criterion was found to be true by the strain analysis which meant that the assumed failure method was correct.

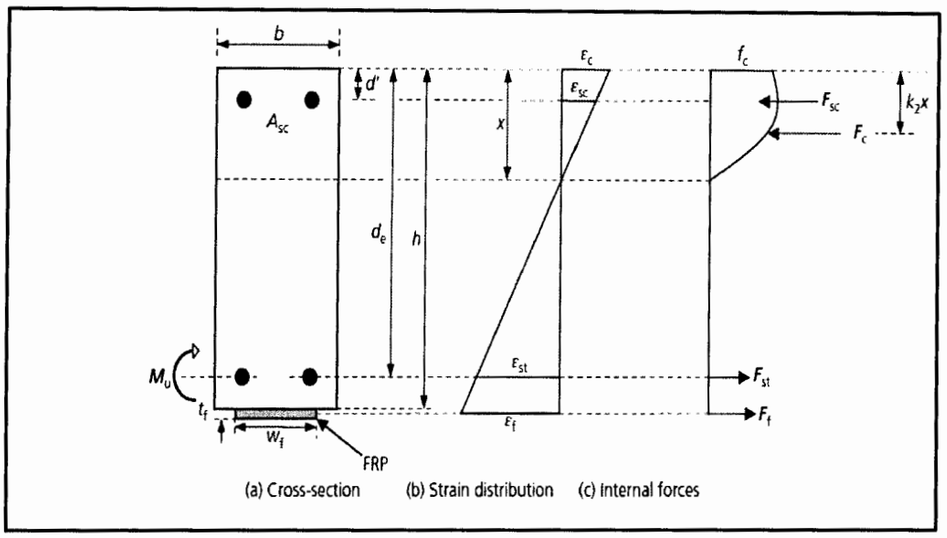

Figure 3.4: Strains and internal forces on CFRP-repaired RC beams at failure (Malumbela et al., 2011)

Failure mode iii (Appendix C) was the only one that satisfied its condition which meant that it was the failure mechanism with which the designed strengthened beam would be governed by. The CFRP length was kept constant for all the strengthened beams at a length of approximately 1700mm. This CFRP plate had longitudinal fibres in an epoxy mortar; the properties of the plate are specified later in the chapter, refer to Table 6.

3.4 Experimental procedure

3.4.1 The extent of damage length

Due to time constraints the process of accelerated corrosion was ruled out and the simulated corrosion, which is described later on in this chapter, chosen as the preferred method. Past research has investigated the effect corrosion on the tensile rebars, compression rebars and stirrups (Shahawy et al., 1999; Allen Ross, 1999; Kachlev et al., 2000). This study on the other hand only focused on corroded longitudinal tensile reinforcement and was not extended to the other rebars. Elgarf (1999) argues that the loss of flexural capacity is likely to be more significant when localized pockets of pitting corrosion occur on the stirrups and longitudinal rein-

forcement bars. Elgarf (1999) also states that large reductions in flexural capacity, strength and rigidity, which render a beam inadequate for serviceability loads are most likely to occur when localized pitting has extended to many sites resulting in extensive and relatively uniform levels of corrosion. It is the uniform level of corrosion mentioned by Elgarf (1999) that is investigated in this study. The extent of corrosion merely refers to the length of this uniform corrosion with the degree of corrosion kept constant for all damaged beams.

Tensile reinforcement was ground (damaged) to achieve 5% reduction of the cross sectional over a uniform length. The strengthened beams were ground to 4 different damage lengths namely: 450mm, 800mm, 1300mm and 1800mm, refer to Figure 3.5. Each beam was loaded in flexure therefore each damage length was duplicated 3 times. The duplication of results was made to ascertain some level of precision and to remove variability within the results thereby allowing for more reliable results to be produced.

A repair height of 105mm was used to resemble field practice objective of clear space enough to clean the reinforcement bars. In addition to using the simulated corrosion method to expedite the experimental program, a polystyrene technique was used, whereby the region where patch repair was required was pre-filled by polystyrene instead of concrete. The retrofit method of choice was a combination of patch repair and externally bonding a CFRP plate to the soffit of a beam.

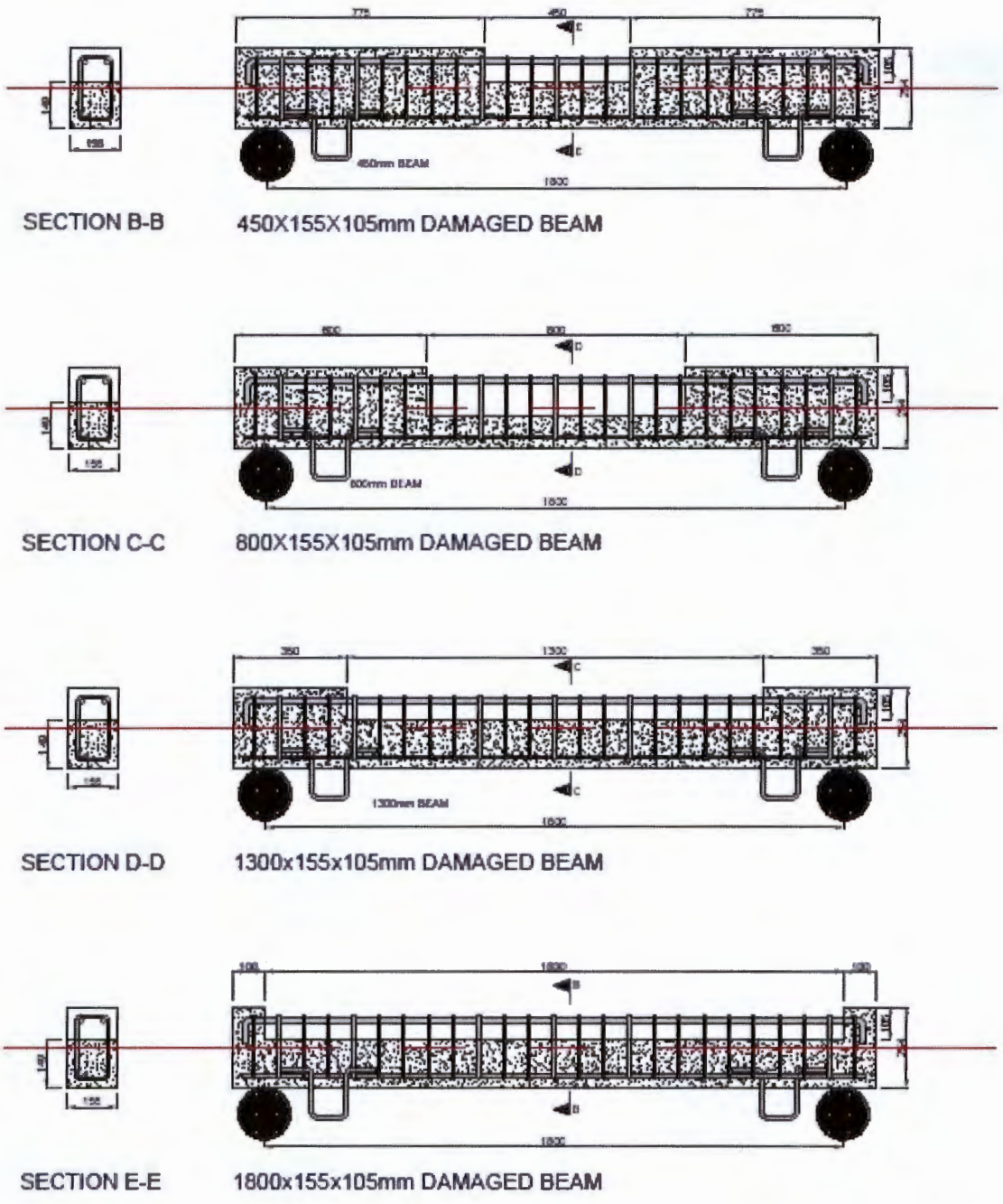

Figure 3.5: Patch repair lengths for the damaged beams

The selection of the patch repair lengths considered the effect of principal stress behaviour of the beams. Equation 3.1 represents the stresses induced in a symmetrical beam when there in bending in two axes and axial loading present (Hibbler, 2008). In the setup of this experiment it is important to note that there were no axial forces nor bending forces about the Y axis. There-

fore when only the middle term, in Equation 3.1 was used since it is the stress induced by bending about the Z axis, as the main cause of the axial direct stress σ_x. The shear force value can be used to calculate the shear stress which is perpendicular to the axial direct stress τ_{xy} using Equation 3.2 below. The reduction of area of steel would result in reduced moment capacity as indicated by Figure 3.6.

The 450mm damage extent was within the maximum bending stress region 3, (Figure 3.6), and zero shear region. In region 3 the stress block at the section was in pure compression and tension. In region 3 the maximum moment resistance of the beams was reduced due to the reduction of tensile steel. The reduction of the tensile steel in the maximum moment region means that there would be a reduction of the principal stresses σ_1, σ_2 and τ_{max}. The damage length of 1800mm was equivalent to the span of the beam therefore extended to region 1 where there is zero moment and maximum shear, as shown in Figure 3.6. At region 1 the direct stress σ_x was zero and therefore the stress block at this section was in pure shear.

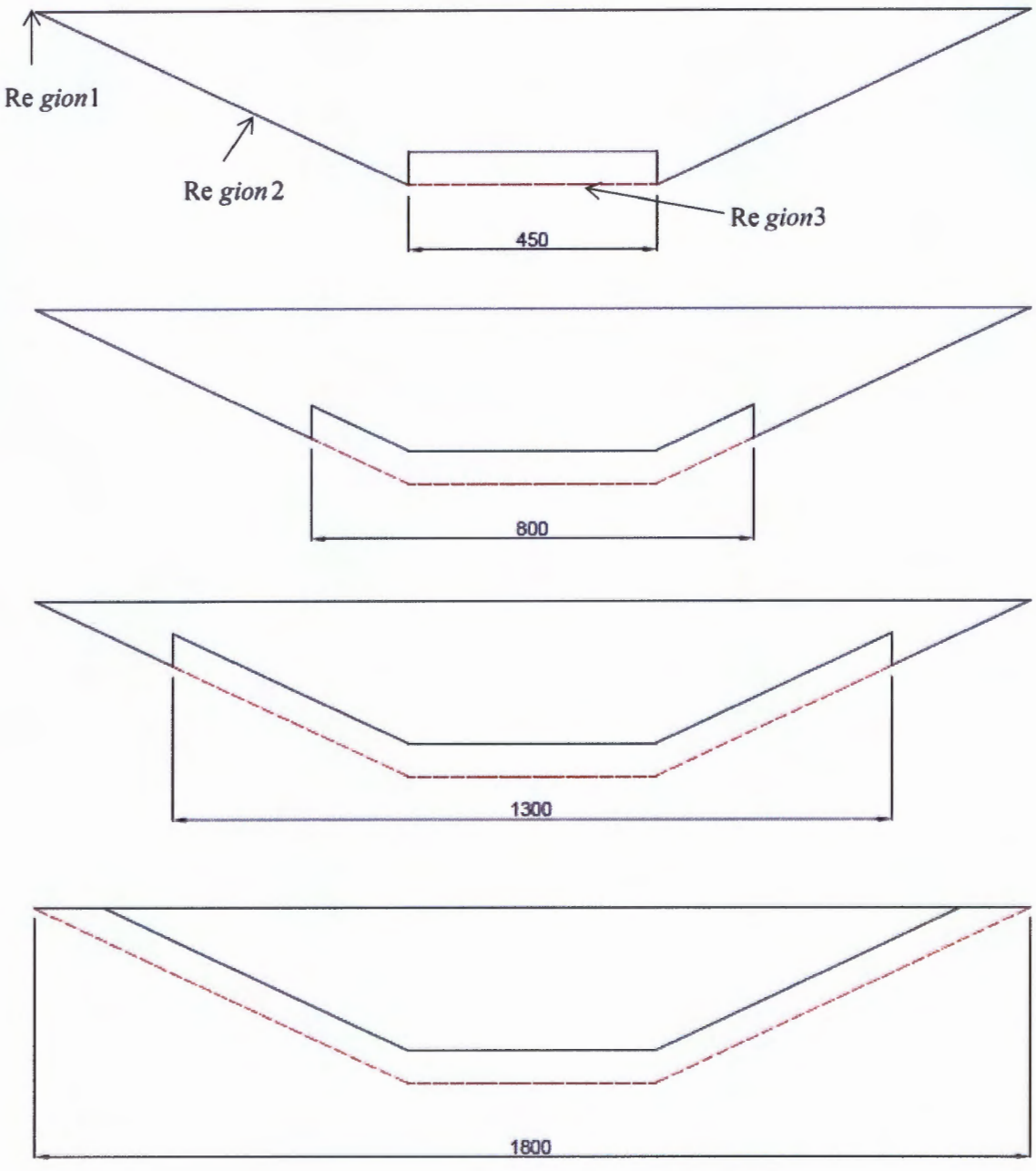

Figure 3.6: Old bending moment diagram (red) and new bending moment diagram (black) after simulated corrosion.

$$\sigma_x = \frac{N}{A} - \frac{M_z y}{I_{zz}} + \frac{M_y z}{I_{yy}} \tag{3.1}$$

Where N = axial load; A = cross sectional are of concrete; M_z = bending moment about the Z axis; M_y = bending moment about the Y axis, I_{zz} = moment of inertia about the z axis, I_{yy} = moment of inertia about the Y axis, y = distance to the centroid; z = distance to the centroid.

$$\tau_{xy} = \frac{VAy}{Ib} \tag{3.2}$$

Where V = shear force, A = cross sectional area of the beam, y = distance to the centroid, I = moment of inertia; b = width of the beam.

When damage by the reduction of steel area was induced in the beams the principal stresses decreasedmaking the beam critical at lower stresses. With increasing damage length there is a consequential decrease in moment resistance of the beam, as shown in Figure 3.4, which in turn cause a reduction in principal stresses.

3.4.2 Simulated corrosion

In past studies many investigations involving corroded beams, which were retrofitted in flexure, have used normal corrosion or accelerated corrosion. Normal corrosion is achieved by exposing the beams to normal corrosion exposure near the sea. Accelerated corrosion is an expedited form of corrosion achieved through electrochemical reaction. With accelerated corrosion the reinforcement is connected to a power supply by means of wires to form the anode while stainless steel forms the cathode. The reaction requires an aqueous solution to complete the circuit which is normally sodium chloride (NaCl) solution of approximately 3-5 % concentration. The length of time for which accelerated corrosion is conducted is determined by Faraday's law, which is governed by the input current and the targeted degree of corrosion.

$$\delta = \frac{Ait}{yZF} \tag{3.3}$$

Where: δ = loss of metal (cm); A = Atomic weight of iron (56 g); i = corrosion current density (Amp/cm^2); t = time elapsed (seconds); Z = valency of the reacting electrode (iron). Commonly taken as 2; F = Faraday's constant (96 500 Amp-seconds); γ = density of material (iron = 7.86 g/cm^3)

For the purpose of this investigation neither normal corrosion nor accelerated corrosion was used but a simulated accelerated corrosion process was performed. The simulated accelerated corrosion involved grinding/milling of steel to achieve the desired degree of corrosion of 5% as shown in figure 3.7 below. Simulated corrosion was chosen due to time constraints.

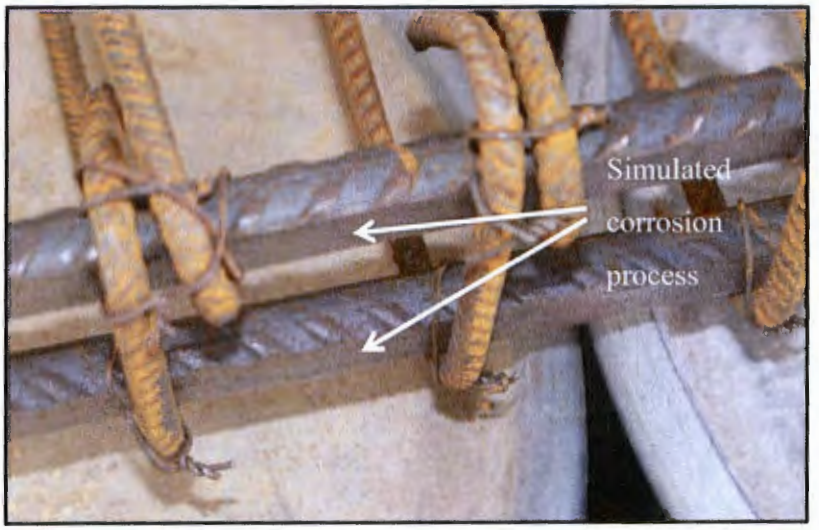

Figure 3.7: Simulated corrosion on the tensile reinforcement

The tensile steel was ground by a milling machine to achieve quality and constant cutting levels. The tensile steel was cut on the soffit perpendicular to cross sectional area. The calculation method for the milling depth required to achieve 5% area loss is provided in Appendix C, refer to Equation C13. The aforementioned calculation result was that a 2mm height would be required to be milled in order to achieve the 5% steel area loss refer to Figure C.1. After the tensile reinforcement had been milled it was tied back to the reinforcement cage.

3.4.3 Workability test

A 2 month program was developed for casting, patch repair and CFRP strengthening of the beams. The beams were cast in four sets, the first three sets had four beams and the last had 3 beams. Each set of beams were cast on the same day. The average strength was obtained for each set from three cubes (Table 5). Only three cubes were cast for each set because the batch quantities were the same on the particular day when a set was cast

Batching was done for the materials to fit into two 50 litre mixers. The batching process was done to determine the amount of materials required to cast a beam. Quality control for the workability of the concrete mixes was performed by means of the slump test, in accordance

with SANS 5862-1:2006. A slump range of 105mm - 130mm was achieved for all the beams. A 5m steel mould was used for casting a maximum of 4 beams at a time. The steel mould was wiped clean of any dirt (rust, dust etc.) before it was oiled. The reinforcement cages were thoroughly cleaned before polystyrene was used to cover the patch repair. Since simulated corrosion was implemented there was no reason to cast concrete in the repair region hence the use of polystyrene. The removal of polystyrene was a relatively easy task when compared to concrete removal that is required when beams undergo accelerated corrosion.

Once polystyrene had been installed on all 12 damaged beams, 25mm cover blocks were attached to the sides of reinforcement cages at strategic points so as to maintain constant cover around the beams. The beams were kept in the steel mould for 7 days to ensure that enough strength had been gained for stripping. A damp hessian cloth was used to cover the exposed portion of the beams while they were in the mould. After stripping was performed the beams were stored upside down at the back of the laboratory and wrapped in a moist hessian cloth, as shown in Figure 3.8 and Figure 3.9. The hessian cloth was kept damp by a watering can which was applied to all the beams every morning up to 28 days.

Figure 3.8: Beams being cured by covering with hessian cloth

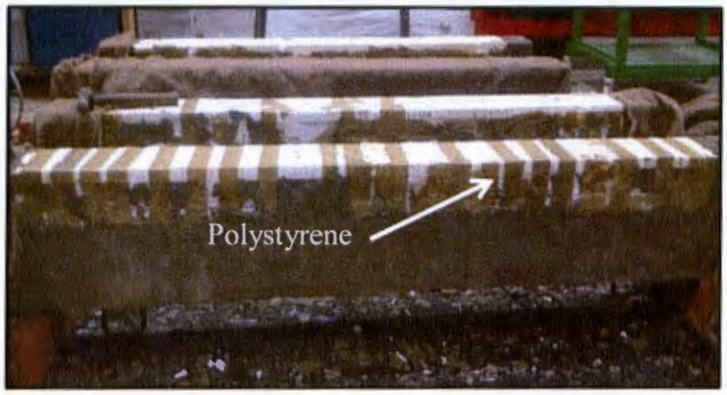

Figure 3.9: Beam after stripping stored upside and hessian cloth wrapping

The Casting program spanned over 1 month. After 14 days of curing the repaired beams were patch repaired and further cured for another 14 days. The Patch repair material was cured for 14 days only due to time limitations but was strategically chosen such that the concrete had gained sufficient strength for the intended tests (Owens, 2012).

3.4.4 Surface Preparation and Patch repair

Prior to strengthening the beams were patch repaired, this was done to emulate field practices. The patch repair method in combination with strengthening was identified as the most effective corrosion rehabilitation method by Malumbela et al. (2011), Rio et al. (2011) and many other researchers. There are various reasons why the combined retrofitting method is favourable; the patch repair allows the removal of rust products, the possibility of coatings to prevent further corrosion and re-passivation of reinforcement. CFRP strengthening has some durability benefits but more than that it can increase the capacity of beams strengthened in flexure beyond the original capacity.

The surface of the concrete that was in contact with polystyrene had a smooth shiny surface after the removal of the polystyrene (Figure 3.10). The smooth surface was roughened through the process of scabbling. The roughened surface, refer to Figure 3.11, was such that the aggregates were exposed.

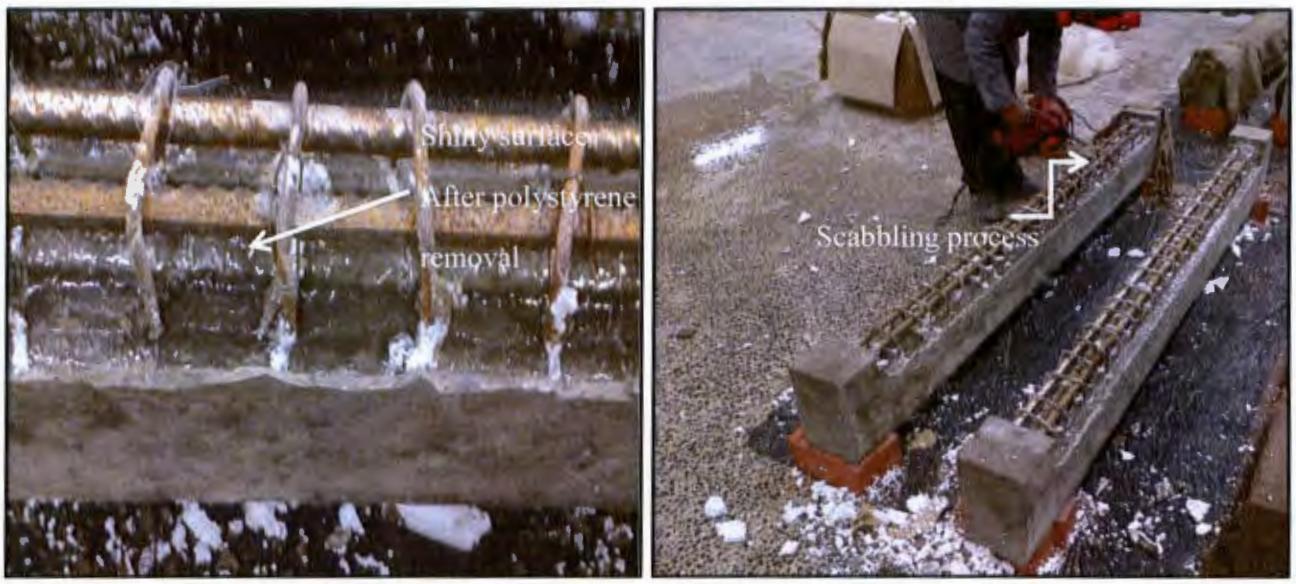

Figure 3.10 Concrete surface after the removal of polystyrene (left) and surface preparation by the scabbling process (right)

After the scabbling process there were dust remnants which would prevent sufficient bond of the patch repair mortar and the concrete substrate. The remaining dust from scabbling was removed with compressed air. Once the surface prepared region was free of dust the clean surface was dampened and wooden moulds sealed onto the beam sides where they were clamped with triangular steel clamps, refer to Figure 3.12b.

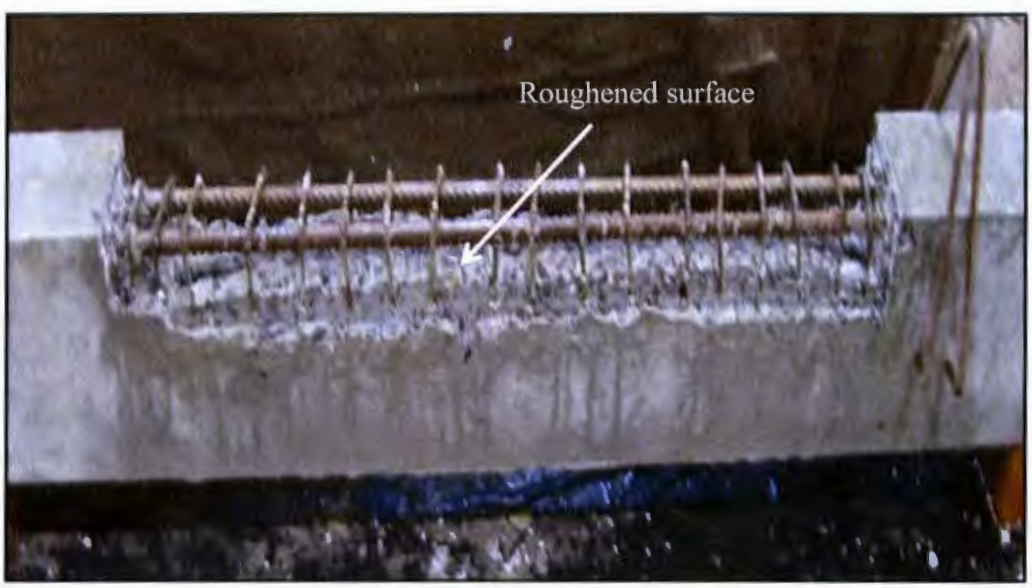

Figure 3.11: Roughened concrete surface

An epoxy adhesive was applied to the dampened rough concrete surface, shown in Figure 3.12, and repair mortar poured in the moulded region. It is important to note that adhesives have often been blamed in the past for not sticking but the source of the trouble generally lay with ignorance due to the lack of specifications. The vital property of adhesives is that they adhere to the relevant substrate surfaces and to maintain good bond with the substrate, this is achieved through surface preparation. The purpose of surface preparation is to remove contamination and weak surface layers, to change the substrate surface roughness at a micro level. The key stages involved in achieving this purpose are:

i. cleaning;
ii. Material removal and surface modification;
iii. Further cleaning (to remove contamination introduced by treatments, such as oil-mist, dust or chemical residues).

The repair mortar was cast into the wooden moulds after epoxy was placed on the roughed surface. The patch repair was levelled with a trowel to maintain a smooth surface. The wooden mould was removed after 24 hours in order to start the curing process with hessian cloth. After 28 days curing for the concrete substrate and 14 days for the patch repair the curing process was halted and the beams painted white, as shown in Figure 3.13. The beams were painted white to enhance the visibility of crack development during testing.

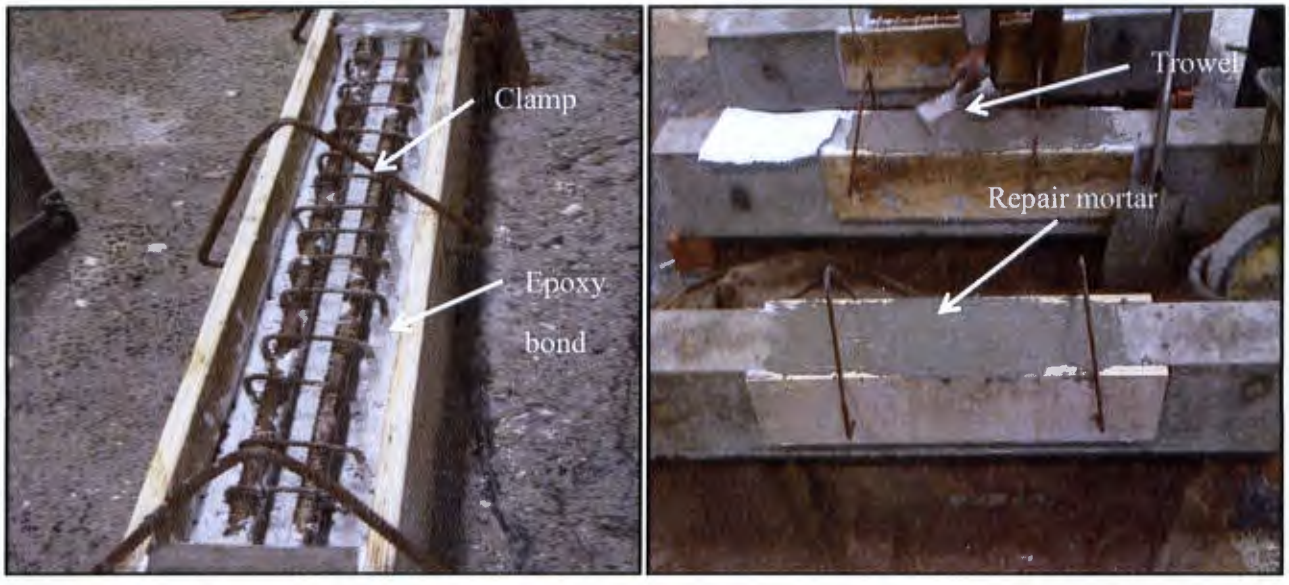

Figure 3.12: Setup of the wooden mould and adhesive epoxy application (left); patch repair application (right)

Figure 3.13: Beams after 28days (left) and beams after being painted white (right)

After patch repairs and painting the beams, surface preparation was conducted on the soffit of the beams for the application of CFRP strengthening.

3.4.5 Strengthening with CFRP

Surface preparation was also required in the region where the CFRP plate was to be bonded. An epoxy adhesive was used to bond the CFRP to the concrete substrate. An applicator was

made for the application of constant epoxy thickness (as shown in Figure 3.14). The CFRP strip used on all strengthened beams were identical in size, 50mm wide x 1.2mm thick and were bonded at the centre of the beam soffit over a length of 1700mm, as shown in Figure 3.15 below.

Figure 3.14: The applicator used to apply a constant epoxy adhesive thickness

Figure 3.15: CFRP plate and FRP wrap configuration

Surface preparation was implemented through sand blasting to roughen the surface so as to allow good adhesion of the CFRP to the concrete substrate. Compressed air was used again to remove the dust created by the scabbling process. The CFRP was cleaned with a commercial product as specified by the producer. Once the CFRP bond had hardened anchorage was pro-

vided at the plate ends bonded by an epoxy impregnation resin, the dimension of the wrap was 0.127mm thick, 150mm wide and 663mm long.

3.5 Material specifications

The reinforcement steel yield strength and ultimate strength as given by the supplier is shown in Table 3 below.

Table 3: Strength of steel used for the reinforcement cage

Reinforcement diameter (mm)	Yield strength (MPa)	Ultimate strength (MPa)
20	502	630
8	250	-

The mix design of the beams done was specified in Fultons (2009). The mix design was done in such a manner as to achieve 50MPa characteristic strength. The final quantities that were obtained for the mix are shown in Table 4. The aggregate materials used were acquired from the Cape Peninsula region. The coarse aggregate used was 19mm greywacke stone; the fine aggregate was Klipheuwel sand and CEM I 52.5N cement.

Table 4: Summary of the required quantities per cubic meter (m^3)

Binder type	w/c	Water (l/m^3)	Cement binder (kg/m^3)	Coarse aggregate (kg/m^3)	Fine aggregate (kg/m^3)
CEM I 52.5N	0.45	195	433	958	845

The design process began with the estimation of the required water content (l/m^3) and water cement ratio. The cement quantity was determined from the water to cement ratio. The coarse and fine aggregate quantities were determined from an Equation 3.7 and 3.8, provided by Addis and Goodman (2009).

$$A = CBD(K - 0.1FM) \tag{3.7}$$

$$S(kg/m^3) = \rho_s\left(1 - \frac{w}{\rho_w} - \frac{c}{\rho_c} - \frac{A}{\rho_a}\right) \tag{3.8}$$

Table 5: Average compressive strength results for a set of beams

Set	Compressive strength (MPa)	Mean compressive strength (MPa)	Standard deviation
S1	53	51	± 1.1
	51		
	50		
S2	53	52	± 0.6
	52		
	52		
S3	52	52	± 1.4
	53		
	50		
S4	52	54	± 2.0
	57		
	53		

Table 6: Properties of the commercial products utilised in the experiment

Property	Patch repairs (28 days)	FRP plate	FRP wrap	Epoxy resin for repair mortar	Epoxy resin for FRP plate	Epoxy resin for FRP wrap
Compressive strength (MPa)	75	-	-	60-70	70-80	-
Tensile strength (MPa)	5.5	3100	4900	18-20	24-27	30
Modulus of elasticity (GPa)	-	165	230	-	11.2	3.8
Thickness (mm)	-	1.2	0.127	-	2	-

3.6 Test setup and instrumentation

3.6.1 Thermography

3.6.1.1 Thermographic camera (Flir i7)

The Flir i7 was used to produce sensitive thermal images to detect the presence of any voids in the FRP bond to the concrete substrate.

The Flir series camera (Figure 3.16) works on an infrared energy detection system as was explained in literature. The camera is a non-contact device that detects infrared energy (heat)

which is converted to an electronic signal and processed to produce a thermal image on a monitor. The main advantage of thermal imaging over other products such as thermometers, with respect to thermal readings in non-contact mode, is that the former scans large areas whereas the latter does single spot measurements.

Figure 3.16: Flir i7 thermographic camera used for void detection

The Flir i7 camera has high accuracy of approximately $\pm 2\%$ or $2°C$. The broad measurement range with a minimum of $-20°C$ and a maximum temperature of $+250°C$. The Flir i7 is the latest camera model in a series of three. The thermal image quality of the Flir i7 is 140x140 pixels. The Flir i7 uses a spotmeter for its measurement functions unlike its counterparts the i3 and the i5 which use the centre spot. The Flir series cameras weigh only 350g and can be easily stored. The Flir i7 is easy to understand and designed for entry level users.

3.6.1.2 Voids detected by Flir i7

A heat source was introduced into the system by means of a commercial halogen light with a nominal power of 500 Watts. The light was shone on the CFRP plate for a short period of time thereafter images were taken with Flir i7 on the CFRP surface. The thermographic camera was able to identify the presence of voids in the epoxy bond, the position where voids were detected are shown in Table 19 of Appendix G. In the same Appendix there are some samples of images taken with the Flir i7, of the repaired and strengthened beams, are in Figure G.1 and Figure G.2.

3.6.2 Cracking behaviour

During testing the cracking behaviour of the beams was monitored after every 10kN load. The beams were loaded up until crushing failure of concrete occurred on the extreme compression zone near mid-span. Figure 3.17 shows the crack mapping and failure mode that was obtained for all the reinforced and strengthened beams.

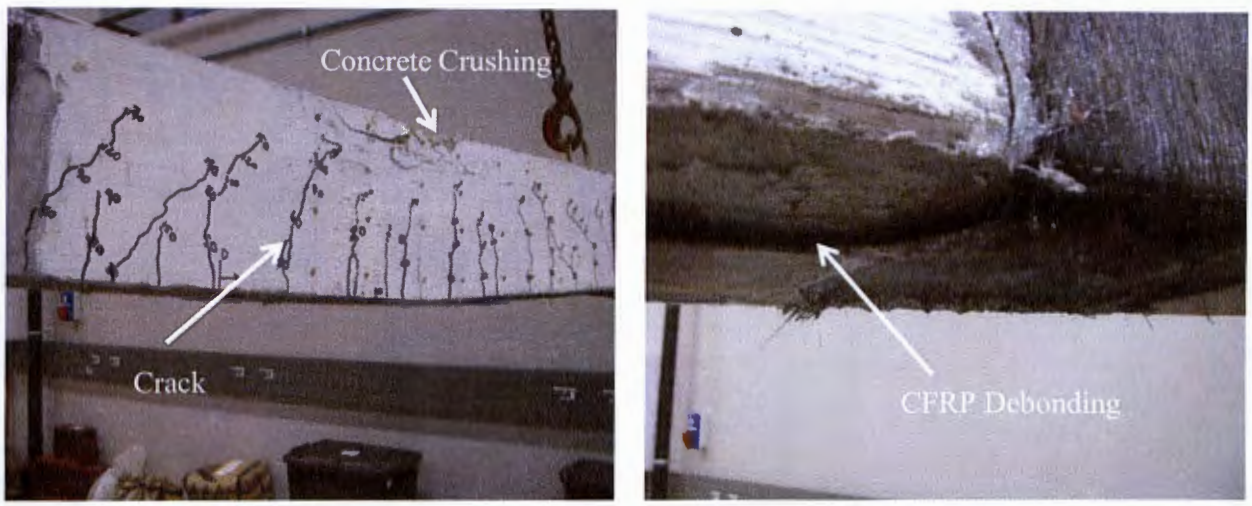

Figure 3.17: Crack mapping and crushing failure mode (left) with CFRP debonding failure mode (right)

The maximum crack width for every beam was measured using a crack width gauge ruler. The average crack spacing of each beam was also determined over the length of the span.

3.6.3 Load-deflection insturments

The load-deflection results were electronically collected by a data acquisition system, as shown in Figure 3.18 below. Five LVDTs and a load cell were connected to a signal conditioning module, refer to figure 3.19. The signal conditioning module was connected to the computer from which a program called Labview was used to extract the deflection and load results as a function of time.

Figure 3.18: Electronic setup for the load and deflection measurements

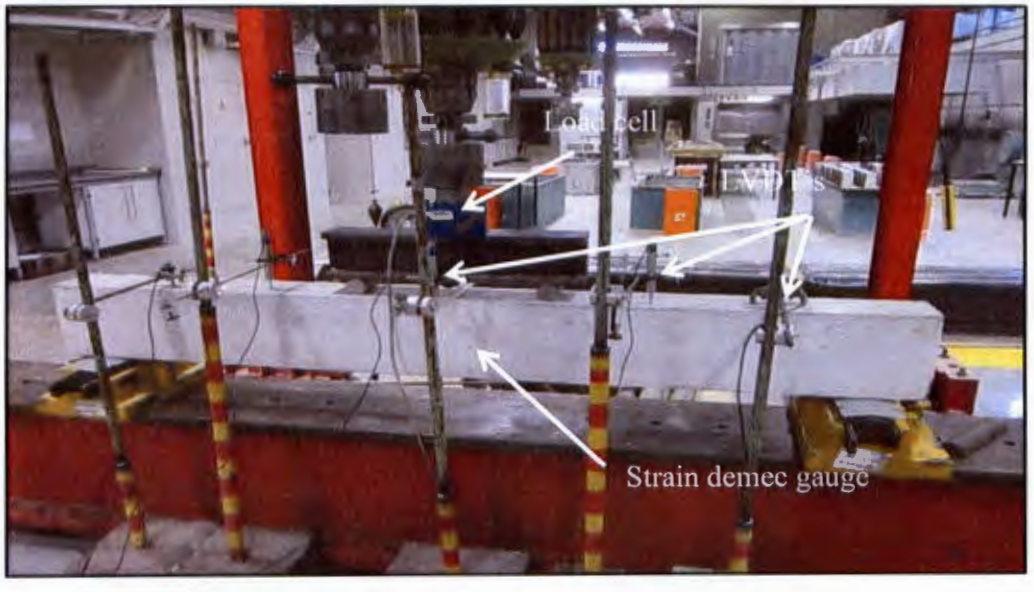

Figure 3.19: Experimental setup for the deflection and load results

All the LVDTs were placed upside down for safety reasons. The load cell was put directly below the hydraulic jack head and on top of the steel I beam, at the centre, used as the load spreader for four point loading. The LVDTs were installed in a symmetric manner, with a LVDT at mid-span, two LVDTS at 450mm on either side of mid-span and the two LVDTs 675mm from mid-span (Figure 3.19). Test equipment was calibrated prior to testing of the beams. The beams were tested in two flexure loading machines: the Wolpert and the Denison.

3.6.4 Demec strain gauge layout

The beams were tested in flexure by means of incremental static loading until failure. All the beams were instrumented to establish the performance of characteristics. Demec targets were used to capture the strain behaviour of the beams at mid-span, as shown in Figure 3.20 below. Some of the demec target results were discarded due to the distorted results caused by the presence of cracks. The demec targets were placed on a 100mm gauge length as specified by the manufacturer. The targets near the top of the concrete and the bottom were placed 30mm from the edges. The middle targets were placed at the heights 105mm and 165mm from the bottom of the beams.

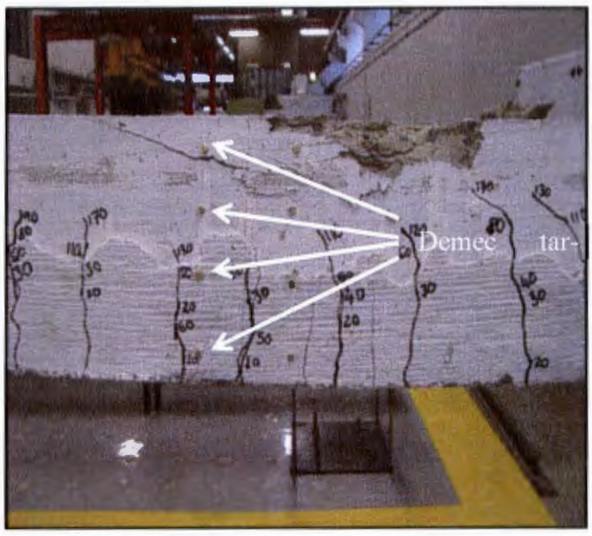

Figure 3.20: Configuration I of the demec strain targets

The extreme compression strain results were used to calculate the predicted neutral axis results for each beam.

An extensometer, Figure 3.21, was used to record the strain values from the demec strain gauges.

Figure 3.21: The extensometer used for the strain measurements

The extensometer can detect strains by measuring the relative movement of the demec strain targets. An extension in the distance between the targets signified the stains in tension whereas a reduction in the distance between the targets was indicative of compressive strains.

3.6.5 FEM results

The FEM results were obtained from a study that was conducted by Mundeli and Moyo (2014) at the University of Cape Town. All parts making up the model were created in Abaqus CAE, which is the graphical user interface in which the models were created, jobs submitted and the results monitored and analysed. Various FEM results are presented in this study; for verification of the input parameters refer to the study conducted by Mundeli and Moyo (2014).

3.7 Chapter summary

The test methodology described in this chapter was designed with the intention of exploring the effect of the extent of damage on patch repaired and strengthened reinforced concrete beams.

The methodology initially provides the design and details of the control beams. It further defines the extent of damage and describes the process of simulated corrosion and the technique used to perform a successful patch repair. After the patch repair, the method of using CFRP plate as a strengthening scheme is described.

Finally the material specifications are provided and the method of testing described for data acquisition process. The methods of static testing that were implemented were designed in such a way to achieve the desired results. The results of the proposed methodology are interpreted in the following chapter.

Chapter 4

4. Results and discussion

4.1 Introduction

This study was part of a larger investigation which was conducted; this study formed the experimental portion whereas the other part was done by the use of finite element modeling (FEM). The aim of the study was to investigate the effect of the extent of damage on the behaviour of the repaired and strengthened beams. A total of 15 beams were cast in the laboratory and investigated. Three of the beams were control beams and the other 12 beams were subjected to damage by means of simulated corrosion. The extent of damage was varied whereby there were the following damage lengths: 450mm, 800mm, 1300mm and 1800mm. The damaged beams were damaged by means of reducing the longitudinal tensile steel area to simulate 5% degree of corrosion. For each damage length there were three identical beams; so the four damage lengths were imposed on 12 beams. The damaged beams were patch repaired and subsequently strengthened with a CFRP plate at the centre on the soffit of the beams. After the beams were cured for 28 days they were tested in flexure loading machine. The experimentation was executed by incremental static loading, as mentioned in the methodology.

The behaviour of the beams that were being investigated in this study included: the effect of voids on debonding failure, the cracking behaviour, load deflection and the neutral axis. Although the idea of using a thermographic camera was a great idea; due to testing constraints the progression of the voids with increasing loads was not captured. The lack of data on void progression during testing made it hard to draw any conclusive results regarding the effect of voids on debonding failure. After testing the positioning of the voids in relation to debonding failure was closely viewed to see if there was any correlation, which was not apparent enough.

The results are presented and discussed in the following order: cracking behaviour and failure mode, load deflection behavior and neutral axis results.

4.2 Cracking behavior and failure mode

4.2.1 Introduction

The crack propagation pattern was unique for every beam but the crack propagation process was similar for all the beams. The failure mode for the all control beams was the same as was the failure mode of the reinforced and strengthened beams. Observations of the crack propagation were made every 10kN and marked clearly. The cracking behaviour of the beams, occurred as predicted by the design method; which was to fail in flexure and in a ductile manner.

The cracking behaviour was observed for the control beams, un-strengthened, and the damaged beams that were consequently repaired and strengthened. The typical control beam crack development and failure mode was observed as shown in Figure 4.1. The cracking behaviour and failure process was as follows:

1. At loads below 30kN, the first cracks were identified within the maximum moment region.
2. The flexural cracks further developed with increasing load as the flexural shear cracks also became present in the shear span.
3. More cracks developed as the load increased up to a certain point, when failure was imminent; at this stage crack widening was evident which was then followed by crushing of concrete.

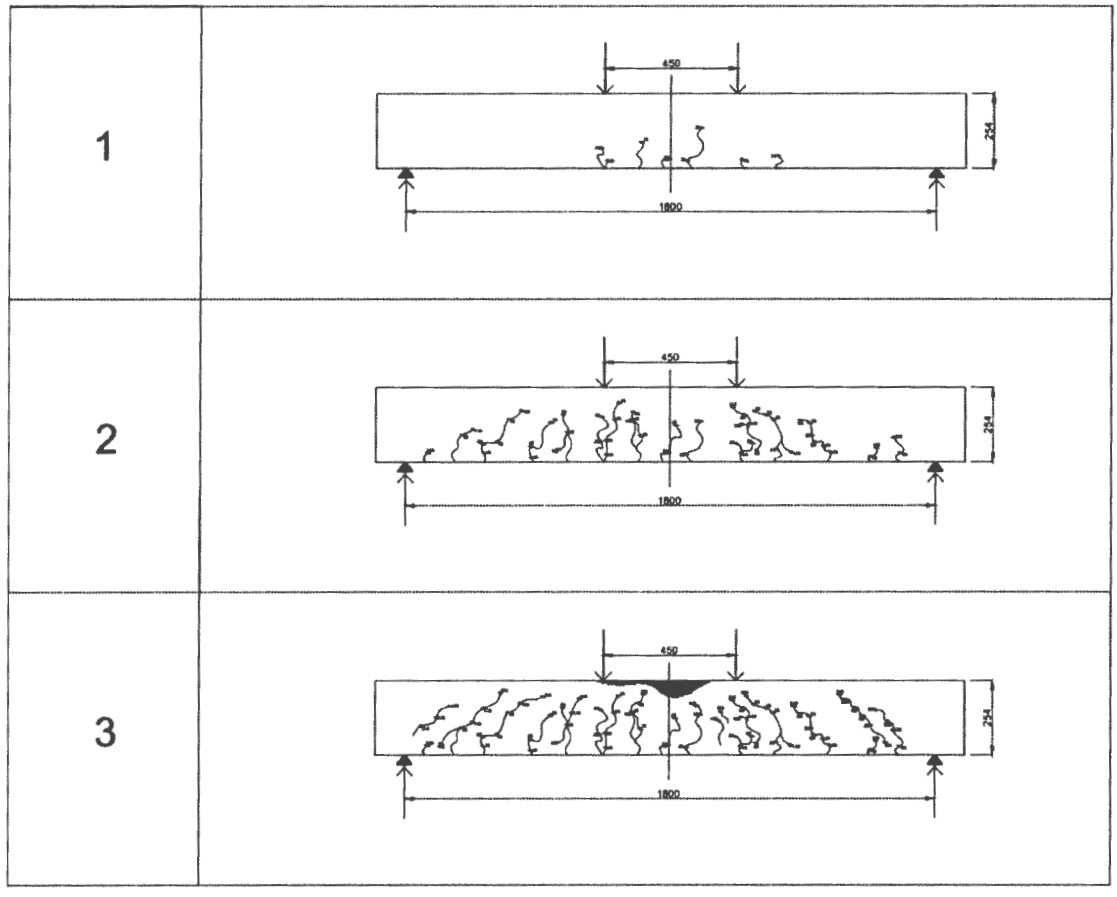

Figure 4.1: Crack propagation and failure mode of control beams

The damaged beams that were repaired and strengthened (RS) beams displayed a similar crack propagation process to that of the control beams but the failure sequence was different. The following observations were made:

1. At low loads flexural cracks developed in the high moment region
2. As the load increased, flexural shear cracks developed near the end supports
3. Debonding of CFRP plate due to splitting of the epoxy bonding agent
4. Compression damage in the form of crushing of concrete in the compression zone near a load application region. In certain cases there was FRP wrap splitting at the CFRP plate end.

The crack propagation and failure process that was observed for the RS beams is shown in Figure 4.2 below:

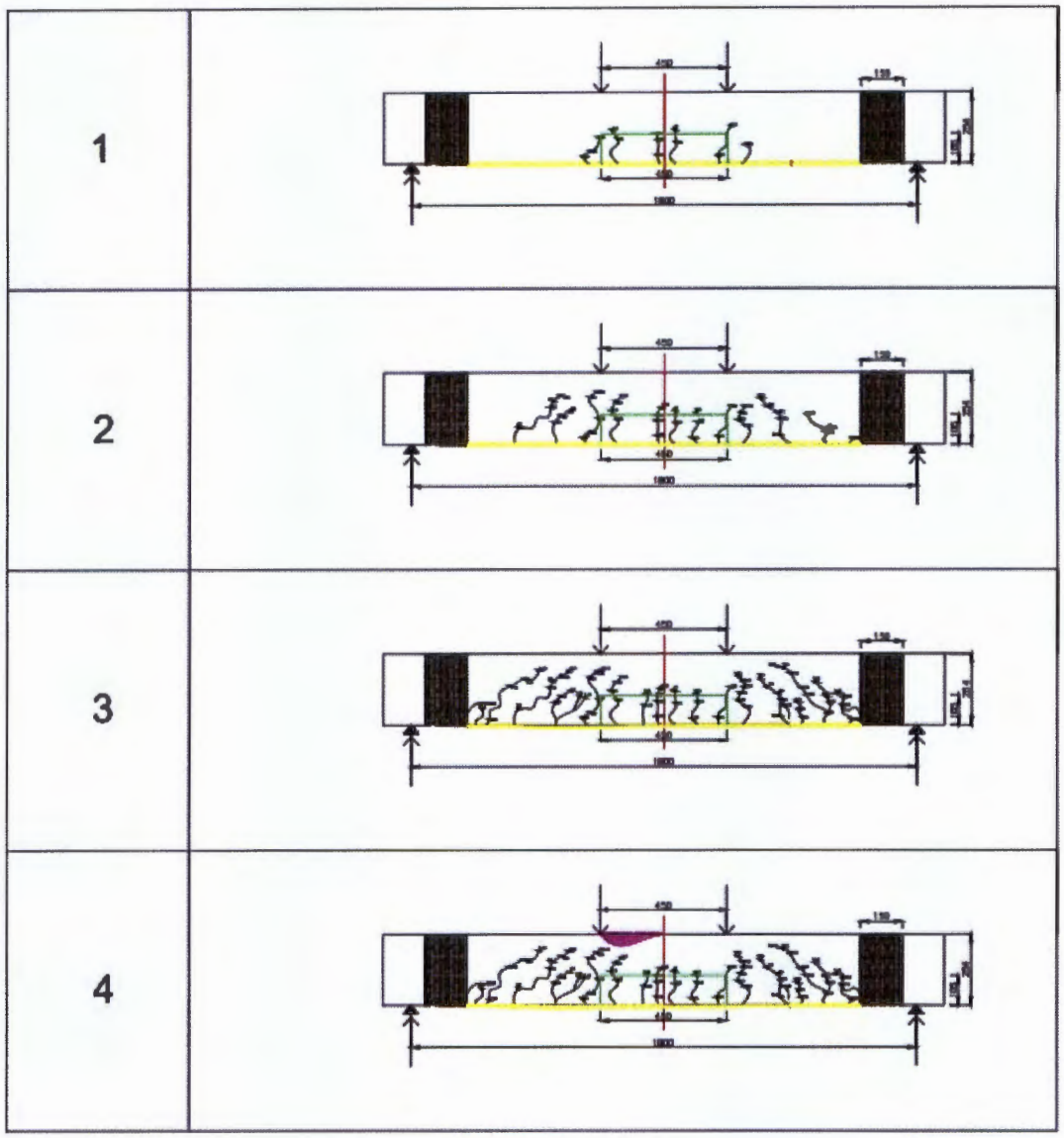

Figure 4.2: Crack propagation and failure mode of RS beams

Photographs taken of beams during testing are presented in the appendices and will be used to illustrate the different forms of damage encountered during testing. The results of the crack progression are presented for each set of identical beams and the discussion of the behaviour of the beams is presented after the crack progression results.

4.2.2 Progression of damage for control beams C1, C2 and C3

The control beam crack propagation behaviour was typical representation of under reinforced beam behaviour. Figure 4.3 below represents the crack propagation formation that was observed for the first control beam (C1). Two initial cracks commenced at a load of 30kN for beam C1. One of the initial cracks occurred within the region of maximum bending whereas the other occurred just left of the maximum moment region. As the load was increased to 40kN and 50kN the flexural cracks in the maximum moment region propagated further. The formation of cracks in the shear span, the region from the edge of the points of load application up to the supports, became obvious from 90kN onwards. The average crack spacing (C_s) of the beam was also observed. The average crack spacing was defined over a length of 1400mm, which was measured 700mm on either side of mid-span, over the number of cracks which occurred within that length. The average crack spacing for control beam C1 was found to be $C_s \approx 93$mm. Beam C1 also had a maximum crack width of $C_m \approx 2.5$mm. Crushing failure of concrete was observed directly below region of load application on the right hand side of mid-span of the beam. The crushing length was also observed, which was defined as the crushing damage length which was measured on the extreme compression fibre. Concrete crushing occurred on the extreme compression face under the applied load on the right over a length of approximately 235mm.

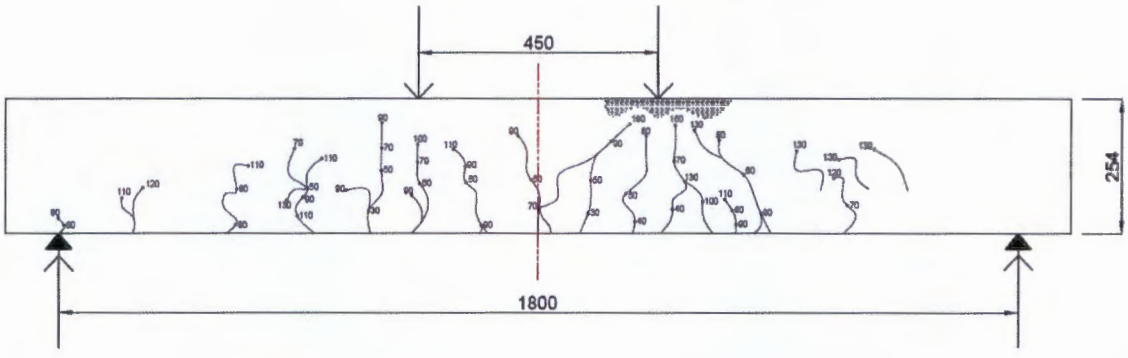

Figure 4.3: Progression of damage observed for beam C1

The observation of the crack propagation of the second and third control beams C2 and C3 is shown in Figure 4.4 and Figure 4.5 respectively. One initial crack was noted at 20kN for control beam C2 in the maximum moment region. More flexural cracks initiated as the load in-

creased to 30kN and 40kN in and near the maximum moment region. Flexural shear cracks became evident at higher loads. The flexural shear cracks propagated towards the points where the loads were applied. The average crack spacing of beam C2 was found to be $\mathbf{C_s} \approx 93$mm, and the maximum crack width of $\mathbf{C_m} \approx$ 1.8mm was observed. Crushing length of concrete occurred from the point load application on the right of mid-span extending 332mm towards the load applied on the left side of the mid-span of the beam.

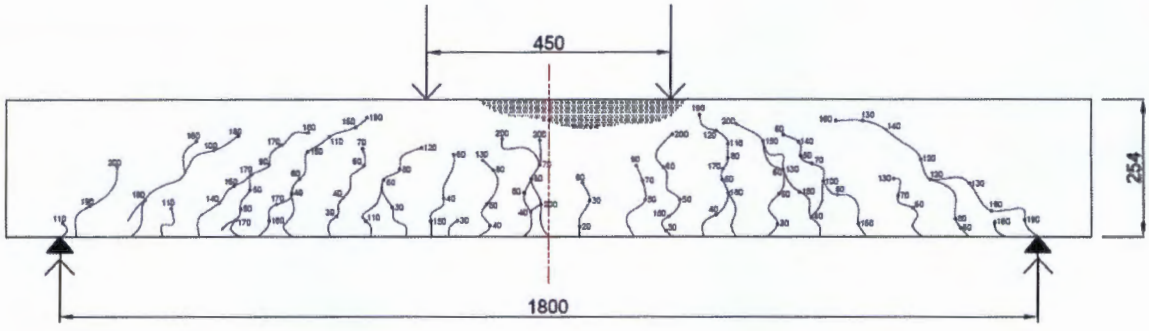

Figure 4.4: Progression of damage observed for beam C2

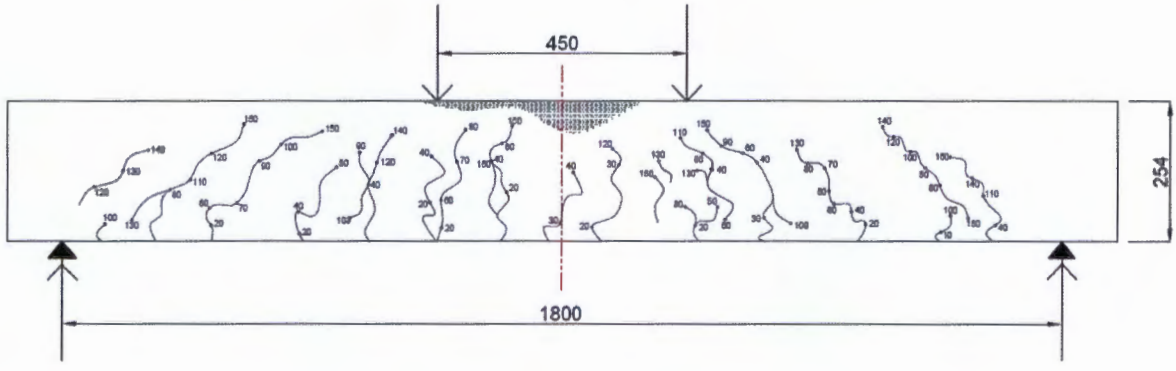

Figure 4.5: Progression of damage observed for beam C3

Control beam C3 had one initial crack which occurred at load of 10kN. Similarly like the other control beams C1 and C2 flexural cracks were observed in and near the maximum moment region and flexural shear cracks developed in the shear span region near the supports. Control beam C3 recorded an average crack spacing of $\mathbf{C_s} \approx$100mm and a maximum crack width of $\mathbf{C_m} \approx$ 2mm. Crushing failure length of concrete in the exteme was approximately 394mm and occurred under the point load on the left of mid-span.

The control beams ultimately failed due to crushing of concrete in the compression zone within/near the maximum moment region. The compression failure was due to the development of high compressive stresses in the compression zone. The maximum crack width also occurred within the maximum moment region due to the development of high tensile stresses on the exteme tension face.drop

4.2.3 Progression of damage for repaired and strengthened beams in set 1 (S1.2, S1.3 and S1.4)

The beams in set 1 were damaged over a length of 450mm and subsequently patch repaired and strengthened. The damage progression that was observed for the set 1 RS beams S1.2, S1.3 and S1.4 are shown in figures 4.6; 4.7 and 4.8 respectively.

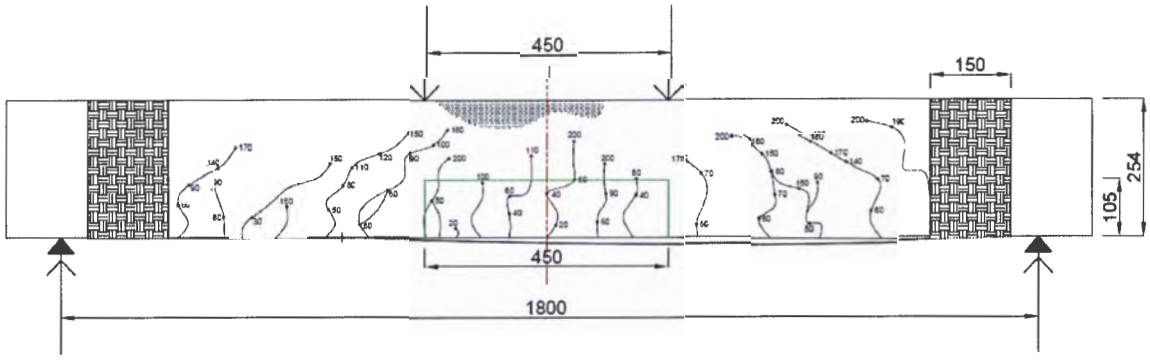

Figure 4.6: Progression of damage observed for beam S1.2

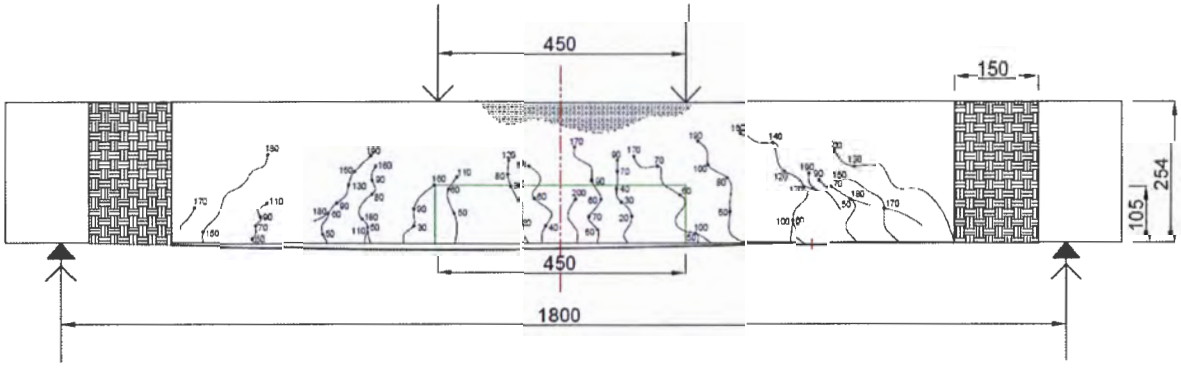

Figure 4.7:Progression of damage observed for beam S1.3

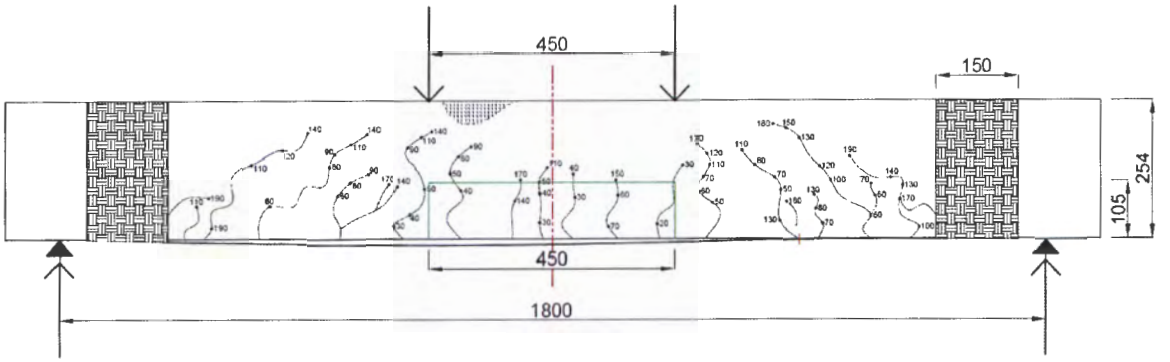

Figure 4.8: Progression of damage observed for beam S1.4

All the set 1 beams experienced first crack at a load of 20kN. For RS Beams S1.2 and S1.3 it was observed that two initial cracks developed within the maximum moment region. When the load was low the flexural cracks formed in the maximum moment region. As the load increased the cracks developed throughout the beam's span with increasing loads finally giving rise to flexural shear cracks in the shear span near the supports. The flexural shear cracks propagated in the direction of the points of load application. The average crack spacing ($\mathbf{C}_s$) of the beams S1.2, S1.3 and S1.4 were found to be 82mm, 70mm and 88mm respectively. Compared to the control beams the set 1 beams displayed a lower average crack spacing. The maximum crack width ($\mathbf{C}_m$) results that were measured were as follows; 1.6mm, 1.1mm and 0.9mm for the RS beams S1.2, S1.3 and S1.4, respectively.

Unlike the control beams debonding failure of the CFRP plate was also observed, for all three beams in set 1, prior to crushing failure of concrete on the extreme compression face of the beam. The cause of debonding couldn't be monitored but a load snapping noise indicated the onset of debonding. Although debonding was evident in all the set 1 beams it did not occur in an identical manner thus no pattern was identified. Debonding occurred near the middle of the shear span on the left of mid-span for beams S1.3 and S1.4. For beam S1.2debonding failure occurred in the right of mid-span, where it progressed right through to the plate end on right support. The FRP wrap on the right side ruptured, as shown in Figure D.1in Appendix D. After debonding had occurred crushing failure commenced although not immediately.The set 1 beams all underwent concrete crushing failure of concrete in the extreme face for beams S1.2, S1.3 and S1.4, with the crushing lengths of approximately 375mm, 312mm and 310mm

respectively. Concrete crushing occurred near the applied load on the left of mid-span for beams S1.2 and S1.4 whereas it occurred on the right of mid-span for beam S1.3.

4.2.4 Progression of damage for repaired and strengthened beams in set 2 (S2.2, S2.3 and S2.4)

Set 2 beams represent the RS beams that damaged to a length of 1800mm. Figures 4.9 4.10 and 4.11 are the diagrams detailing the damage progression observed for the beams S2.2, S2.3 and S2.4, as shown below.

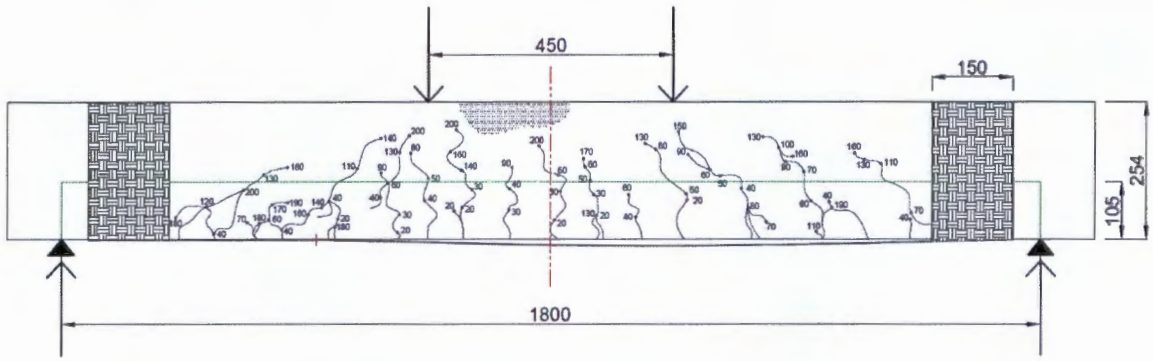

Figure 4.9: Progression of damage observed for beam S2.2

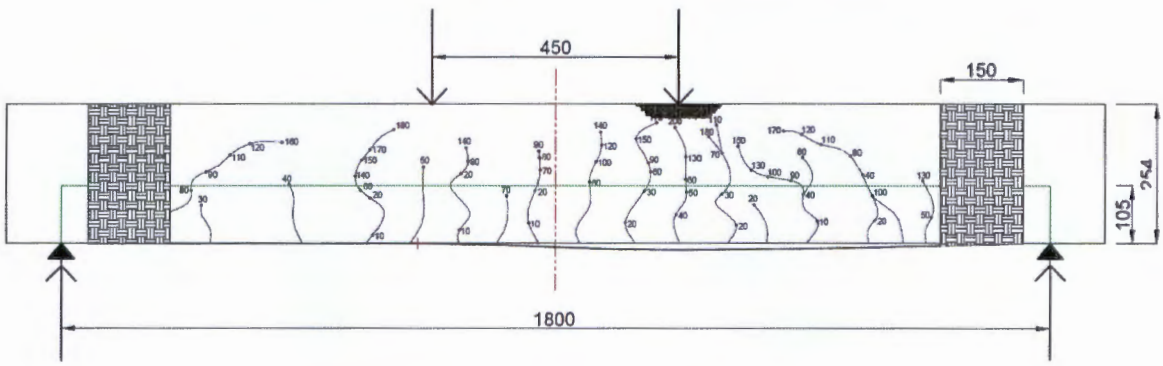

Figure 4.10: Progression of damage observed for beam S2.3

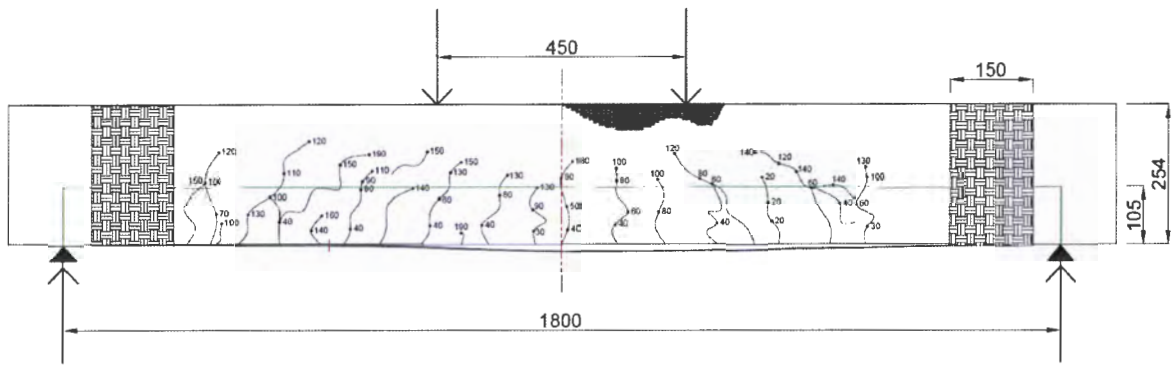

Figure 4.11: Progression of damage observed for beam S2.4

For two of the three set 2 beams the first crack occurred at20kN for RS beams S2.2 and S2.3 respectively. Meanwhile the first crack was lower for beam S2.4 with a load of 10kN. The damage progression of the beams in set 2 commenced in a similar fashion as the control beams and set 1 beams. The average crack spacing ($\mathbf{C_s}$) for beams S2.2, S2.3 and S2.4 were found to be 74mm, 88mm and 70mm respectively. It should be noted that the beams in set 2 all had an average crack spacing that was lower than the control beams. The maximum crack widths ($\mathbf{C_m}$) of 1.3mm, 1mm and 1.6mm were measured for beams S2.2, 2.3 and S2.4 respectively.

Debonding failure was again observed for all the beams in set 2, in as similar manner to the set 1 beams, and was trailed by crushing failure on concrete in the extreme compression face of the beams. Epoxy bond splitting was observed with the CFRP still intact for all strengthened beams in set 2. Debonding position was similar for all the beams in set 2, debonding was between the left shear span up to the FRP wrap on near the right support. Soon after debonding concrete crushing on the extreme face of the beams were observed with the crushing lengths of 230mm, 150mm and 315mm for RS beams S2.2, S2.3 and S2.4 respectively. The concrete crushing occurred in the region where the point load on the right of mid-span was applied for beams S2.3 and S2.4; whereas concrete crushing for beam S2.2 occurred near the point load on the left of mid-span.

4.2.5 Progression of damage for repaired and strengthened beams in set 3 (S3.2, S3.3 and S3.4)

The third set of beams were damaged and repaired over 1300mm length. The crack propagation diagrams for beams S3.2, S3.3 and S3.4 are shown in figures 4.12, 4.13 and 4.14 respectively.

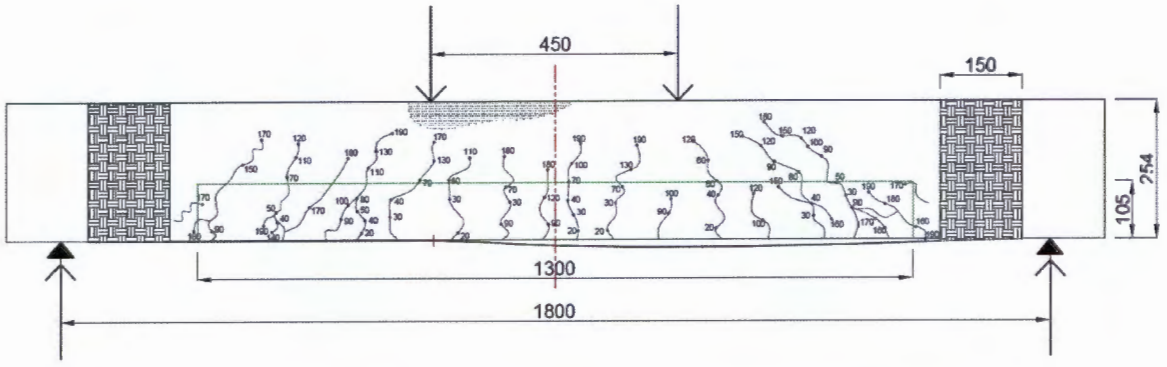

Figure 4.12: Progression of damage observed for beam S3.2

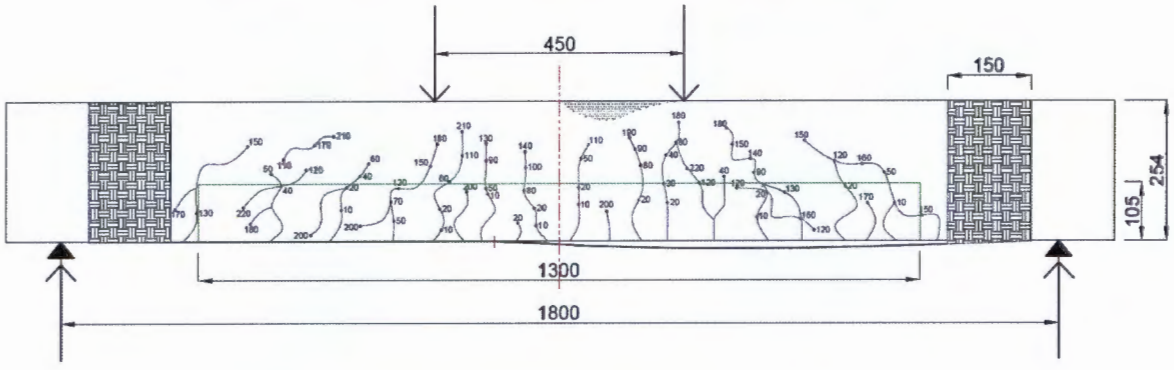

Figure 4.13: Progression of damage observed for beam S3.3

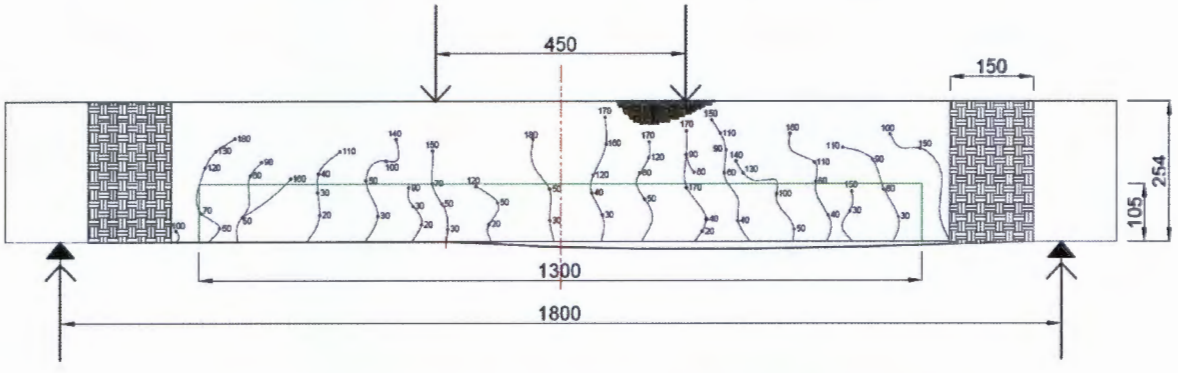

Figure 4.14: Progression of damage observed for beam S3.4

The crack propagation pattern was identical to the set 2 beams that were tested before. The first cracking loads of 10kN was observed for beam S3.3 and 20kN beams S3.2 and S3.4. At loads below 30kN flexural cracks initiated around the maximum moment region. The crack development of the flexural cracks and flexural shear cracks was similar to the other RS beams. The average crack spacing (C_s) of beams S3.2, S3.3 and S3.4 were 82mm, 70mm and 78mm re-

spectively. The maximum crack width of (C_m) 0.7mm, 1.7mm and 1.3mm were measured for-beams S3.2,S3.3 and S3.4 respectively.

Like the RS beams tested before debonding failure trailed by crushing failure of concrete in the extreme compression face was obtained for the set 3 beams. Debonding extended through the FRP wrap on the right side for beam S3.4, (Figure D.2 in Appendix D). Concrete crushing length that were observed for beams S3.2, S3.3 and S3.4 were 305mm, 283mm and 228mm respectively. Concrete crushing occurred around the point load on the right of mid-span for beams S3.3 and S3.4 meanwhile concrete crushing occurred around the load on the left of mid-span for beam S3.2.

4.2.6 Progression of damage for repaired and strengthened beams in set 4 (S4.1, S4.2and S4.3)

Lastly were the set 4 beams whichhad an extent of damage of 800mm, which is the second smallest damage/repair length. The crack propagation diagrams for beams S4.1, S4.2 and S4.3 are represented by Figures 4.15,4.16 and 4.17respectively below.

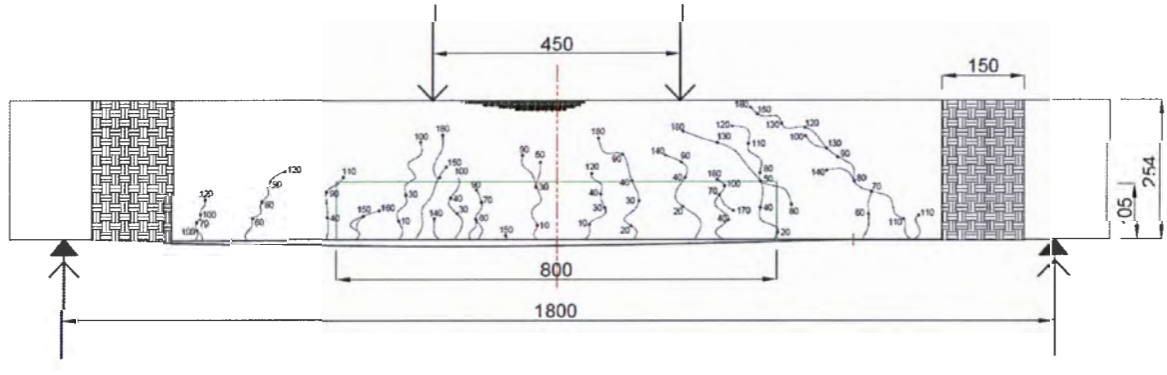

Figure 4.15: Progression of damage observed for beam S4.1

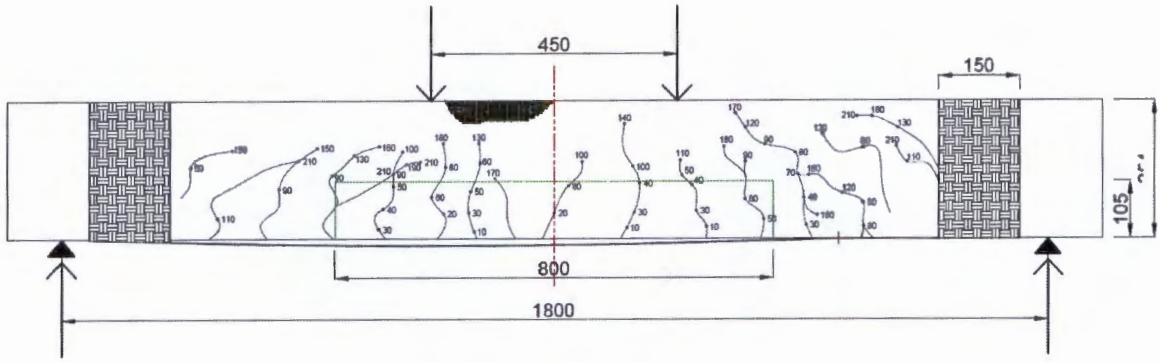

Figure 4.16: Progression of damage observed for beam S4.2

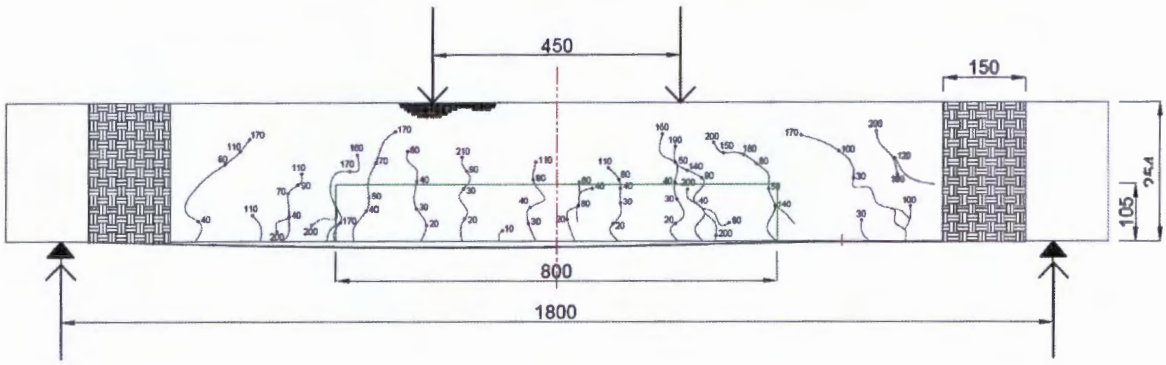

Figure 4.17: Progression of damage observed for beam S4.3

All the set 4 beams first crack(s)occurred at a load of 10kN. The failure mode of the set 4 beams was similar to the other RS beams. The average crack spacing (C_s) of beams S4.1, S4.2 and S4.3 were 67mm, 100mm and 78mm respectively. The maximum crack width (C_m) of 1.4mm and 1.1mm were measured from beams S4.3 and S4.2 respectively, unfortunately the crack width for beam S4.1 was not obtained.

The beams in set 4 underwent debonding failure before concrete crushing failure in the extreme compression zone. Thedebonding for beam S4.2 extended through the FRP wrap on the left, refer to Figure D.3 of appendix D. concrete crushing occurred near the applied load on the right of mid-span for all set 4 beams. The concrete crushing length that was measured for the beams S4.1, S4.2 and S4.3 were 296mm, 284mm and 268mm respectively.

4.2.7 Comparative analysis

The crack propagation of all the RS beams was as predicted by the strengthening ratio equations in the CFRP design in Appendix C. It was observed that flexural cracks were vertical and dominant in and around the region of maximum moment. Flexural shear cracks were also observed near the supports in the shear span and inclined towards the loading points. The type of crack formation that was observed in this particular study can be explained on the basis of shear span to effective depth ratio. According to Robberts and Marshall (2008) we may expect the type of failure observed in this experiment when the shear span to effective depth ratio is in between 6 and 2.5, the beams used in this experiment had a shear span to effective depth of 3.2. The initial cracks in the beams initiated when the principal stresses of the concrete was reached in tension. The concrete cracks at low loads because concrete is weak in tension but strong in compression. From the results it was evident that the addition of the patch repair material and the CFRP plate did indeed alter the crack spacing and crack width of the CFRP strengthened beams as expected. The section that follows attempts to discuss the effect that the extent of damage may have had on cracking behavior of the RS beams and comparisons drawn to the control beam behaviour. Furthermore the experimental results that were obtained from this investigation are compared to the finite element modelling (FEM) results that were obtained in a parallel study.

4.2.7.1 The effect of the extent damage length on the crack propagation process

A summary of the results from the cracking behavior all 15 beams is provided in Table 12 in Appendix D. For analytical purposes the results of the identical beams was averaged and is presented in Table 7 below. From Figure 4.18 it can be seen that the cracking load initiated relatively higher for the control beam as compared to the RS beams, although the RS beams were supposed to crack at higher loads due to the high strength of the patch repair material. The FEM results were similar to the results that were obtained from the experiment ,refer to Figure 4.19. There was no evident solution for reason why the RS beams displayed lower cracking loads than the control beams.

Table 7: Average results of cracking behaviour observed during testing

Beam name	Beam damage length (mm)	First crack (kN)	Average spacing C_s (mm)	Maximum crack width C_m (mm)
control	0	20	95	2.1
set 1	450	20	79	1.2
set 4	800	10	79	1.3
set 3	1300	17	76	1.3
set 2	1800	17	76	1.3

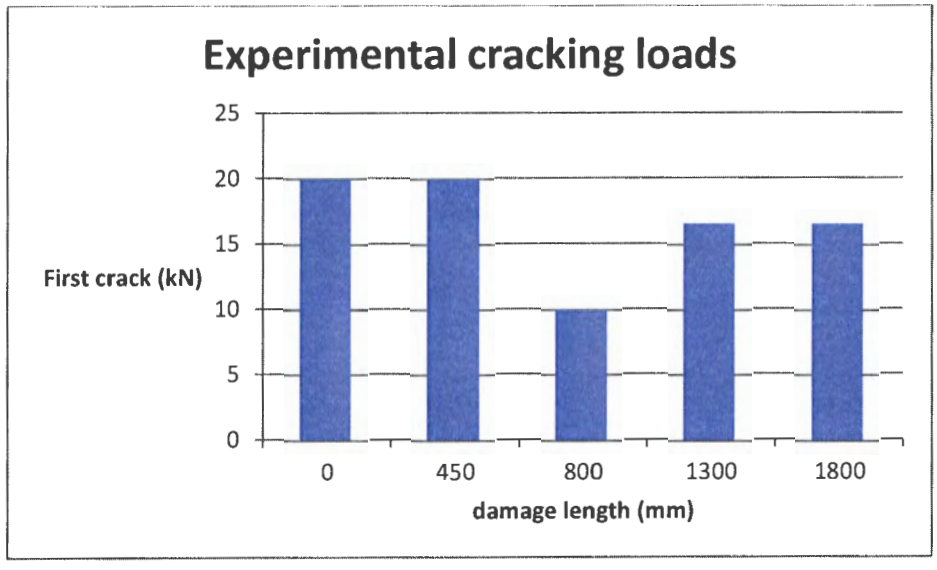

Figure 4.18: Experimental cracking loads

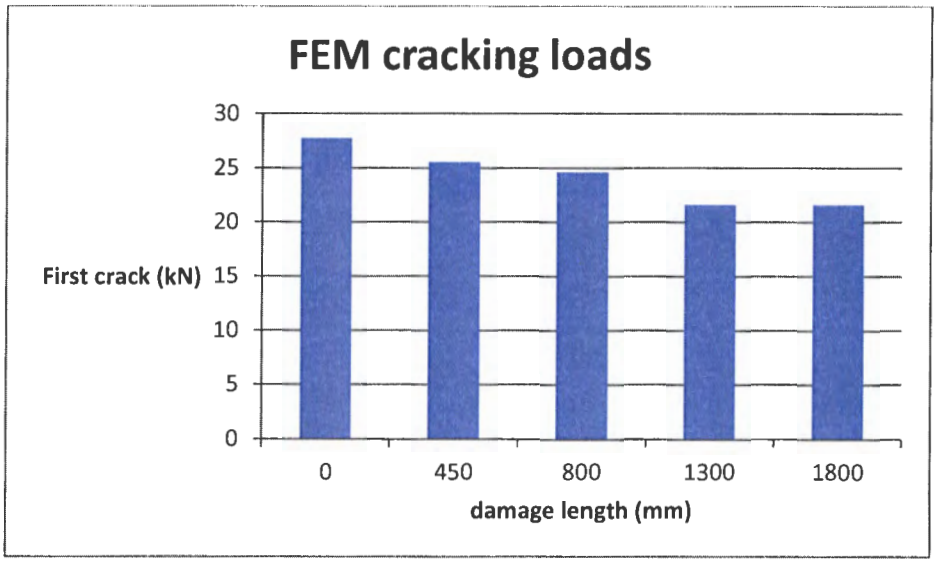

Figure 4.19: FEM cracking loads

The first crack always occurred at mid-span on the extreme tension face of the beam and extended upwards towards the compression face. The average crack width of the control beams was larger than the average crack width of the RS beams. The wider crack width of the control beams was due to the lack of restrictive compressive forces that are transferred to the crack by the composite action of the epoxy and CFRP. The RS beam with the 450mm damage extent had the lowest crack width of all the other RS beams. The remaining RS beams had the same average crack width of 1.3mm. The higher crack width of the RS beams with the larger damage length could be attributed to the higher load capacity which they experienced.

The patch repair-concrete substrate interface remained intact from the naked eye which implied a good bonding behaviour. The crack spacing of the RS beams were higher than the control beams, refer to Figure 4.20. The average crack spacing of the control beams was higher than all the RS beams with95mm. It was also observed that for increasing damage extent there was a decrease in average crack spacing. The beams with 450mm and 800mm damage extent had an average crack spacing of 79mm whereas the beams with the damage extent of 1300m and 1800mm had an average crack spacing of 76mm.Although it was expected that the RS beams would have a lower amount of cracks for increasing damage extent, due to the higher tensile strength of the repair material than the concrete substrate, it is believed that the addition externally bonded CFRP plate created a tensioning stiffening effect that altered the expected cracking behaviour. Hollaway (1999) describes how the addition of the composite plate to the soffit

of the beam restricts the widening of cracks (also referred to as tension stiffening). The tension stiffening effect offers restrictive compressive force to the potential crack widening thereby promoting the formation of other cracks nearby to relieve the high stresses.

It is important to note that tensile stresses that are transferred to the FRP induce interfacial stresses between the FRP and concrete which can lead to debonding near the cracks if high enough.

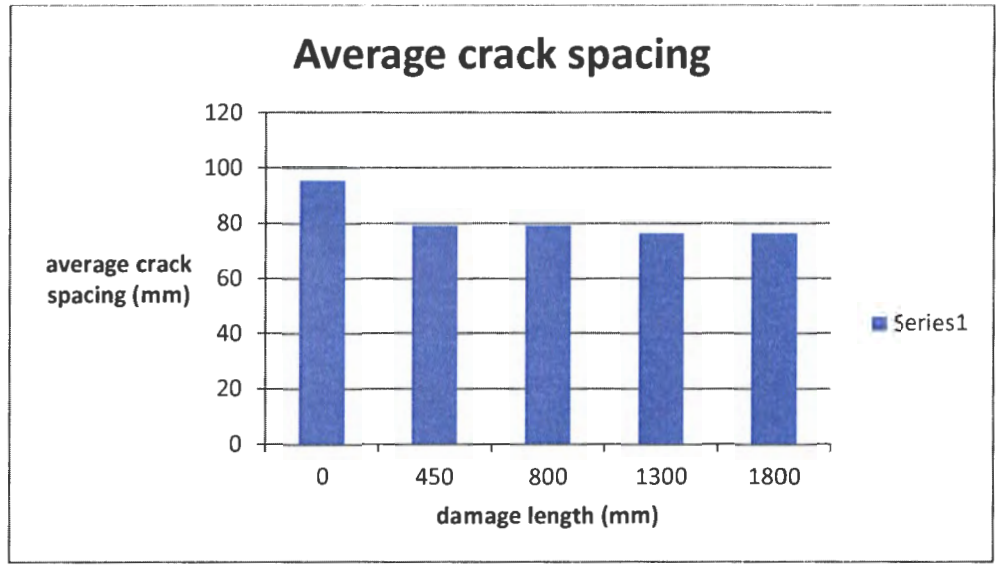

Figure 4.20: Average crack spacing for varying damage extent

At high loads numerous cracks had formed to the point where the interfacial stresses lead to the debonding of the CFRP plate due to epoxy bond splitting for all the repaired and strengthened beams.

4.2.7.2 The effect of extent of damage on the failure mode

Brittle debonding failure of CFRP by means of epoxy bond splitting was observed for all strengthened beams. Although it was hard to detect the debonding origins, an accurate prediction can be made through deductive reasoning. Buyukozturk et al. (2004) mentions how debonding occurs in regions of high stress concentrations in strengthened members which are often associated with material discontinuities and near cracks. After yielding the crack propagation slowed immensely but the widening of flexural cracks in the maximum moment region initiated. This widening of the flexural cracks may have caused high interfacial stresses in the

epoxy bonding agent thereby inducing Intermediate Crack (IC) debonding. Debonding failure was identified earlier in the literature chapter as being a major problem in past experiments. This was pointed out by Bonacci et al. (2001) in a database of 23 different studies leading up to 1999 it was found that 63% of the strengthened beams failed by debonding. In another study by Ceci et al. (2012) there was 184 beams which were identified as undergoing IC debonding failure. As stated by many researchers in the past debonding failure was a problem in the study as it presents brittle failure and under utilizes the CFRP plate.

4.3 Load - Deflection analysis

4.3.1 Introduction

In this section a discussion of the mid-span load deflection results is presented. The current evaluation utilizes data obtained from an electronic measurement system located at the mid-span of the tested beam from the hydraulic actuator (force load). Data was collected well beyond debonding failure up until crushing of concrete was observed in the extreme compression zone. The load-deflection results of all the beams are presented in Table 13 and Table 14 in Appendix E. The comparative results of the RS beams relative to the average control beam are shown in the Table8 below.

The results obtained from the load-deflection curves were as follows: yield, peak and ultimate loads and displacements. The yield load was of interest because it is important detail for the consideration of under-reinforced beam design. The experimental yield load results were noted at the points where the second change in stiffness was observed. The peak load was important for observing the effect of CFRP strengthening. Loading the beams to ultimate failure ensured that the ductility results could be analysed, as ductility is important with regards to design. Two forms of ductility are described in this chapter, ultimate ductility being the first relates to ultimate failure by crushing of concrete in the extreme compression zone. The other form of ductility refers to debonding ductility. The ductility mentioned in this study refers to the displacement ductility which refers to displacement ratio i.e. for ultimate ductility refers to the ratio of

the displacement at ultimate failure to the displacement at yield $\left(\frac{\mu_f}{\mu_y}\right)$, and debonding ductility is the ratio of displacement at debonding to the displacement at yield $\left(\frac{\mu_d}{\mu_y}\right)$.

Table 8: Results from the load-deflection behaviour beam results

Beam	Yield load (%)	Peak load (%)	Normalized ultimate ductility $\left(\frac{\mu_f}{\mu_y}\right)$	Normalized debonding ductility $\left(\frac{\mu_d}{\mu_y}\right)$
S1.2	20.9	22.7	0.4	0.6
S1.3	7.1	11	0.3	0.7
S1.4	2.9	5.3	0.3	0.9
S2.2	13.6	11.9	0.3	0.8
S2.3	30	32	0.4	0.7
S2.4	18.2	17.2	0.4	1
S3.2	6.9	9.6	0.4	0.6
S3.3	30.1	25.6	0.3	0.4
S3.4	-0.5	-3.4	0.3	0.5
S4.1	7.9	10.1	0.4	0.6
S4.2	27.1	29.2	0.3	0.5
S4.3	16.6	22	0.3	0.7

The load-deflection relationship enabled further interpretation of the beam behaviour, where the different stages of occur. Crack initiation was not clearly visible from the experimental results although the point of yield of the control beams and the RS beams was evident. The lack of distinct linear phases for pre-cracking stiffness and post cracking stiffness were the result of the behaviour that was not perfectly linear elastic, as theory would suggest. Furthermore from the load deflection graph the peak load, debonding load and ultimate loads were identified. Figure 4.21 illustrates the typical behaviour that was observed for the control beams and the RS beams.

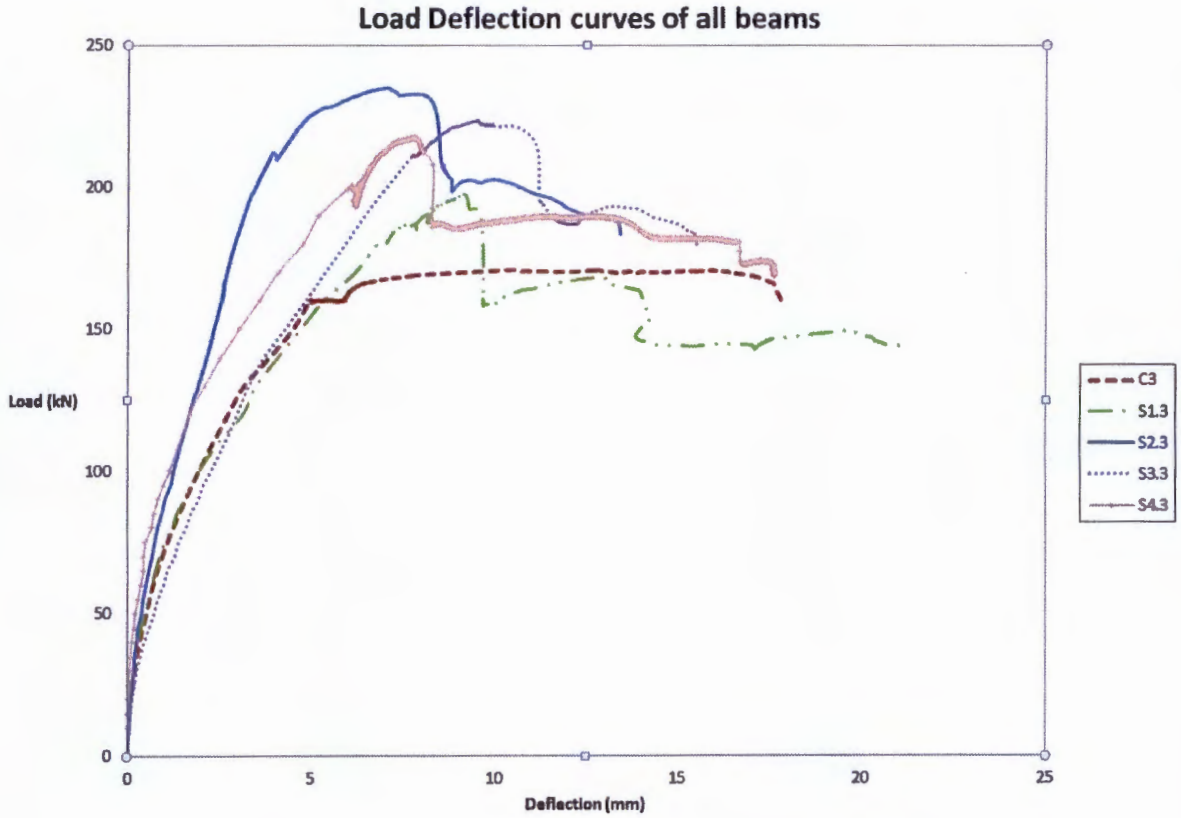

Figure 4.21: Load- deflection of one beam from each set

From the comparison of the control beam behaviour to the RS beams it was evident that the control beams were more ductile than the RS beams. The reduced ductility of the RS beams was expected as it has been shown in many studies which were mentioned in chapter 2. Although the ductility of the RS beams reduced there was an increase in yield strength and peak load when compared to the control beams which was also expected, as it is well known fact of CFRP strengthening as indicated in literature. Due to the variation of results of the identical beams there is no definite typical load-deflection relationship that can be provided to compare the control beams and the RS beams. It was also observed that there was a trend in terms of load increase in relation to extent of damage but that is covered later in this section.

4.3.2 Load deflection results for the experimental beams and FEM

4.3.2.1 Load-deflection yield and peak load results for control beams

The yield and peak load results from the load-deflection relationship are provided in the Appendix E in Table 13. The Behaviour of the control beams is shown in Figure 4.22 below. From

the figure we can see that the control beam the load-deflection stiffness was indeed divided into 3 regions namely pre-cracking stiffness, post cracking stiffness and post yielding stiffness. The change in stiffness just indicates the change in stiffness due to crack initiation where the tensile concrete is rendered null and void in terms of tensile forces. In theory when cracking occurs the tension forces only act on the tension reinforcement bars (rebars). Another point of interest is the point of yielding, where the RC beam load remains relatively constant with increasing displacement. The aforementioned behaviour where the beams displace at a constant load is where the concept of ductility plays in. The ductility of the control beams was very ductile; which means that the under reinforced design method did achieve the desired ductility. The Yield loads of the control beams were found to be 183kN and 160kN for control beams C1 and C3 respectively. The yield load from FEM beam was in between that of the two aforementioned control beams. The data from beam C2 was unfortunately lost and could not be recovered.

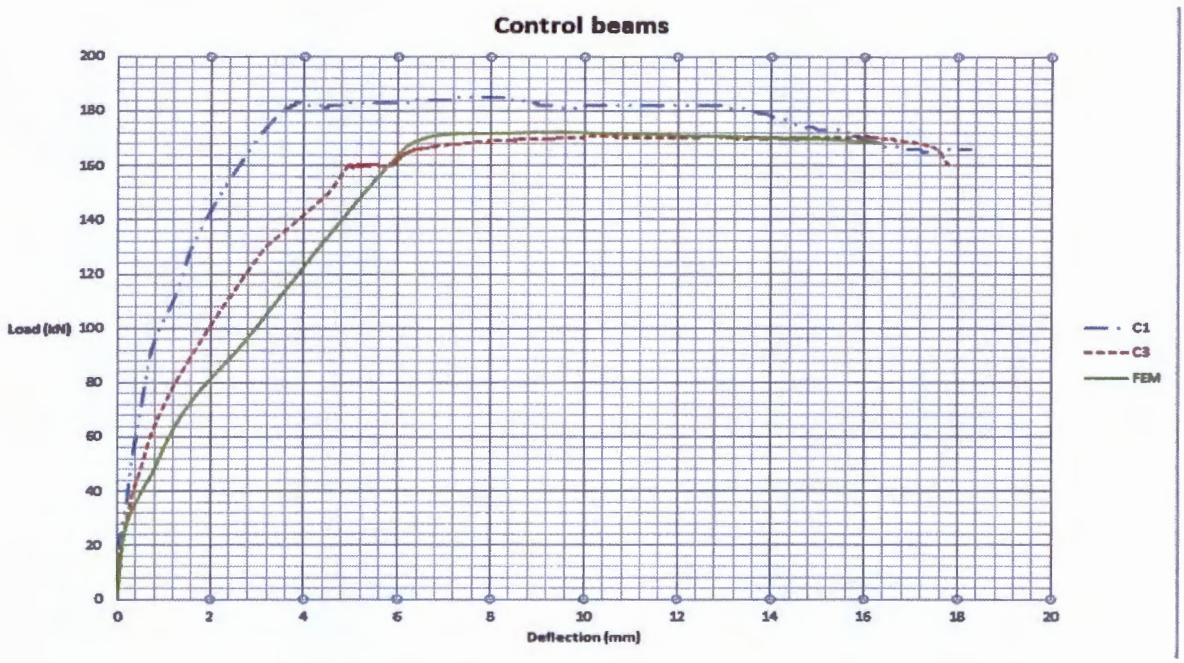

Figure 4.22: Load-deflection behaviour of retrofitted beams C1, C2 and C3

The peak loads of the experimental control beams were 185kN and 171kN for beams C1 and C3 respectively. The peak load for FEM beam was the same as the yield load.

4.3.2.2 Load-deflection yield and peak load results for RS beams

The load-deflection of the RS beams was also captured well but the pre-cracking stiffness and post cracking stiffness was not perfectly linear. However the yield point, peak load and debonding of CFRP were captured well as shown for the beams with 450mm damage (set 1) by Figure 4.23 below. The yield loads of theset 1 beams higher than those of the control beams with the following load results; 207kN, 184kN and 177kN for RS beams S1, S2 and S3 respectively. The peak load results of the set 1 beams were; 218kN, 198kN and 188kN for the RS beams S1, S2 and S3 respectively.

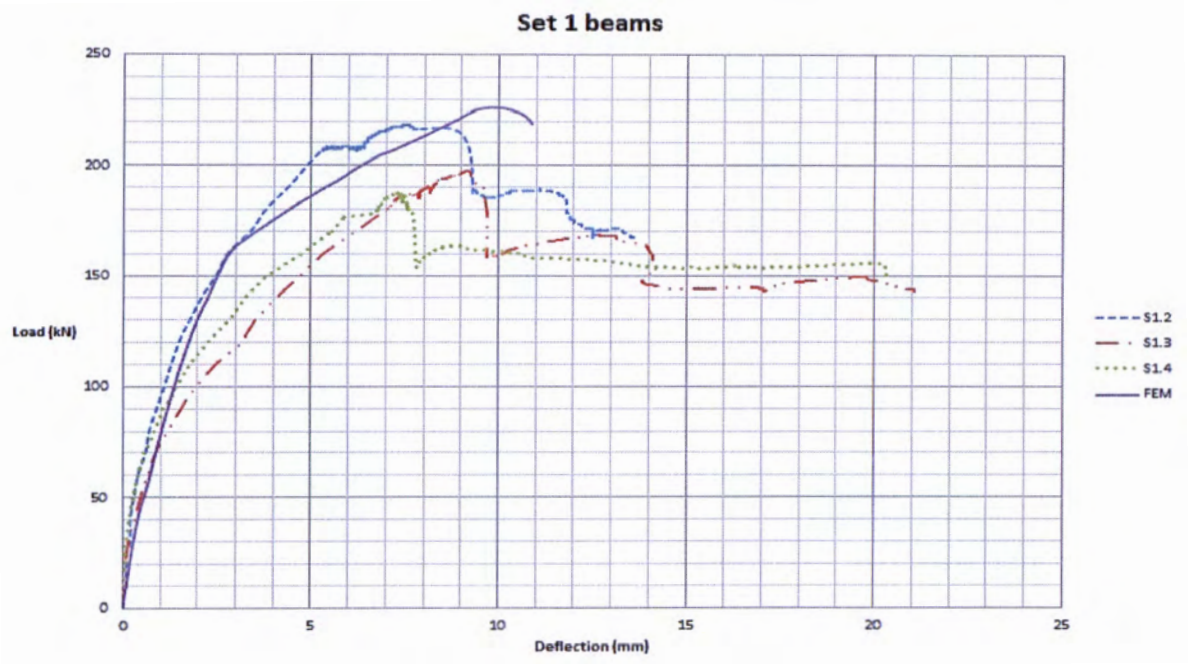

Figure 4.23: Load-deflection behaviour of RS experimental beams S1.2, S1.3 and S1.4 and FEM

The load-deflection behaviour of the RS beams with the 800mm damage extent (set 4) are shown in Figure 4.24 below. There was a good correlation of the experimental results and the FEM beam. The yield loads and peak loads were found to be higher than the control beam results. The load results for beams S4.1, S4.2 and S4.3 were 185kN, 218kN and 200kN respectively for the yield loadswhereas the peak loads were 196kN, 230kN and 217kN respectively.

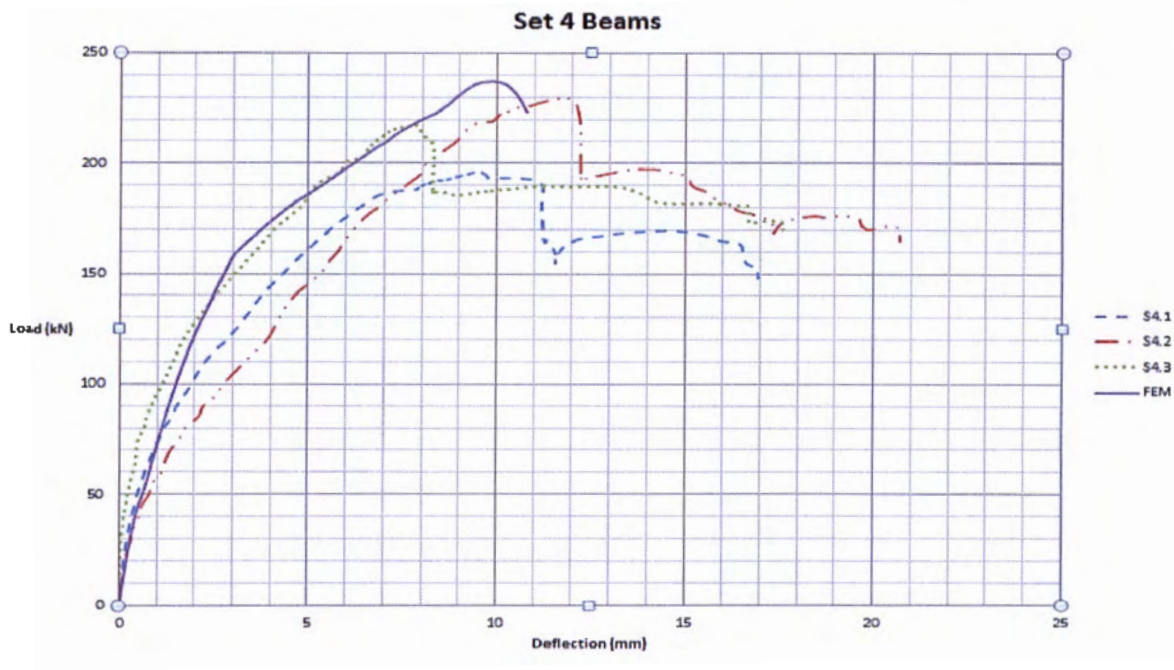

Figure 4.24: Load-deflection behaviour of RS beams S4.1, S4.2, S4.3 and FEM

Figure 4.25 and Figure 4.26 illustrate the load-deflection behaviour of the RS beams with the 1300mm (set 3) and 1800mm (set 2) damage extent, respectively. The yield loads and peak loads were found to be higher than the control beam results, with the exception of beam S3.4. The yield loads for RS beams S3.2 and S3.3 were 184kN and 223kN respectively; the peak loads results were 195kN and 224kN respectively. The RS Beam S3.4 had a higher yield load, of 171kN, and peak load, 172kN, than control beam C3 but lower yield and peak loads than beam C1.The load results for RS beams S2.2, S2.3 and S2.4 were 195kN, 223kN and 203kN respectively for the yield loads whereas the peak loads were 199kN, 235kN and 209kN respectively. The higher yield and peak loads results of the RS beams compared to the control beam results confirm an already well known fact of the ability of external strengthening to increase the strength of damaged reinforced concrete beams.

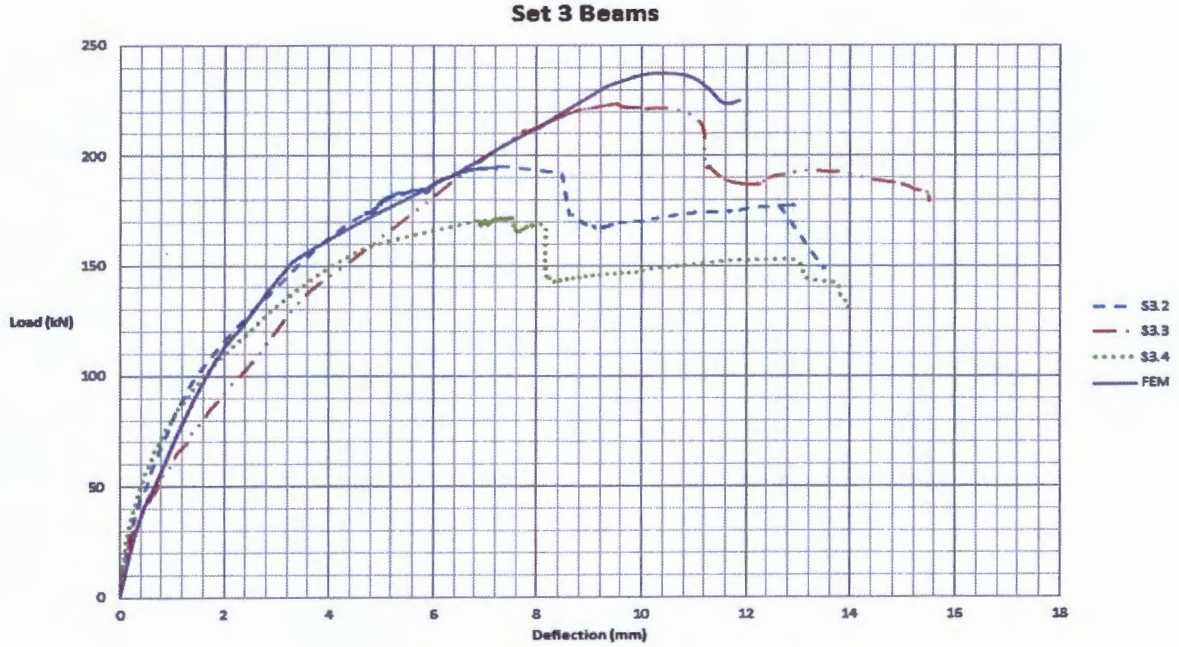

Figure 4.25: Load-deflection behaviour of RS beams S3.2, S3.3,S3.4 and FEM

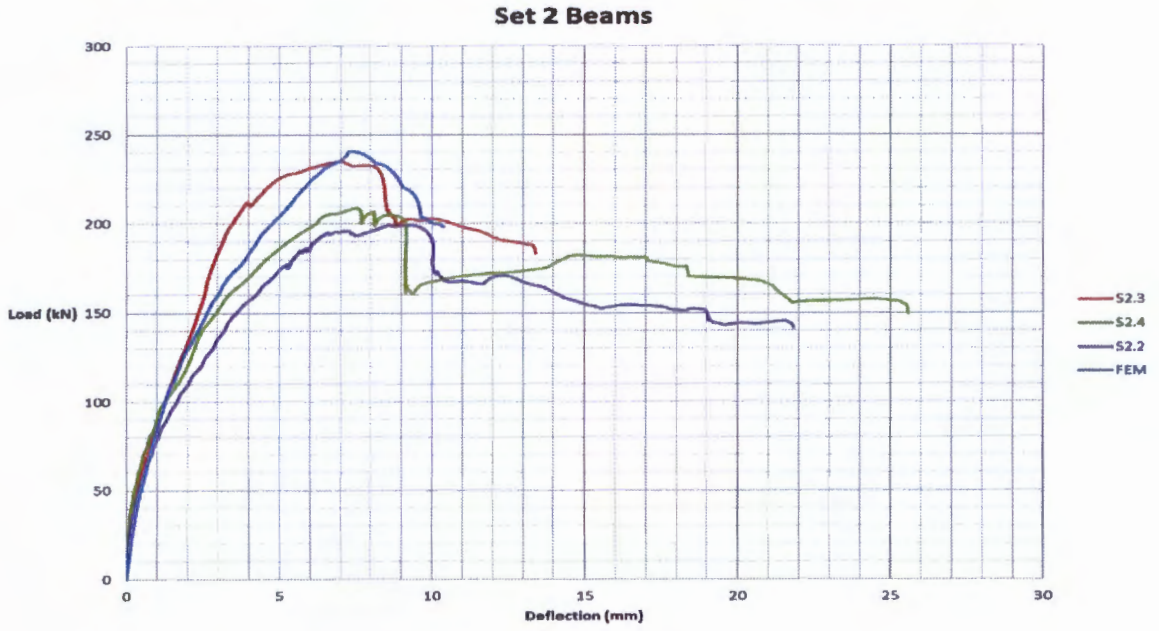

Figure 4.26: Load-deflection behaviour of RS beams S2.2, S2.3, S2.4 and FEM

The design method used, from Taljsten (2006), was successful in that the RS beams yielded before the debonding failure occurred. It was observed that debonding failure soon occurred after yielding for all RS beams. The debonding is depicted in the load deflection curves by the sudden drop in load carrying capacity at a specific displacement, refer to Figure 4.1. After debond-

ing the RS beams were loaded further, where it was noticed that the beams returned to what appeared as the load carrying capacity of the un-strengthened capacity of the damaged beams, up until crushing (ultimate) failure was observed.

4.3.3 Comparison of the different sets of beams to the control beam

Tables15 and 16 in Appendix E provide the average mid–span load deflection results of the repaired and strengthened beams and the control beam.

The post yield stiffness of the control beams (Figure 4.22) reached what appeared to be a plateau , after yielding, up to failure where the concrete in extreme compression zone underwent crushing failure. It was observed that identical beams yielded with different results. The difference in the load deflection behaviour of identical beams can be attributed to the difference in concrete micro-structure which results in different crack propagation path for each beam subsequently affecting stiffness results of the beams.

The combined retrofit method of patch repairs and strengthening seemed to have provided the desired effect of restoring the capacity of damaged beams, in fact the yield load results and peak loads were higher than the control beam results with the exception of beam S3.4. Repaired and strengthened (RS) beam S3.4 displayed a decrease in yield load of 0.5% and a decrease in peak load of 3.4%, the lower yield load and peak load. The deviation of beam S3.4 from the results of the other RS beams could have been caused by anything from irregularity of steel to the debonding failure nature of the RS beam. The rest of the retrofitted beams all displayed increases in yield load capacity in the range of 2.9% - 30% when compared to the average control beam yield load. The yield displacements of the RS beams were higher than that of the control beams average yield displacement of 4.5mm. The increase in the peak loads of the RS beams was in the range 5.3% - 32.0%.

The ductility results confirmed findings of past studies whereby the majority of repaired and strengthened beams had a lower ductility than the control beams. The debonding ductility and the ultimate ductility of the RS beams were in the range of 0.3 - 0.4 and 0.5-1 respectively, refer to Table 8. The decrease in ductility was caused by the brittle debonding failure of the CFRP.

4.3.4 The effect of damage length on yield load, peak load, rigidity and ductility

Patch repair combined with CFRP strengthening retrofit method restored the damaged beams load carrying capacity but reduced the ductility of the beams when compared to the control beams, refer to Table 9. After evaluating each of the RS beams results relative to the average control beam results the next stage was to evaluate the effect of damage length on the retrofitted beams. An evaluation was carried out on the average results of each set of beams in order to establish any patterns present. The main focus of this study was on the experimental results but the investigation was part of a larger study where finite element modeling (FEM) was also carried out. The specifics of the properties input into the FEM are not specified in this study as this was not the aim of this study but the FEM results, Table 10, were used in this discussion for comparison.

Table 9: average results compared to the control beams

Beam	Experimental yield load (%)	Peak load (%)	Rigidity (%)	Normalized ultimate ductility $\left(\frac{\mu_f}{\mu_y}\right)$	Normalized debonding ductility $\left(\frac{\mu_d}{\mu_y}\right)$
450mm	10,3	13	-20	0,72	0,33
800mm	17,2	20,4	-26,9	0,60	0,33
1300mm	12,2	10,6	-29,1	0,49	0,31
1800mm	20,6	20,4	-5.1	0,82	0,37

Table 10: Finite Element Modelling (FEM) results

Beam	FEM yield load (%)	FEM peak load (%)	Normalizeddebonding ductility	Post crack rigidity (kN/mm)
Control	0	0	1	15.6
450mm	10,2	23.8	1.17	31.9
800mm	13.1	27.32	1.08	30.6
1300mm	18.9	27.37	0.92	25.5
1800mm	9.6	-	-	-

The average yield and peak load results of the RS beams were higher than that of the average control beam results. The FEM results further confirmed the higher yield and peak load results.

4.3.4.1 The effect of damage length on yield load and peak load

Figure 4.27 shows the average yield load results for all the different groups of beams, as found in Table 9, for experimental beam results which increased by 10.3%, 17.2% and 20.6% for beams with the 450mm, 800mm and 1800mm patch repair respectively. The beam with the 1300mm patch repair had a yield load increase of 12.2% but was not increasing in proportion according to increasing damage extent; this was mainly due to the result of the outlier beam S3.4.

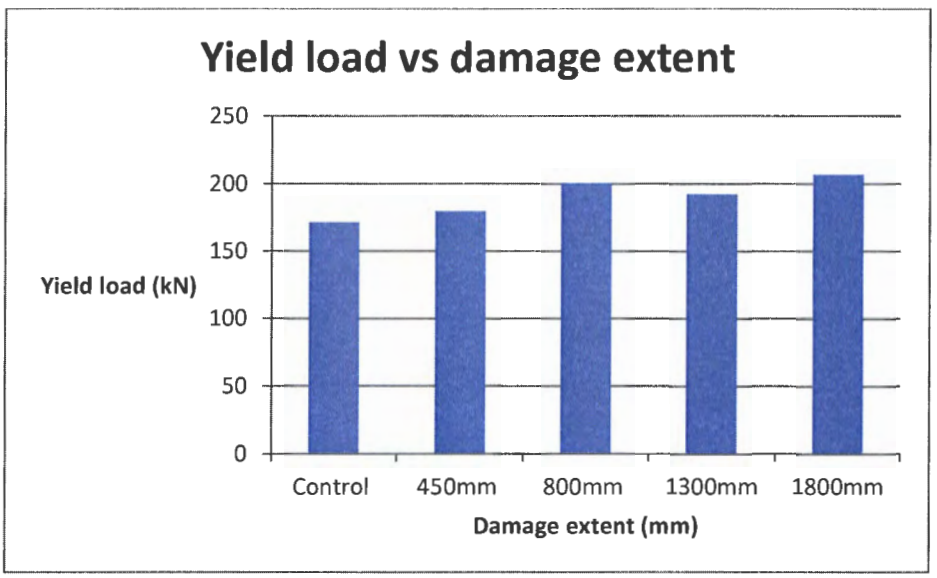

Figure 4.27: Average yield load results for the differentgroups of beams

The FEM yield load results from the load – strain curves correlated better with the experimental yield load results; as opposed to the FEM load-deflection results. A similar trend was observed in the FEM results with an increase in yield loads of 10.2%, 13.1% and 18.9% for beams with the 450mm, 800mm and 1300mm patch repair.

Similar to studies conducted by Malumbela et al. 2011 and Ray et al. 2011 the average peak loads of the RS beams were higher than the average control beam peak load, refer to Figure 4.28 below.

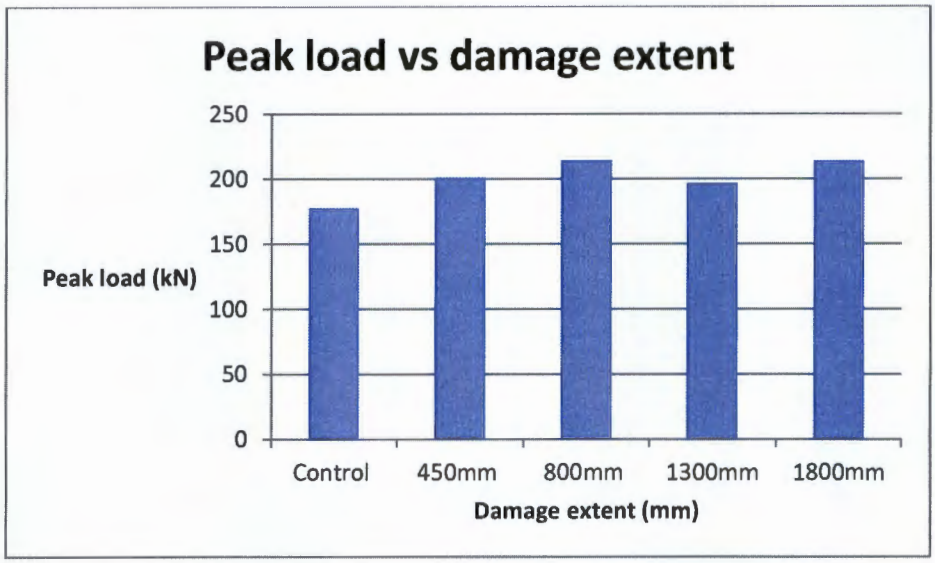

Figure 4.28: Average peak load results for the different groups of beams

It was observed that increasing damage lengths; 450mm, 800mm and 1800mm had a correlation to higher peak loads of 13%, 20.37%, 20.44% respectively. The peak load of the beam with the 1300mm damage length was 10.6% higher than the control beam but lower than all the other retrofitted beams, the set 3 result was affected by the S3.4 beam result. The FEM results also presented a similar trend to the experimental results with increases of 23.83%, 27.32% and 27.37% for beams with damage lengths of 450mm, 800mm and 1300mm respectively.

From the results a conclusion was drawn that the extent of damage was completely outweighed by the strength provided by the patch repair material. The increase in yield loads and peak loads for increasing patch repair lengths could have been due to the higher strength offered by the patch repair material, considering that the strengthening technique used was identical for all RS beams. Although the patch repair had more influence on the beam behaviour it is possible that if the degree of damage was increased from 5% to 15% the extent of damage may become a major influence on the RS beam behaviour than the repair materials.

4.3.4.2 The effect of damage length on ductility and rigidity of RS beams

The ductility results were in agreement with the findings from past studies in that the retrofitted beams were less ductile than the control beams. The ductility results of the RS beams is provided in Figure 4.29 below. The average normalized ultimate ductility results for the damage lengths of 450mm, 800mm and 1300mm appeared to be a declining with the vales 0.72, 0.60

and 0.49 respectively. The beam with the 1800mm damage length had the highest ultimate ductility value of 0.82 but was still less ductile than the control beam.

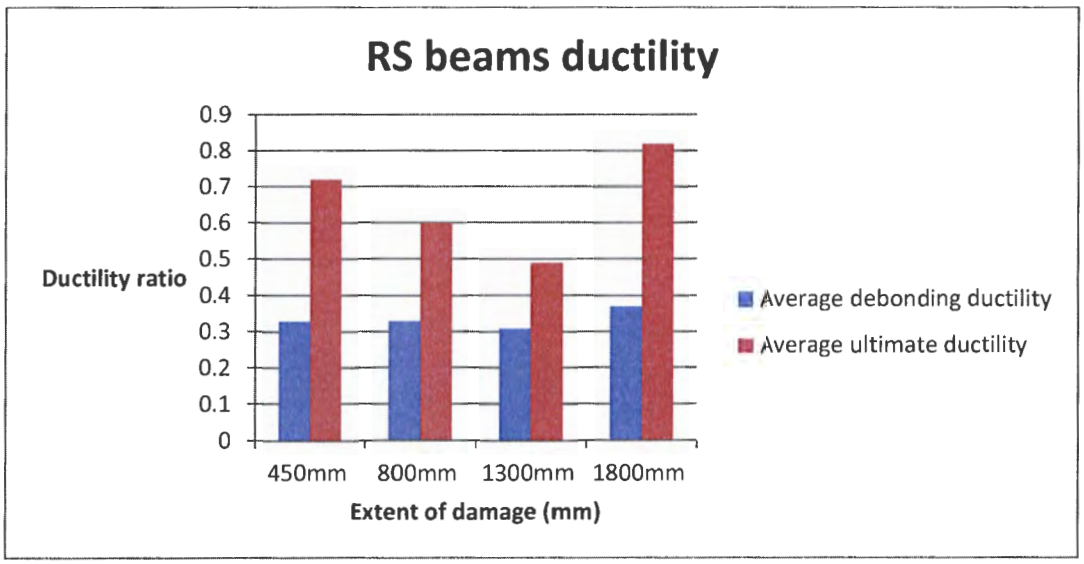

Figure 4.29: Ductility results for the RS beams

The experimental results made interpretation difficult with regards to the post cracking rigidity of the RS beams compared to the control beams, as was mentioned earlier. The experimental average rigidity results of the beams with the damage lengths of 450mm, 800mm and 1300mm indicated a decrease in rigidity of 20%, 26.9% and 29.1% respectively. In contrast the beam with the 1800mm damage length had the least decrease in rigidity of 5.1%. The decrease in rigidity of the retrofitted beam contradicts observations that have been made in other studies by Masoud et al. (2008) and Ray et al. (2011). The lower stiffness of the retrofitted damaged beams in comparison to the control beams could be due to the relation of the concrete used to the size of CFRP plate. In this experiment the concrete used was generally higher than that used in past experiments. The higher concrete strength could mean that the concrete had a higher stiffness in relation to the CFRP plate stiffness thus making strengthening less effective with regards to rigidity. A similar pattern was observed in FEM rigidity results where there was a decrease in rigidity for increasing damage extent; 450mm, 800mm and 1300mm. The FEM control beam was however less rigid than the RS beams which contrasts the experimental results.

4.3.4.3 The effect of damage length on the design

The behaviour of the RS beams was very interesting and may have implications in design. The beams with large damage lengths were weaker and therefore require a higher amount of FRP area. When designing for the amount of FRP required for the damaged beams equation 1 of appendix B was used. In the equation the area of FRP is equated to the moment loss due to the degree of corrosion. The problem in the design is that the damage length is assumed to have no effect on the beams behaviour whereas we have seen that damage length does have an impact on the peak load and yield load. A reduction factor could be introduced to account for the damage length, where the damaged beams with the long damage lengths should have a lower moment capacity. The lower moment capacity of the damaged beams with large damage lengths would require a larger amount of FRP such that the behaviour is similar to the damaged beams with the smaller damage length.

4.4 Neutral Axis

The horizontal strains on the concrete surface were measured at mid-span as was mentioned in the methodology. The strain measurements were disrupted by the propagation of cracks in-between the demec targets, therefore only the compression strain measured near the extreme compression face was used. The measured compression strain at mid-span was also used to calculate the strain in the tension steel, compression steel and CFRP. An attempt was also made to capture vertical strains at the concrete substrate – patch repair interface for some of the retrofitted beams. The mid-span strains results were collected from both sides of the reinforced concrete beams and the average used as a better representation of the strain profile across the width of the beams.

The NA presented in Table 11 is measured from the extreme compression face going down the depth of the beam. The NA was calculated from horizontal force equilibrium at the mid-span section, similarly to the design process calculation of the NA at crushing failure of concrete after yielding of tensile reinforcement.

Table 11: Average neutral axis results at first crack and at tension steel yielding

Beam	Yield neutral axis (mm)	Calculated neutral axis at ultimate failure (mm)	Compression rebar strain	Tension rebar strain
control	49.3	41.6	890	2917
450mm	64.51	56.7	1471	3341
800mm	55.02	56.7	999	2823
1300mm	59	56.7	1218	3042
1800mm	61.88	56.7	1363	3199

The depth of the neutral (NA) axis shifted towards the extreme compression face with increasing loads. The average NA of the control beams occurred at 49.3mm, this is compared to the expected NA of 41.6mm at ultimate failure by crushing of concrete after yielding of tensile steel. A similar pattern was observed with the RS beams as the NA at the point of yielding of tensile steel was higher than the predicted NA at failure. The increasing of the NA with increasing loads was similar to what was observed by Tigeli et al. (2013). Although for the control beam Tigeli et al. (2013) observed that the NA of the neutral axis was unchanged.

The depth of the NA was higher for RS beams than the control beams. Again this result was similar to the study carried out by Tigeli et al. (2013)

4.5 Chapter summary

This chapter presented the experimentaland FEM results of the control beams and the RS beams.

The results were presented in terms of cracking behaviour, load-deflection and strain behaviour of the concrete. The cracking behaviour initiated with vertical flexural cracks but as the load increased flexural shear cracks started to develop in the direction of the applied loads. The addition of the CFRP in flexure changed the cracking behaviour slightly; the first crack developed earlier for a larger damage extent. It was also observed that for the average crack spacing of RS beams was lower than the control beams; furthermore for increasing damage extent there was a decrease in average crack spacing. The largest crack width, in the maximum moment zone, at failure was larger for control beams as opposed to the RS beams. The RS beams failed by the debonding of CFRP plate due to epoxy splitting subsequently by crushing of concrete in the extreme concrete compression zone.

The load deflection behaviour of the RS beams was in agreement with literature. The addition of CFRP plate increased the yield and peak loads of the RC beams despite induced damage in the beams to simulate accelerated corrosion. The RS beams were less ductile than the control beams. The extent of damage did have an effect on the behaviour of RS beams. There was an increase in yield loads for increasing damage extent, with the exception of the beams with the 1300mm damage, for both the experimental results and the FEM. There was also an increase in peak loads for increasing damage extent. A decrease in debonding and ultimate ductility was observed for increasing damage extent with the exception of the beams with the 1800mm damage length. The rigidity of the RS beams was less than the control beams; with the trend indicating decreasing rigidity for increasing damage extent.

The neutral axis results at yield were also observed; the addition of CFRP seems to have increased the neutral axis depth. For beams with the damage extent of 450mm, 1300mm and 1800mm damage there was an increase in neutral axis depth

Chapter 5

5. Conclusions and Recommendations

In the past reinforced concrete beams have been found to be structurally deficient during their service life. There are various reasons that have been provided to explain the causes of the premature deterioration of beams i.e. corrosion of reinforcement, accidents, poor design and workmanship. As such rehabilitation and retrofitting of structural deficient reinforced concrete beams has become a popular remedial measure instead of complete replacement of the deficient beams, wherever possible.

The aim of this dissertation has been to study the behaviour of reinforced rectangular concrete beams subjected to simulated acceleration corrosion damage and subsequently repaired with cementitious patch repair mortar and externally strengthened using CFRP. The study was spurred by a gap in literature where it was noted that there are not many studies on patch repaired and strengthened beams.

The study was conducted using a total of 15 RC beams of the dimensions 2000mm x 254mm x 155mm, 3 were control beams the remaining 12 beams were damaged by simulated acceleration corrosion subsequently patch repaired and strengthened. Past literature has used accelerated corrosion to represent the natural corrosion that has been observed on the deteriorating beams. Reinforced concrete beams develop concrete cracks during their service life due to shrinkage and cracking of concrete. Cracked concrete allows for exacerbated deterioration of the passivation layer caused by a unique set of conditions (presence of moisture, chlorides and oxygen) which allows for the formation of a chemical reaction that neutralizes the alkaline properties of concrete. Pitting corrosion then occurs where there is no passivation layer. In some instances maybe in an accident situation; larges pieces of concrete would dismantle from the reinforced concrete member thereby exposing the reinforcement to corrosion. Elgarf (1999) argues that when localized pitting has extended too many sites it would result in extensive and relatively uniform levels of corrosion. It is the uniform level of corrosion mentioned by Elgarf (1999) that is investigated in this study; it is also the same uniform corrosion that has been investigated past studies.

The damaged beams were subjected to 5% simulated corrosion. Four damage extents were investigated: 450mm, 800mm, 1300mm and 1800mm. For each damage extent there were three identical beams. The damaged beams were patch repaired and externally strengthened on the beams soffit with CFRP.

There was a good correlation between the experimental results and numerical results that were obtained in a study conducted by Mundeli and Moyo (2014). In the experiment the beams were all tested statically under four point loading. Crack formation was mapped with a marker at intervals of 10kN. The mid-span load deflection results and strains at mid-span in compression zone were collected. The tested beams all failed as predicted by the design procedures used.

5.1 Cracking behaviour

All 15 beams underwent flexural failure whereby the tensile steel yielded and crushing failure of concrete occurred at the end.

The crack propagation for control beams initiated with flexural cracks near mid-span. As the loads increased more flexural cracks developed in the shear span in the direction of the applied loads. After yielding almost no new cracks formed but the widening of the near mid-span region occurred. Widening of cracks at occurred at mid-span, crushing failure then occurred at the extreme compression zone near the load application point.

The crack propagation sequence of the RS beams was similar to the control beam behaviour but prior to concrete crushing there was intermediate crack debonding failure of CFRP due to epoxy splitting. Debonding failure was caused by the interfacial stresses induced by the flexural cracks. The influence of voids could not be detected towards debonding failure.

The experimental average cracking load of the control beams was higher than the rest of the RS beams; this was confirmed by the FEM results. There was a decrease in cracking loads for increasing damage extent. The average crack spacing of the control beams was found to be higher than that of the RS beams; furthermore it was observed that there was a decrease in average crack spacing for increasing damage extent.

5.2 Load-deflection behaviour

All the patch repaired and strengthened beams had higher yield loads and peak loads in the range of 2.9%-30 and 5.3%-32%, respectively, than the control beams. The increased strength of the patch repaired and strengthened beams were at the expense of ductility, the debonded ductility was in the range of 0.3-0.4 whereas the ultimate ductility was in the range of 0.5-1.

Both the experimental and numerical results indicate that the extent of damage does have an influence on the load deflection behaviour of RS beams. It was observed that for increasing patch damage extents; 450mm, 800mm and 1800mm there was an increase in average yield loads and average peak loads. RS beam S3.4 was identified as the cause for the deviation of set 3 beams from the rest of the RS beams. The FEM load-deflection results displayed similar trends to the experimental results but the yield load results were quite the opposite. Although the FEM yield load results from the load-strain results were in agreement with the experimental results where there was an increase in yield loads for increasing damage extent of 450mm, 800mm and 1300mm. The FEM peak load results from the load-deflection curve were also found to increase for increasing damage extent of 450mm, 800mm and 1300mm.

The increase in strength of the RS beams compared to the control beams occurred at the expense of ductility. For increasing damage extents; 450mm, 800mm and 1300mm there was a decrease in average ductility. Likewise with the FEM results the ductility was found to be decreasing for increasing patch repair lengths of 450mm, 800mm and 1300mm. The control beam was less rigid than the RS beams according to the FEM results; it was also observed that for increasing damage extent for the 450mm, 800mm and the 1300mm there was a decrease in rigidity. The same decrease in rigidity was observed in the average experimental results for increasing damage extent of 450mm, 800mm and 1300mm although the control beam was stiffer than the RS beams.

5.3 Neutral axis

The neutral axis of the control beam was higher than the RS beams. For increasing damage extent of 450mm, 800mm and 1300mm there was a decrease in the neutral axis when the yielding of the tensile steel reinforcement occurred. The neutral axis at yield was higher than the neutral axis at failure for all the beams which shows that the neutral axis decreases with increasing load up to failure.

5.4 Summary

Much of the concluded work is based on physical observations that were made during the testing procedure. Other results were collected electronically to develop the load deflection behaviour of the tested beams. Comparison of the results obtained in this study cannot be made to previous studies as this is the first time a study of this nature has been conducted. The behaviour of RS beams are indeed affected by the length of damage extent and have to be considered from a design perspective. The relation of presence of voids in relation to the debonding nature of RS beams has not been established but further research in this regard would be advised. The addition of CFRP in flexure does increase the strength of the damaged beams beyond their original capacity if designed for accordingly.

5.5 Recommendations

On the basis of the findings and conclusions, the following recommendations are made:

- Research into the effect of different degrees of corrosion 10% and 15%, by means of accelerated corrosion when combined with varying damage extents.
- Investigate the effect of sustained loading on the RS beams with varying levels of damage. Sustained loading is a more realistic loading scenario encountered on the bridge structures.
- Investigate the effect of damage extent on shear strengthening of rectangular beams.
- Using intermittent anchorage along the span of the beam could prevent the debonding failure, therefore indirectly utilising the CFRP properties to its maximum potential.
- Future studies should investigate the progression of voids for they may have a role in the debonding behaviour of strengthened beams. Monitoring voids can be conducted in-between the load increments.
- Using thermographic cameras to qualitatively define defects. This would require the design of a testing setup which will leave enough space for thermographic observations. Consultation with a specialist in thermography is also advised.
- Observations should be made on strains in the tensile longitudinal reinforcement and strains of the CFRP plate at mid-span.
- To minimise any mistakes during the casting phase concrete should be ordered on the same day and all the beams cast on the same day. This will decrease the variations in results with the same configuration.
- The use of strain gauges to monitor the neutral axis, tensile steel strains and the CFRP strain profile. This would provide a wider picture into the behaviour of strengthened damaged beams. The strain measurements at the mid-span of the beams would be the most important.
- Vertical strain measurements at the interface of the repair mortar and the concrete substrate
- The use of high speed camera to capture the crack propagation patterns on the reinforced concrete beams

5.6 Limitations

The following limitations to the research conducted were identified below;

- The varying concrete strengths increased the complexity of the study further, in future the same concrete mix, ordered from mixing plants
- Strain gauges on the tensile steel, concrete surface and CFRP would have provided better and more information on the behaviour of patch repaired and strengthened beams
- Thermographic monitoring of the epoxy bond at the CFRP-concrete interface could provide information on the source of debonding failure i.e. flexural cracks or discontinuities mainly voids

Bibliography

Addis, B. and Goodman, J, 2009. Concrete mix design. In Fulton's concrete technology. 9th ed. G. Owens, Eds. Cape Town: Cement and Concrete Institute.

Allen Ross, D. M. 1999. Strengthening of reinforced concrete beams with externally bondedcomposite laminates. ACI Structural Journal, 8.

Almusallam, A. a., 2001. Effect of degree of corrosion on the properties of reinforcing steel bars. Construction and Building Materials, 15(8), pp.361–368.

Almusallam, A.A. and Al-gahtani, A.S. 1996. Effect of reinforcement strength corrosion on bond. , 10(2), pp.123–129.

Al-Saidy, A. H., Al-Harthy, A. S., Al-Jabri, K. S. and Al-Shidi, N. M. 2010. Structural performance of corroded RC beams repaired with CFRP sheets. Composite Structures 92.

ASCE, M. Bonacci, J.F. and Maalej, M. 2001. Behavioural trends of RC beams strengthened with externally bonded FRP. Journal of composites for construction, pp.102–113.

ASCE, M., Macri, B.M. and Bren, S. F. 2004. Effect of Carbon-Fibre-Reinforced Polymer Laminate Configuration on the Behaviour of Strengthened Reinforced Concrete Beams.

Ashour, A. F., El-Refaie, S. A. and Garrity, S. W. 2004. Flexural strengthening of RC continuous beams using CFRP laminates. Cement and Concrete Composites, 26(7), pp.765–775.

Balaguru, P., Nanni, A. and Giancaspro, J. 2009. FRP Composites for reinforced and presterssed concrete structures. New York: Taylor and Francis.

Ballim, Y., Alexander, M. and Beushausen, H. 2009. Durability of concrete. In Fulton's concrete technology. 9th ed. G. Owens, Eds. Cape Town: Cement and Concrete Institute.

Bank, L. C. 2006. Compositers for construction: Structural design with FRP materials. John Wiley and Sons, Inc.

Benjeddou, O. Ouezdou, M. Ben and Bedday, A. 2007. Damaged RC beams repaired by bonding of CFRP laminates. Construction and Building Materials, 21(6), pp.1301–1310..

Bentur, A.Berke, N. Diamond, S. 1997. Steel corrosion in concrete: fundamentals and civil engineering practice. London: E and FN Spon

Bisby, L. A., Ranger, M. and Williams, B. K. 2003. Reinforced concrete structures with fibre-reinforced polymers. ISIS Canada design manual no. 3. Canadian Network of centres of excellence on intelligent sensing for innovative structures, Winnipeg Manitoba Canada.

Bonacci, J.F., and Maalej, M. 2000. Externally bonded fibre - reinforced polymer for rehabilitation of corrosion damaged concrete beams. ACI structural Journal,97(5).

Buyukozturk, O., Gunes, O. and Karaca, E. 2004. Progress on understanding debonding problems in reinforced concrete and steel members strengthened using FRP composites. Construction and Building Materials, 18(1), pp.9–19.

Cabrera, J. G. 1996. Deterioration of concrete due to reinforcement steel corrosion. Cement and Concrete Composites, 18(1), pp.47–59.

Cairns, J., Plizzari, G.A., Du, Y., Law, D. W. and Franzoni, C. 2005. Mechanical properties of corrosion damaged reinforcement, ACI Materials Journal.

Camata, G., Spacone, E. and Zarnic, R. 2007. Experimental and nonlinear finite element studies of RC beams strengthened with FRP plates. Composites Part B: Engineering, 38(2), pp.277–288.

Ceci, A.M., Casas, J.R. and Ghosn, M. 2012. Statistical analysis of existing models for flexural strengthening of concrete bridge beams using FRP sheets. Construction and Building Materials, 27(1), pp.490–520.

David, E., Djelal, C. and Buyle-Bodin, F. 1998. Repair and strengthening of reinforced concrete beams using composite materials.2nd international PhD symposium in civil engineering Bhudapest , pp.1–8.

Elgarf, S. M. 1999. Flexural strength of concrete beams with corroding reinforcement. ACI Structural Journal, 12.

Esfahani, M.R., Kianoush, M.R. and Tajari, A. R. 2007. Flexural behaviour of reinforced concrete beams strengthened by CFRP sheets. Engineering structures 29, pp.2428–2444.

Fayyadh, M. M. and Abdul Razak, H. 2012. Assessment of effectiveness of CFRP repaired RC beams under different damage levels based on flexural stiffness. Construction and Building Materials, 37, pp.125–134.

Galietti, U., Lurprano, V., Nenna, S., Spangnolo, L. and Tundo, A. 2007. Non-destructive defect characterization of concrete structures reinforced by means of FRP. Infrared physics and technology 49, pp. 218-223.

Hibbler, R. C. 2008. Mechanics of materials 7th edition. Pearson educuation South Asia Pte Ltd.

Hollaway, L. C. and Leeming, M. B.1999. strengthening of reinforced concrete structures using externally bonded composites in structural and civil engineering. Cambridge: Woodhead publishing limited.

Hollaway, L.C. 1999. An experimental study of the influence of plate end anchorage carbon fibre composite plates used to strengthen reinforced concrete beams. COMPOSITE STRUCTURES.

Robberts, J. M. and Marshall, V. 2008.Analysis and design of concrete structures.University of Pretoria.

Khalifa, A. and Nanni, A. 2002. Rehabilitation of rectangular simply supported RC beams with shear deficiencies using CFRP composites. Construction and building materials 16, pp.135–146.

Lai, W. L., Kou, S. C., Poon, C. S., Tsang, W. F. and Lee, K. K. 2013. A durability study of externally bonded FRP-concrete beams via full-field infrared thermography (IRT) and qausi-static shear test. Construction and building materials 40, pp. 481-491.

Lee, H. S., Noguchi, T. and Tomosawa, F. 2002. Evaluation of the bond properties between concrete and reinforcement as a function of the degree of reinforcement corrosion. Cement and Concrete Research, 32(8), pp.1313–1318.

Lu, X.Z.,Teng, J. G., Ye, L. L. and Jiang, J. J. 2005. Bond–slip models for FRP sheets/plates bonded to concrete. Engineering Structures, 27(6), pp.920–937.

El Maaddawy, T. and Soudki, K., 2005. Carbon-Fibre-Reinforced Polymer Repair to Extend Service Life of Corroded Reinforced Concrete Beams. Journal of composites for construction, pp.187–195.

Maierhofer, Ch., Arndt, R., Rollig, M., Rieck, C., Walther, A., Scheel, H. and Hillemeier, B. 2006. Applicationof impulse-thermography for non-destructive assessment of concrete structures. Cement and concrete composites 28, pp. 393-401.

Maldague, X., Galmiche, F. and Ziadi,A.2002. Advances in pulsed phase thermography. Infrared Physics and Technology, 43(3-5), pp.175–181.

Maldague, X. P. 1993. Nondestructive evaluation of materials by infrared thermography. London: Springer-Verlag London Limited.

Marco Arduini and Antonio Nanni, M. A. 1997. Behaviour of precracked reinforced concrete beams strengthened with carbon FRP sheets. Journal of composites for construction, 10.

Malumbela, G., Alexander, M. G. and Moyo, P., 2011, Load-bearing capacity of corroded, patched and FRP repaired RC beams. Magazine of concrete research 63(11): 797-812

Malumbela, G., Alexander, M. G. and Moyo, P., 2011. Model for cover cracking of RC beams due to partial surface steel corrosion. Construction and Building Materials, 25(2), pp.987–991.

Malumbela, G., Alexander, M. G. and Moyo, P., 2010. Variation of steel loss and its effect on flexural capacity of RC beams corroded and repaired under load. Construction and Building Materials, 24:1051–59.

Mangat, P.S. and Elgarf, M .S. 1999. Bond characteristics of corroding reinforcement in concrete beams.Materials and structures, Vol. 32, pp.89–97.

Morgan, D.R. et al., 1996. Compatibility of concrete repair materials and systems. Construction and building materials, Vol. 10(1), pp 57 - 67.

Mundeli, S. and Moyo, P. 2014. Behaviour of RC beams patch repaired and strengthened with FRP composites: A numerical study. University of Cape Town.

Neagoe, C.A., 2011. Concrete beams reinforced with CFRP laminates. Departament Resistencia de Materials i Estructures a l'Enginyeria (RMEE).

Nounu, G. and Chaudhary, Z.-U.-H., 1999. Reinforced concrete repairs in beams. Construction and Building Materials, 13(4), pp.195–212.

Obaidat, Y.T. et al., 2011. Retrofitting of reinforced concrete beams using composite laminates. Construction and Building Materials, 25(2), pp.591–597.

Owens, G. Ed. 2012. Cementitious materials. Fundamentals of concrerte 2nd edition Cape Town. Cement and Concrete Institute.

Pešić, N. and Pilakoutas, K. 2003. Concrete beams with externally bonded flexural FRP-reinforcement: analytical investigation of debonding failure. Composites Part B: Engineering, 34(4), pp.327–338.

Río, O. et al., 2005. Behaviour of Patch-Repaired Concrete Structural Elements under Increasing Static Loads to Flexural Failure. Journal of materials in civil engineering, pp.168–178.

Saadatmanesh, H. Ehsani, M. 1991. RC beams strengthened with GFRP plates. I: experimental study. ASCE J Struct Eng 1991; 117:3417-33.

Sahamitmongkol, R. et al., 2008. Flexural Behavior of Corroded RC Members with Patch Repair – Experiments and Simulation. Journal of advanced concrete technology, Vol. 6(2), pp.317–336.

Shahawy, M. A., Arockiasamy, M., Beitelman, T. andSowrirajan, R. 1996. Reinforced concrete rectangular beams strengthened with CFRP laminates. Composites Part B, 225-233.

South African National Standards. 1994. Code of practice - structural use of concrete: Part 1: reinforced concrete. (SANS10100-1: 1994). Pretoria: SANS Standards.

South African National Standards. 2006. Concrete tests - Compressive strength of hardened concrete. (SANS5863: 2006). Pretoria: SANS Standards.

Schlaich, J., Schiifer, K. and Jennewein, M. 1991. using strut-and-tie models. PCI journal.

Smith, S.. and Teng, J. 2002. FRP-strengthened RC beams. I: review of debonding strength models. Engineering Structures, 24(4), pp.385–395.

Smith, S.T. and Teng, J. G. 2001. Interfacial stresses in plated beams. Engineering Structures 23(7), pp.857–871.

Spadea, F. B. 1998. Structural behaviour of composite reinforced concrete beams with externally bonded CFRP. Journal of composites for construction, 10.

Seracino, R. 2004. FRP Composites in Civil Engineering. 2nd international conference on FRP composites in civil engineering, CICE-2004 Adelaide, Australia. Balkema Publishers.

Taljsten, B. 2006. FRP strengthening of existing concrete structures: design guidline. Lulea: Lulea University printing office.

Tigeli, M., Moyo, P. and Beushausen, H. 2011. Behaviour of corrosion damaged reinforced concrete beams strengthened using CFRP laminates. Proceeding international symposium on nondestructive testing of materials and structures, NDTMS-2011, Istanbul, Turkey.

Toutanji, H., Zhao, L. and Zhang, Y. 2006. Flexural behaviour of reinforced concrete beams externally strengthened with CFRP sheets bonded with an inorganic matrix. Engineering Structures, 28(4), pp.557–566.

Triantafillou, T. and Plevris, N. 1992. Strengthening of RC beams with epoxy-bonded fibre-composite materials. Material structures25, pp. 201-211.

[Online] Available from: http://www.microtech.co.za/flir_products.htm [Accessed 1st October 2013].

Appendices

A) Appendix A: Design of rectangular reinforced concrete beam

The beam design was in accordance with SANS10100-1. The FRP design guideline of choice was that by Taljsten (2006).

The beams were designed with the following assumptions according to SANS10100-1:

- Plane sections remain plane which relates to Bernoulli's formula
- Simplified stress block was chosen
- For a cracked cross section the tensile concrete was ignored
- Perfect bonds were assumed for steel with concrete and reinforcement

The RC beam was designed in accordance with the ultimate limit state specifications of SANS 10100-1, Edition 2.2, 2000. The beam has been designed under-reinforced so as to ensure yielding of the steel.

Ultimate limit design:

The design is for four point loading scenario, where the distance in between the loads centre to centre is 450mm and the shear span is 675mm. The distance in between the supports is 1800mm.

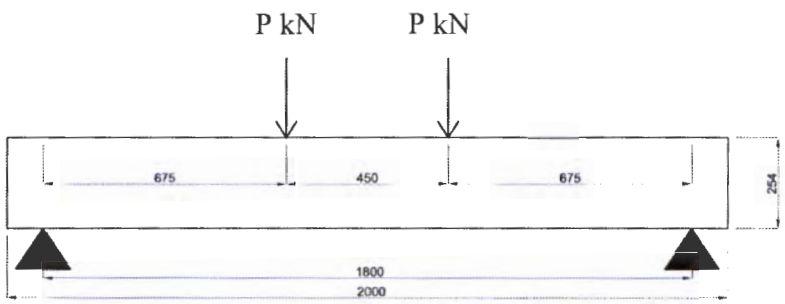

Figure A.1: Dimensions (mm) of beam span

Self-weight of beam (DL) = γ_c x volume

= 24kN / m^3 x 2 x 0.155 x 0.254

= 1.9kN

LL = 80kN (estimation)

Load combination = 1.6LL + 1.4DL

= 1.6(80) + 1.4(1.9)

= 129.15

» 130kN

(each load = 65kN)

Design for flexure:

M_{max} = 0.675 x 65 = 44kNm

f_{cu} = 50 N/mm^2

f_y= 502 N/mm^2

f_y' = 250 N/mm^2

γ_m = 1.15

b = 155mm

h = 254mm

cover = 25mm

K'= 0.156 (redistribution of bending moments does not exceed 10%)

Estimate compression reinforcement diameter of 8mm

Estimate tension reinforcement diameter of 20mm

Estimate shear link diameter of 8mm

∴d'= cover + diameter of shear links + 0.5(diameter of compression reinforcement)

= 25 + 8 + 0.5(8)

= 37mm

∴d = h – cover – diameter of shear links – 0.5(diameter of tension reinforcement)

=254 – 25 – 8 – 0.5(20)

= 211mm

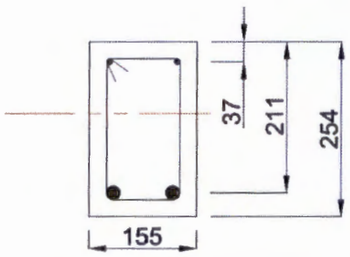

Figure A.2: Dimension (mm) of compression and tension reinforcement

$$K = \frac{M}{bd^2 f_{cu}} = \frac{44 \times 10^6}{155 \times 211^2 \times 50} = 0.128$$

K ≤ K' ∴ compression steel is not required; however 2 compression steel bars of 8mm diameter (2Y8) will be included to hold up the shear links,

∴A_s'=100.5mm^2

$$z = d(0.5 + \sqrt{0.25 - \frac{K'}{0.9}} = 211\left(0.5 + \sqrt{0.25 - \frac{0.156}{0.9}}\right) = 164mm$$

z ≤ 0.95d = 200mm

$$A_s = \frac{M}{0.87 f_y z} = \frac{44 \times 10^6}{0.87 \times 502 \times 164} = 614mm^2$$

∴ provide 2Y20 bars (A_s=628mm^2)

Check:

$$f_s = \frac{2}{3} f_y \times \frac{A_{s,req}}{A_{s,prov}}$$

$$mf = \frac{2}{3} \times 502 \times \frac{614}{628}$$

$$= 327\ N/mm^2$$

$$= 0.55 + \frac{477 - f_s}{120\left(0.9 + \frac{M}{bd^2}\right)}$$

$$= 0.55 + \frac{477 - 327}{120\left(0.9 + \frac{44 \times 10^6}{155 \times 211^2}\right)}$$

$$= 0.722$$

$$\frac{l}{d} = \frac{1800}{211} = 8.5$$

$$\frac{l}{d} = 8.5 < 20mf = 14.44$$

(therefore ok)

Design for shear:

M_{max}= 44kNm

V = 65kN

f_{cu} = 50 N/mm^2

f_{yv}= 250 N/mm^2

γ_m= 1.25

a_v = 675mm

d = 211mm

$$2.5 < \frac{a_v}{d} = 3.2 < 6$$

∴flexural cracking will be the most likely mode of shear failure

$$v = \frac{V}{bd} = \frac{65 \times 10^3}{155 \times 211} = 1.99\ N/mm^2 < 4.75\ N/mm^2 < 0.8\sqrt{f_{cu}} = 5.66$$

$$v_c = \frac{0.75}{\gamma_m}\left(\frac{f_{cu}}{25}\right)^{\frac{1}{3}}\left(\frac{100A_s}{bd}\right)^{\frac{1}{3}}\left(\frac{400}{d}\right)^{\frac{1}{4}} = \frac{0.75}{1.25}\left(\frac{50}{25}\right)^{\frac{1}{3}}\left(\frac{100 \times 628}{155 \times 211}\right)^{\frac{1}{3}}\left(\frac{400}{211}\right)^{\frac{1}{4}} = 1.10$$

$$v = 1.99 > (v_c + 0.4) = 1.5$$

∴ provide links along the whole length of the beam and

$$A_{sv} = \frac{b \times s_v (v - v_c)}{0.87 f_{yv}}$$

Using $A_{sv} = 2\frac{\pi D^2}{4} = 2 \times \frac{\pi \times 8^2}{4} = 100.5mm^2$

and solving for S_v:

$$s_v = \frac{A_{sv} \times 0.87 \times f_{yv}}{b(v - v_c)}$$

$$= \frac{100.5 \times 0.87 \times 250}{155(1.99 - 1.10)}$$

$$= 158.5mm > 0.75d = 158.3$$

∴ provide 24Y8 shear links at minimum spacing of 80mm so as to ensure the mitigation of shear failure.

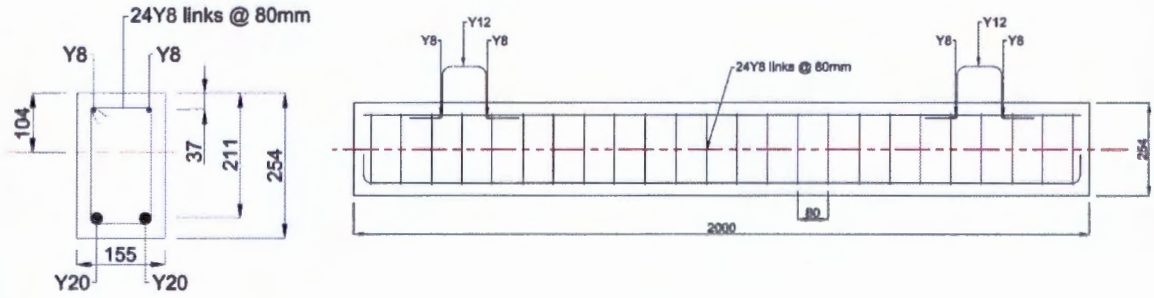

Figure A.3: Layout of reinforcing steel

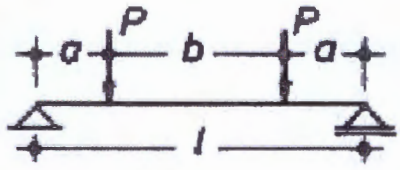

Figure A.4: Point load configuration

E_c = 30 GPa

E_s= 200 GPa

$l = 1800\text{mm}$

$a = 675\text{mm}$

$$\alpha_e = \frac{E_s}{E_c} = \frac{200}{30} = 6.67$$

$$I = \frac{bh^3}{12} + (\alpha_e - 1)(A_s + shift^2) + (\alpha_e - 1)(A_s' + shift^2)$$

$$= \frac{(155)(254)^3}{12} + (6.67 - 1)(596.9 + 107^2) + (6.67 - 1)(100.5 + 67^2)$$

$$= 211.8 \times 10^6\, mm^4$$

$$\delta = \frac{Pl^3(3\alpha - 4\alpha^3)}{24E_cI} \qquad where \quad \alpha = \frac{a}{l} = \frac{675}{1800} = 0.375$$

$$\delta = \frac{(65 \times 10^3)(1800)^3(3(0.375) - 4(0.375)^3)}{24(30 \times 10^3)(211.8 \times 10^6)}$$

$$\delta = 2.27mm < \frac{L}{d} = \frac{2000}{211} = 9.5mm$$

B) Analysis of reinforced concrete beam

$$x = \frac{A_s \times 087 f_y - A_s' fy}{0.45 f_c b} = 99mm \tag{B1}$$

$$\frac{d'}{d} = \frac{37}{211} = 0.18 < 0.2 \tag{B2}$$

$$\frac{d'}{x} = \frac{37}{99} = 0.37 < 0.5 \tag{B3}$$

$$\frac{x}{d} = \frac{99}{211} = 0.47 < 0.5 \tag{B5}$$

$$\varepsilon_s = \left(\frac{d-x}{x}\right)\varepsilon_{cu} = \left(\frac{211-99}{99}\right) \times 0.0035 = 3.8 \times 10^{-3} > \frac{0.87 f_y}{E} = \frac{0.87 \times 502}{200 \times 10^3} = 2.2 \times 10^{-3} \tag{B6}$$

$$\varepsilon_s' = \left(\frac{x-d'}{x}\right)\varepsilon_{cu} = \left(\frac{99-37}{37}\right) \times 0.0035 = 2.5 \times 10^{-3} > \frac{0.87 f_y}{E} = \frac{0.87 \times 250}{200 \times 10^3} = 1.25 \times 10^{-3} \tag{B7}$$

Therefore both the longitudinal tensile and compressive reinforcement yields before failure.

Check steel yielding before failure:

C) FRP design

Estimation of required FRP area:

$$A_f = \frac{\Delta M}{0.9h\varepsilon_f E_f} = \frac{1761597.8}{0.9\times 254\times 1.8\times 165\times 10^3} = 7.78mm^2 \quad \text{(C1)}$$

The smallest CFRP plate size that the commercial producer had was A_f= 60mm^2.

$$M = A_s' f_s'(\beta x - d_s') + A_s f_s(d_s - \beta x) + (\frac{h-x}{x}\varepsilon_{cu})E_f A_f(h - \beta x) \quad \text{(C2)}$$

$$= 101.5\times 250(0.9\times 56 - 37) + 597\times 502(211 - 0.9\times 56) + \left(\frac{254-56}{56}\right)\times 0.0035\times 165000\times 60(254 - 0.9\times 56)$$

$$= 71.5kNm$$

Failure criterion (Taljsten 2006):

The assumptions that were made for CFRP design were as follows:

- There exists a perfect bond between CFRP and concrete substrate (full composite action) and the repair material, such that strain compatibility exists.
- The stress strain relationship of CFRP was assumed as linear elastic behaviour up to failure.
- The stress strain relationship of steel was assumed as elastic perfectly plastic
- Concrete simplified stress block was used
- The effect of patch repairs in the force equilibrium was neglected

$$\rho_{fi} = \frac{\alpha v_1 f_{cc} - \rho_s f_y + \rho'_s f'_y}{\left(\varepsilon_{cu}\left(\frac{h}{v_1 d_s} - 1\right) - \varepsilon_0\right)\times E_f} \quad \text{(C3)}$$

$$= \frac{0.9\times 0.582\times 40 - \left(\frac{628}{155\times 211}\right)\times 502 + \left(\frac{100.5}{155\times 211}\right)\times 250}{\left(0.0035\left(\frac{254}{0.582\times 211} - 1\right) - 0\right)\times 165\times 10^3} = 2.2\times 10^{-2}$$

$$\rho_{f2} = \frac{\alpha v_1 f_{cc} - \rho_s f_y + \rho'_s \varepsilon_{cu}\left(1 - \frac{d'_s}{v_1 d}\right)E_s}{\left(\varepsilon_{cu}\left(\frac{h}{v_1 d_s} - 1\right) - \varepsilon_0\right) \times E_f} \quad \text{(C4)}$$

$$= \frac{0.9 \times 0.582 \times 40 - \left(\frac{628}{155 \times 211}\right) \times 502 + \left(\frac{100.5}{155 \times 211}\right) \times \left(1 - \frac{37}{0.582 \times 211}\right) \times 200 \times 10^3}{\left(0.0035\left(\frac{254}{0.582 \times 211} - 1\right) - 0\right) \times 165 \times 10^3} = 2.3 \times 10^{-2}$$

$$\rho_{fu} = \frac{\alpha v_1 f_{cc} - \rho_s f_y + \rho'_s \varepsilon_{cu}\left(\frac{x - d_s}{h - d_s}\right)\varepsilon_f}{\varepsilon_f \times E_f} \quad \text{(C5)}$$

$$= \frac{0.9 \times 0.582 \times 40 - \left(\frac{628}{155 \times 211}\right) \times 502 + \left(\frac{100.5}{155 \times 211}\right) \times \left(\frac{118 - 37}{254 \times 37}\right) \times 0.017}{0.017 \times 165 \times 10^3} = 4.32 \times 10^{-3}$$

$$\rho_{fn} = \frac{\alpha f_{cc} \frac{h v_2}{d_s} - \rho_s f_y + \rho'_s \varepsilon_{cu}\left(1 - \frac{d'_s}{v_2 h}\right)E_s}{\varepsilon_f \times E_f} \quad \text{(C6)}$$

$$= \frac{0.9 \times 40 \times \frac{254 \times 0.161}{211} - \left(\frac{628}{155 \times 211}\right) \times 502 + \left(\frac{100.5}{155 \times 211}\right) \times \left(1 - \frac{37}{0.161 \times 254}\right) \times 200 \times 10^3}{0.017 \times 165 \times 10^3} = -2.80 \times 10^{-4}$$

$$\rho_{f0} = \frac{\alpha f_{cc} \frac{d'_s v_3}{d_s} - \rho_s f_y + \rho'_s \varepsilon_{cu}\left(1 - \frac{1}{v_3}\right)E_s}{\left(\varepsilon_{cu}\left(\frac{h}{v_3 d'_s} - 1\right) - \varepsilon_0\right) \times E_f} \quad \text{(C7)}$$

$$= \frac{0.9 \times 0.582 \times 40 \times \frac{37 \times 1.56}{211} - \left(\frac{628}{155 \times 211}\right) \times 502 + \left(\frac{100.5}{155 \times 211}\right) \times \left(1 - \frac{1}{1.56}\right) \times 200 \times 10^3}{\left(0.0035\left(\frac{254}{1.56 \times 37} - 1\right) - 0\right) \times 165 \times 10^3} = 1.24 \times 10^{-3}$$

$\rho_{f1} > \rho_{fn}, \rho_{fo}$ Which means the strengthened beams should fail by yielding of longitudinal steel reinforcement and crushing of concrete.

Failure criterion (ISIS Canada 2006):

Force equilibrium:

$$T_f + T_s = C_c + C_s \tag{C8}$$

$$\alpha f_{cc} bx + A'_s f'_y = A_s f_y + \left(\frac{h-x}{x}\varepsilon_{cu}\right)E_f A_f \tag{C9}$$

$$0.9 \times 40 \times 155x^2 + 100.5 \times 250x = 628 \times 502x + (h-x)E_f \times A_f$$

$$x = 123mm$$

Computing the quadratic equation yields a neutral axis of 123mm

$$\varepsilon_{frp} = \varepsilon_{cu}\left(\frac{h-c}{c}\right) = 0.0035\left(\frac{254-123}{123}\right) = 0.0038 < 0.0085 \tag{C10}$$

$$\varepsilon_s = \varepsilon_{cu}\left(\frac{d-c}{c}\right) = 0.0035\left(\frac{211-123}{123}\right) = 0.026 > \varepsilon_y \tag{C11}$$

$$\varepsilon'_s = \varepsilon_{cu}\left(\frac{c-d'}{c}\right) = 0.0035\left(\frac{123-37}{123}\right) = 0.0024 > \varepsilon'_y \tag{C12}$$

Calculation of required depth of milling to achieve the 5% steel area loss: $\frac{1}{2}\vartheta$

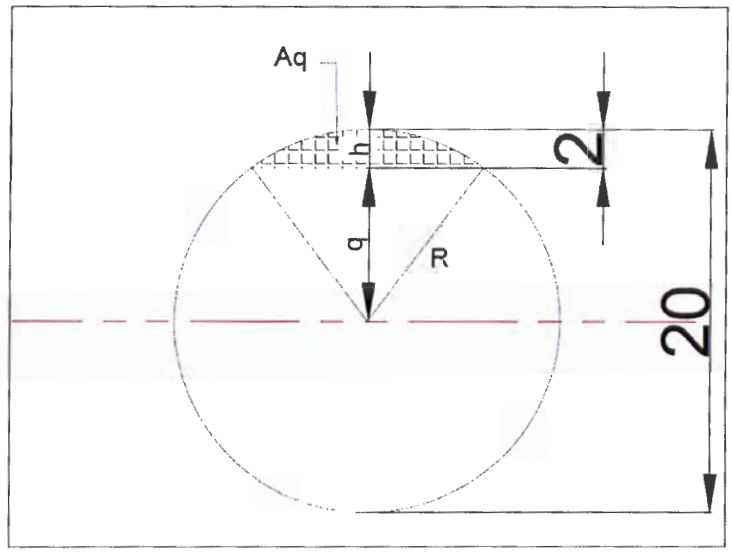

Figure C.1: Reinforcement bar indicating the 5% area loss and required milling depth

$$A_q = \frac{1}{2}R^2\vartheta - \frac{1}{2}R^2 \sin\vartheta \tag{C13}$$

$$A_q = \frac{1}{2}R^2(\vartheta - \sin\vartheta)$$

Where $\cos\left(\frac{\vartheta}{2}\right) = \frac{q}{R}$ m therefore $\vartheta = 2\arccos\left(\frac{q}{R}\right)$

$$A_q = \frac{1}{2}R^2\left(2ar\cos\left(\frac{q}{R}\right) - \sin\left(2ar\cos\left(\frac{q}{R}\right)\right)\right) \tag{C14}$$

The calculations were further confirmed through the integration method:

$$A_q = \iint_{Aq} 1dA = \int_{\vartheta_0}^{\vartheta_1}\int_{q\cos ec\vartheta}^{R} r dr d\vartheta \tag{C15}$$

Where:

$$r\sin\vartheta \geq q; \vartheta_0 = \arcsin\left(\frac{q}{R}\right) and \vartheta_1 = \pi - \vartheta_0$$

$$r \geq q\cos ec\vartheta$$

$$A_q = \frac{1}{2}R^2(\vartheta_1 - \vartheta_0) - \frac{q^2}{2}(\cot\vartheta_0 - \cot\vartheta_1) \tag{C16}$$

A_q=5% of the total area of the tension reinforcement bars

D) Pictures of Debonding failure of CFRP and FRP wrap

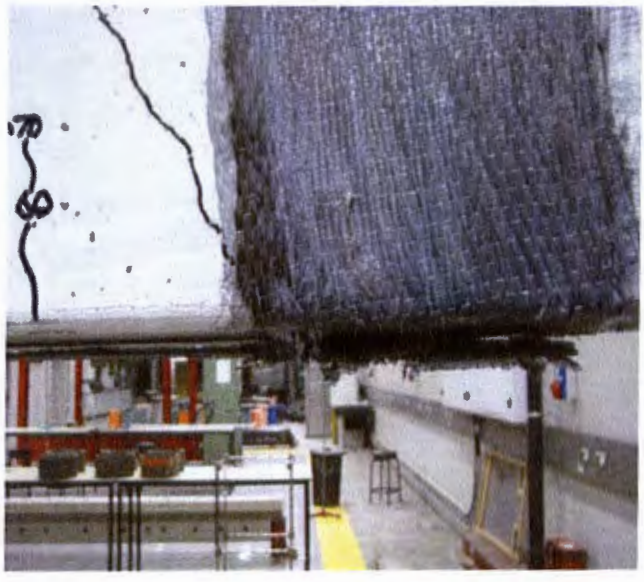

Figure D.1: Fractured FRP wrap near the right end support (beam S1.2)

Figure D.2: Debonding of FRP wrap with partial fracturing of FRP wrap (BeamS3.4)

Figure D.3: Debonding of FRP wrap on the left end (beam S4.2)

Table 12: Results from crack mapping of the beams

Beam No.	First crack (kN)	Average crack spacing C_s(mm)	Maximum crack width C_m (mm)
C1	30	93	2.5
C2	20	93	1.8
C3	10	100	2
S1.2	20	82	1.6
S1.3	20	70	1.1
S1.4	20	88	0.9
S2.2	20	74	1.3
S2.3	20	88	1
S2.4	10	70	1.6
S3.2	20	82	0.7
S3.3	10	70	1.7
S3.4	20	78	1.3
S4.1	10	67	_
S4.2	10	100	1.1
S4.3	10	78	1.4

E) Load-deflection behaviour

Table 13: Mid-span load deflection results

Beam	Yield load (kN)	Yield Dis-placement (mm)	Peak load (kN)	Debonding load (kN)	Debonding displace-ment (mm)	Ultimate (crushing) load (kN)	Ultimate dis-placement (mm)
C1	183	3,9	185			166	18,3
C3	160	5,1	171			159	17,8
S1.2	207	5,5	218	216	8,8	169	13,6
S1.3	184	7,4	198	198	9.,2	143	21,1
S1.4	177	5,9	188	187	7,4	149	20,3
S2.2	195	6,8	199	199	9,5	141	21,8
S2.3	223	4,8	235	232	8,1	183	13,4
S2.4	203	6,4	209	201	9,1	150	25,6
S3.2	184	5,5	195	192	8,5	149	13,5
S3.3	223	9,4	224	221	10,6	180	15,5
S3.4	171	7,2	172	168	8,2	131	14,0
S4.1	185	7,2	196	192	11,1	148	16,9
S4.2	218	9,4	230	230	11,8	165	20,7
S4.3	200	6,3	217	217	7,7	169	17,6

Table 14: Shows the rigidity, ultimate ductility and debonding ductility results

Beam	Rigidity (N/mm)	Ultimate ductility	Debonding ductility
C1	40,6	4,7	-
C3	29,4	3,5	-
S1.2	34,7	2,5	1,6
S1.3	22,4	2,8	1,2
S1.4	27,1	3,5	1,3
S2.2	26,0	3,2	1,4
S2.3	43,2	2,8	1,7
S2.4	30,4	4,0	1,4
S3.2	30,4	2,4	1,5
S3.3	22,8	1,6	1,1
S3.4	21,3	2,0	1,1
S4.1	24,6	2,4	1,5
S4.2	22,3	2,2	1,3
S4.3	30,0	2,8	1,2

Table 15: Experimental average load-deflection results

Beams (mm)	Yield load (kN)	Yield displacement (mm)	Debonding load (kN)	Debondingdisplacement (mm)	Ultimate load (kN)	Ultimate displacement (mm)
Control	172± 12	4,5	-	-	163± 4	18,1
450mm	189± 13	6,3	200± 12	8,4	154± 11	18,3
800mm	201± 14	7,6	213± 16	10,2	161± 9	18,4
1300mm	192±22	7,4	194± 22	9,1	153± 20	14,3
1800mm	207± 12	6	211± 15	8,9	158± 18	20,3

Table 16: Experimental average load-deflection results continued

Beams (mm)	Peak load (kN)	Rigidity (kN/mm)
Control	178± 12	35
450mm (set 1)	201± 13	28
800mm (set 4)	214± 14	25.6
1300mm (Set 3)	197± 21	24,8
1800mm (Set 2)	214± 15	33,2

Table 17: FEM results

Beam	Yield strength (kN)	Yield displacement (mm)	Peak load (kN)	Peak displacement (mm)	First crack load (kN)	First crack displacement (mm)
Control	172	9.42	172	9.42	28	0.2
450mm	190	5.37	226	9.84	26	0.23
800mm	195	5.79	237	9.87	25	0.23
1300mm	205	7.4	237	10.4	22	0.22
1800mm	189	-	-	-	25	-

F) Neutral axis and strain results

Table 18: Experimental results for: neutral axis, tension steel strain, compression steel strain and CFRP strain at mid-span as determined from the compression strain

Beam	Yield load (kN)	Compression strain (at yielding)	Neutral axis (mm)	Tensile steel strain	Compression steel strain	CFRP strain
C1	183	940	50.5	2991	251	3792
C3	160	840	48.1	2844	194	3595
S1.2	207	1484	64.7	3353	636	4339
S1.4	177	1458	64.3	3328	619	4304
S2.2	195	1097	57.3	2945	389	3769
S2.4	203	900	52.7	2700	269	3434
S3.2	184	804	50.3	2569	213	3257
S3.3	223	1150	58.4	3005	421	3852
S3.4	171	1700	68.3	3552	779	4622
S4.1	185	942	53.8	2756	294	3509
S4.2	218	1855	70.7	3684	884	4813
S4.3	200	1290	61.2	3158	510	4064

G) Thermography

Table 19: Position where voids were detected in the RS beams prior to loading

Beam	Position of void(s)
S1.3	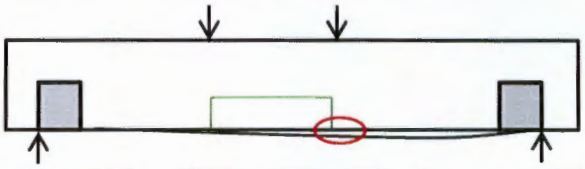
S1.4	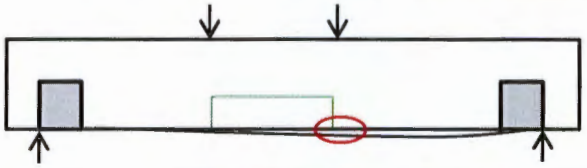
S2.4	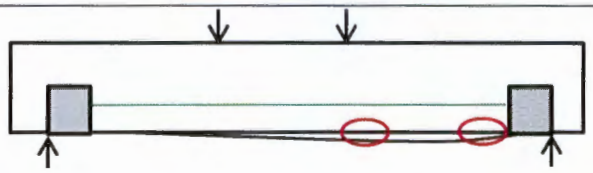
S3.3	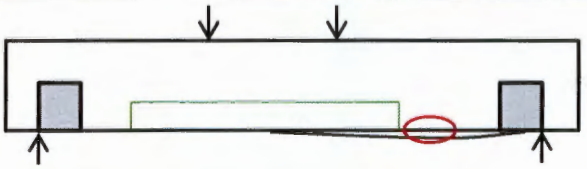
S3.4	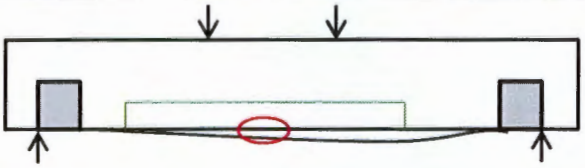
S4.2	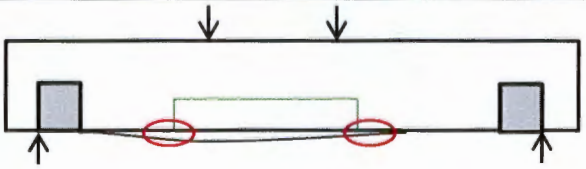
S4.3	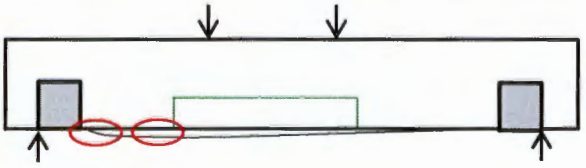

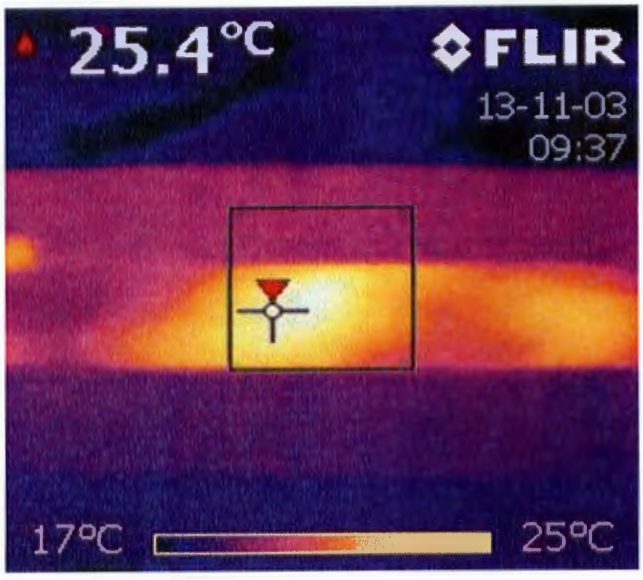

Figure G.1: Image of detected voids present in the epoxy bond of beam S1.3

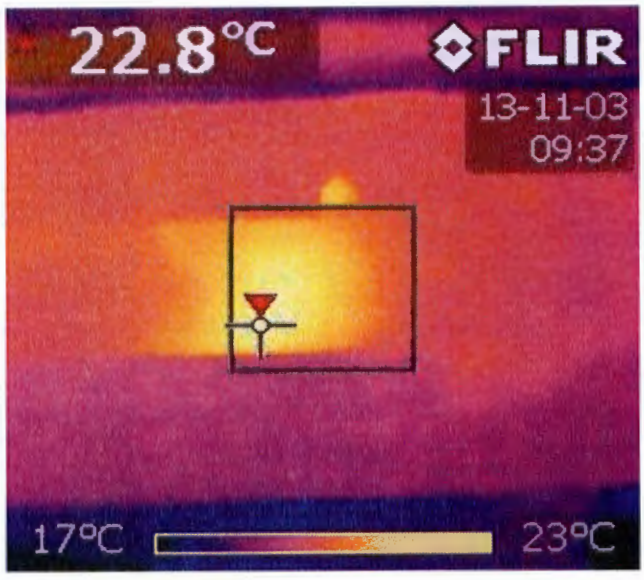

Figure G.2:Image of detected voids present in the epoxy bond of beam S1.4